Dynamics and Fuel Cycle Analysis of a Moderated Molten Salt Reactor

Károly Nagy

Moderated Molten Salt Reactor   Károly Nagy

TUDelft

Delft
University of
Technology

Challenge the future

Dynamics and Fuel Cycle Analysis of a Moderated Molten Salt Reactor

Károly Nagy

Dit proefschrift is goedgekeurd door promotor:
Prof. dr. ir. T.H.J.J. van der Hagen

Copromotor: Dr. ir. J.L. Kloosterman

Samenstelling promotiecommissie:

Rector Magnificus,	Voorzitter
Prof. dr. ir. T.H.J.J. van der Hagen,	Technische Universiteit Delft, promotor
Dr. ir. J.L. Kloosterman,	Technische Universiteit Delft, copromotor
Prof. dr. R.J.M. Konings,	Technische Universiteit Delft
Prof. dr. I. Pazsit,	Chalmers University of Technology, Sweden
Prof. dr. M. Makai,	Budapest University of Technology and Economics, Hungary
Prof. dr. ir. C.R. Kleijn,	Technische Universiteit Delft
Dr. H.C.P.E. Kuipers,	Shell Nederland B.V.

Dynamics and Fuel Cycle Analysis of a Graphite-Moderated Molten Salt Nuclear Reactor

Proefschrift

ter verkrijging van de graad van doctor
aan de Technische Universtiteit Delft,
op gezag van de Rector Magnificus
prof. ir. K.C.A.M. Luyben,
voorzitter van het College voor Promoties,
in het openbaar te verdedigen
op maandag 10 september 2012 om 15:00 uur

door

Károly NAGY

Master of Science in Engineering Physics,
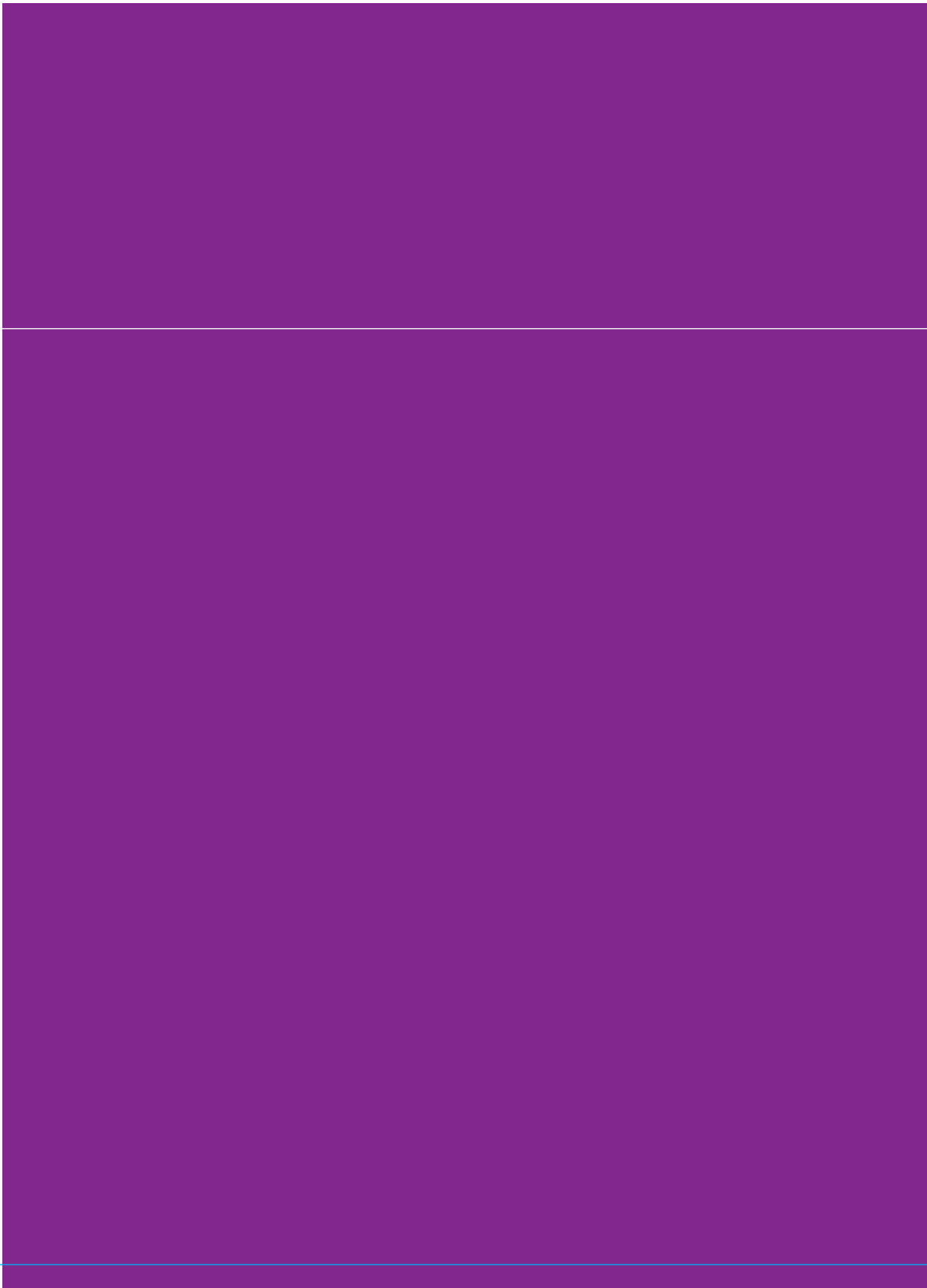Budapest University of Technology and Economics

geboren te Szolnok, Hongarije

To my patient
little family

Contents

Chapter 1

Introduction

This section gives an overview of the Molten Salt Reactor (MSR) and its associated fuel cycle. The first section is a general description of the reactor system, while Chapter 1.2 gives an introduction to the thorium fuel cycle. Next, the technical challenges of a moderated MSR and the research efforts associated with those are addressed. The last part of this chapter gives the objective and an outline of this thesis.

1.1   Molten Salt Reactors

The Molten Salt Reactor (MSR) is a certain type of a nuclear reactor, which is a device to initiate and control a self-sustaining nuclear chain reaction. Nuclear reactors consists of fuel and coolant. The fission reaction takes place in the fuel and the heat produced there is removed by the coolant. Optionally, the high-energy neutrons produced in the fission are slowed down in the moderator. This technique is widely used in nuclear reactors because slow energy neutrons are more likely to initiate new fission events. In most of the reactor types, the fuel is a solid material which contain fissile nuclei, typically ^{235}U. Water is widely used as coolant but some reactor types employ inert gases like helium or molten metals like sodium. Water is an excellent moderator, so water-cooled reactors, which are the most prevalent, are moderated by the coolant as well. The use of a solid moderator is also possible, the best example of that is graphite.

Initially, ten countries joined together to form the Generation IV International Forum (GIF) (Generation IV International Forum, 2002) to develop the future generation of nuclear energy systems. With other countries joining the GIF, this is the main research initiative for nuclear energy development to date. The objective for the generation IV nuclear systems is to provide energy in a reliable and safe way together with reduced long-lived nuclear waste production and increased economic competetiveness. Six promising reactor concepts were selected, these are the Supercritical Water Reactor (SCWR), the Gas Cooled Fast Reactor (GCFR), the Sodium Cooled Fast Reactor (SFR), the Lead Cooled Fast Reactor (LFR), the Very High Temperature Reactor (VHTR), and the MSR. The aim of the GIF is to allow deployment of these reactors before 2030.

The MSR employs a circulating liquid fuel which is a mixture of molten salts. This fuel can be readily transported by pumps and pipes between a simple core (typically containing graphite moderator) and external heat exchangers. The produced heat is removed from the core by the salt itself. The reactor vessel and the piping is designed so that criticality can be achieved only in the core. Heat from the radioactive primary salt is transferred to a clean intermediate salt that then transfers heat to either a steam or gas cycle (see Figure 1.1). MSR can be built with or without solid moderator in the core. Fluoride salts are usually considered for the primary loop of the reactor and the preferred cation components are Li, Be, Na, Zr because the fluoride salts of alkali metals have low vapor pressure and do not produce radiolytic gases. The actinides are dissolved in the salt mixture in a form of fluoride salt as the solubility of actinides is high. The MSR has several advantages and unique characteristics:

- MSRs have good neutron economy which results in high specific power. Furthermore, continuous removal of absorbing nuclides allows operation as actinide burner or as breeder/high conversion ratio reactor.
- The molten fluoride salts have low vapor pressure. Thus, the reactor can operate on atmospheric pressure with only low stresses on the structure.
- MSRs can be suppliers of process heat due to their high temperature operation.
- The safety of the reactor can be ensured by the negative temperature feedback of the fuel salt and the fail-safe drainage to the emergency dump tanks. These tanks are located below the primary loop and the geometry of those is designed to prevent re-criticality of the fuel salt. The dump tanks are separated from the primary loop by salt freeze plugs. These are actively cooled so loss of electricity in the plant or overheating of the fuel salt melts those and gravity drains the fuel salt into the tanks.
- A hypothetical release of radioactive material during an accident would be modest compared to other reactor types due to the low inventory of plutonium, Minor Actinides (MA) (elements heavier than plutonium) and volatile Fission Products (FP) in the salt.
- Molten fluoride salts are excellent coolants, with a 25 percent higher volumetric heat capacity than pressurized water and nearly five times that of liquid sodium. That greater heat capacity results in more compact primary loop components like pumps and heat exchangers.
- Various actinide feeds can be added to the fuel salt without the blending and fuel fabrication needed by solid fuel reactors.
- The fuel salt can be processed (refueling and FP removal) during the opeation of the reactor. Thus, MSRs have potentially high availability.
- The reactor can use ^{232}Th or ^{238}U as a fertile material dissolved as fluorides in the salt.
- Removal of FP can reduce the absorption enough to allow breeding in the thermal energy range using the thorium fuel cycle.

The liquid fuel of the MSR allows for the removal of FP and actinides from the salt during operation. Several techniques were developed which aim to remove a group of elements from the salt (the different processes are explained in detail in Chapter 2.3):

- Gaseous FP are not retained in the salt and migrate to the free surfaces. In order to speed up this process, helium bubbles are introduced to the salt, which are removed in another point of the primary loop together with the collected gaseous FP. This off-gas system removes some of other non-soluble FPs, which are typically noble metals. These FP can be collected on regularly replaced metal sponges as well.
- The fluoride volatilization process is used to remove uranium from the molten salt. In this process, the UF_4 content of the salt is converted to UF_6 gas which is easily collected.
- Three- and four-valent, soluble lanthanides and actinides can be removed with vacuum distillation of the molten salt. This process is very attractive because it does not involve any chemical reaction but it does not differentiate between the different elements.
- More complex chemical processes can separate two-, three- and four-valent elements (usually lanthanides from thorium) but none of those has been tested on large scale applications.
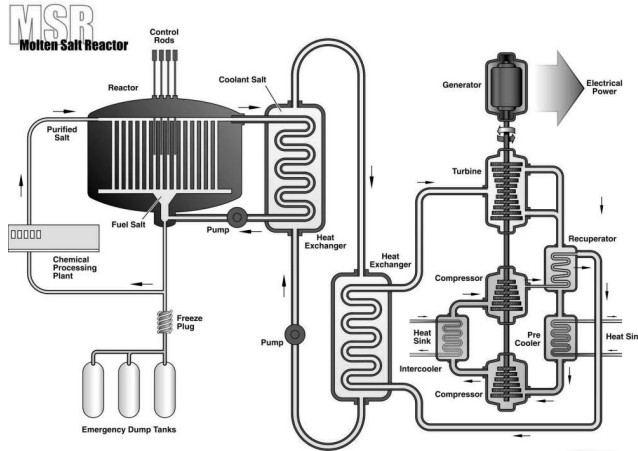
Figure 1.1: The design of a MSR (Generation IV International Forum, 2002). The fuel salt flows into the reactor core and the heat exchanger. The sub-critical emergency dump tanks are separated from the loop by a salt freeze plug. A small stream of the fuel salt is processed in the chemical plant. An intermediate loop of fuel salt transfers the heat to a gas cycle.

There are several fuel cycle options for the MSRs. First, a high conversion ratio once-through actinide burning cycle, which means no soluble FP and actinide is removed from the salt during the lifespan of the salt. In this case, the fuel can be enriched uranium, denaturated ^{233}U (^{233}U - ^{238}U mixture) with the possibility of adding thorium, or plutonium and MA. This option can be operated with minimum chemical processing. Second, breeding can be achieved using the thorium fuel cycle if proper salt purification processes are employed. The last option is actinide (Pu and MA) burning with recycling to reduce the long-lived nuclear waste.

1.2   The thorium fuel cycle

All nuclear power reactors operational in the world use uranium fuel, enriched in the fissile isotope ^{235}U up to 5%. During the enrichment process large amounts of depleted uranium are produced and during the irradiation of the fuel plutonium and heavier elements (Am, Cm etc.) are produced. There is currently not much use of depleted uranium; and the elements heavier than plutonium, the MAs together with plutonium, unless it is reprocessed - are mainly responsible for the long-term radiotoxicity of the spent nuclear fuel.

Thorium is 3 to 4 times more abundant in the earth crust than uranium and is only made up of one isotope, ^{232}Th. This is not a fissile isotope; thus, thorium itself is not a fuel but it has to be irradiated by neutrons first to produce the fissile isotope ^{233}U. This way

new fissile material can be bred and the fissile material resources can be enlarged. This is very different from the uranium fuel cycle, which usually employs an enrichment process because of the low, 0.7%, ^{235}U content of the natural uranium.

From the mid 50s to the 70s there was a worldwide interest to develop thorium fuel cycles in order to supplement uranium reserves. The feasibility of thorium utilization was demonstrated in light water reactors, heavy water reactors, high temperature reactors, liquid metal fast breeder reactors and molten salt reactors (IAEA, 2005). In experimental and power reactors, thorium based ceramic fuels had been used with high or low enriched uranium as driver fuel. In the USA, two boiling water reactors, the BORAX IV and Elk River (Kazimi, 2003), the pressurized water reactor Indian Point (Babcock and Wilcox, 1963) and the Shipping Port light water breeder reactor (Clayton, 1993) were operated with thorium fuel. Several HTGRs were used to demonstrate the feasibility of thorium fuels, such as the AVR (Ziermann, 1990) and THTR (Schwarz and Baumer, 1988) in Germany, Peach Bottom (Everett and Kohler, 1978) and Fort St Vrain in the USA and the DRAGON in UK.

Thorium has always been considered as an option, even for fusion-fission hybrids or more exotic systems (Teller, 1978), but the research of thorium fuel cycles was cancelled after the discovery of new uranium deposits. However, the need for higher burnup, improved waste form characteristics and proliferation-resistance (reduction of plutonium inventories) has recently led to a renewed interest in thorium fuel cycles. In India, the long-term nuclear strategy is based on thorium and a strong research programme of thorium fuels and fuel cycles is carried out. As a demonstration, some 3 tonnes of thorium oxide pellets have been irradiated in the CIRUS and DHRUVA research reactors. The irradiated thorium was reprocessed and the recovered ^{233}U has been utilized in the KAMINI research reactor. Furthermore, thorium is used in the blanket of the FBTR and for flux flattening of initial core after start-up in the PHWRs of India (Balakrishnan and Kakodkar, 1994). Research and development are conducted for construction of an advanced heavy water reactor.

The fertile isotope of the thorium fuel cycle is ^{232}Th which forms ^{233}U after a neutron capture followed by two beta decays. The intermediate products are ^{233}Th and ^{233}Pa which have a half-life of 22.3 minutes and 27 days, respectively. The dynamics of this fuel cycle differ from the uranium cycle because of the relatively long half-life of ^{233}Pa, while ^{239}Np, the isotope in the same position in the uranium fuel cycle has a half-life of 2.35 days. As it will be shown later, this difference has a significant impact on the fuel cycle.

The thorium fuel cycle has several advantages over the uranium cycle:

- The absorption cross-section of ^{232}Th for thermal neutrons is three times that of ^{238}U, which is the fertile isotope of the uranium fuel cycle. Thus, thorium is better fertile material in thermal reactors, but ^{238}U (depleted uranium) is superior to it in fast reactors.
- The reproduction factor (the number of new neutrons generated by fission per neutron absorbed in a given nuclide, represented as η) for the fissile ^{233}U nuclei is greater than 2 over a wide range of the thermal neutron spectrum, not like for ^{235}U and ^{239}Pu (see Figure 1.2). It is easy to see that $\eta = 2$ is the theoretical lower limit for breeding, as one neutron per fission is necessary to maintain the chain reaction and another one is needed to convert one fertile nucleus to a fissile one. Thus, the thorium fuel cycle can

operate with fast, epithermal or thermal spectra, contrary to the uranium cycle in which breeding can be obtained only with a fast neutron spectrum.

- The capture-to-fission ratio (denoted as α) of ^{233}U is lower than for ^{235}U and ^{239}Pu in the thermal range. This allows for smaller critical load for thermal reactors and shows a big difference if a thermal thorium breeder is compared with a fast breeder reactor.

- The thorium fuel cycle produces less long lived radiotoxic waste than the current fuel cycle. Because of the low α value of ^{233}U, less plutonium and MA is produced during the irradiation of the fuel. Furthermore, ^{232}Th is a lighter isotope than ^{238}U. Thus, more neutron captures are necessary to produce MA from ^{233}U. However, there are other radionuclides such as ^{231}Pa, ^{229}Th and ^{230}U which may have long term radiological impact as well.

- Thorium based fuels have intrinsic proliferation resistance due to the radioactivity of the unirradiated ^{233}U (Gat and Engel, 2000). This radioactivity comes from ^{232}U which has a half-life of 73.6 years and it is produced via (n,2n) reactions with ^{232}Th, ^{233}Pa and ^{233}U. The daughter products of ^{232}U have short half-life and some like ^{212}Bi and ^{208}Tl emit high-energy gamma radiation. The latter isotope decays emitting a 2.6-MeV gamma. This hard gamma emission requires substantial shielding and remote operations to handle the ^{233}U already after very short time (days) after it is purified. Furthermore, the ease
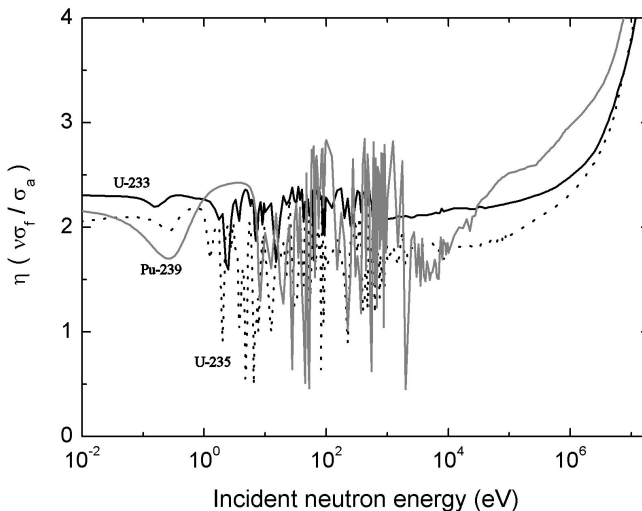
Figure 1.2: The reproduction factor η as a function of incident neutron energy for several fissile nuclides. ^{233}U is superior to the others in the thermal and epithermal energy range.

of detecting the telltale gamma makes clandestine operations almost impossible. ^{233}U contaminated with ^{232}U is generally not acceptable as fissile material for weapons due to its limited shelf time. The handling of ^{233}U becomes hazardous after a short time without shielding and remote operations. The thorium fuel cycle has no enrichment step; thus, the number of handling steps is reduced and safety is increased.

- It is worth mentioning, although it is outside the scope of this thesis, that thorium oxide fuels have superior chemical and physical properties compared to the uranium based fuels.

Of course, there are some challenges associated with the thorium fuel cycle. First, the long half-life of ^{233}Pa lowers the ^{233}U production rate in a breeder reactor because the protactinium can capture a neutron before it decays to uranium and the ^{234}U, the product of this process, is not fissile. The strong gamma radiation of the irradiated thorium makes the fuel proliferation resistant but it also makes remote and automated reprocessing and refabrication of the (solid) fuel necessary. Finally, large scale processes which separate thorium from plutonium and FPs are not yet developed.

1.3 Overview

The first research program on the MSR was conducted at the Oak Ridge National Laboratory. During this program, two demonstration reactors, the Aircraft Reactor Experiment (ARE) (Bettis et al., 1957a) and the Molten Salt Reactor Experiment (MSRE) (Haubenreich and Engel, 1970), were built and succesfully operated. Although the ARE operated only 9 days in 1954 (Bettis et al., 1957b), the experiment answered several important questions. First, it was found (Ergen et al., 1957) that a reactivity insertion results in a shorter reactor period when the fuel is circulated, due to the loss of delayed neutrons emitted in the portion of the fuel located in the primary loop. On the other hand, a large excess reactivity has to be added to bring the reactor on a very short period because the short lived precursors, which decay before could leave the core, are effective in stabilizing the reactor. Furthermore, it was observed that xenon and other volatile fission products are not retained in the molten salt (Savolainen, 1955). The operation time of the MSRE was much longer than that of the ARE as it reached criticality in 1965 and was finally shut down in 1969. The MSRE served mostly as a material test for fuel, moderator and structural material and the problems which arose during operation were solved later in the program. These problems were the tritium production of ^{7}Li, corrosion of the metal structure caused by tellurium and hardening of the metal alloys under irradiation.

The main goal of the MSR project at ORNL was a breeder reactor which uses the thorium fuel cycle. After enough knowledge was gained on the chemistry of fluoride salts and the compatibility of those with graphite, the conceptual design of a one-fluid graphite-moderated breeder reactor was finalized. This reactor was called the Molten Salt Breeder Reactor (MSBR) (Robertson, 1971). This reactor design had a complex graphite structure which divided the core into a well-moderated central zone and under-moderated

zones close to the reflectors. The reactor employed a salt processing scheme which assumed that the whole volume of the primary salt was treated in 10 days. The scheme itself consisted of a removal process of volatile fission products and selective removal of soluble fission products and transuranic elements together with the removal and storage of protactinium. A disadvantage of the MSBR design was the short lifespan of the graphite core. The replacement of the graphite was needed every four years of operation because of the dimensional changes of the graphite structure caused by high-energy neutrons.

1.3.1   Reactor design

The research program at ORNL was finished in 1976 and real interest raised only in the end of the 1990s. In 2001, the MOST project (Renault et al., 2005) started which aimed to provide a state-of-the-art review of the molten salt technology. Among other reactor designs, the MSBR was investigated and the reactivity feedback coefficients calculated in this project did not correspond with the original calculations from ORNL. According to the new results (Kophazi et al., 2003), the MSBR can have a positive feedback on temperature variations due to the positive contribution of the graphite (the feedback mechanisms are explained in Chapter 4.1). The outstanding breeding ratio of the MSBR was found be difficult or impossible to reach because the high fuel processing performance required to achieve it is not feasible (Uhlir et al., 2003). These problems, together with the short lifespan of the graphite, are the major shortcomings of the MSBR and the one-fluid graphite-moderated breeder MSR designs in general. Several solutions were proposed in the literature to solve one or more of these.

First, the positive feedback of the graphite can be lowered by placing isotopes with capture resonances in the thermal range into the reactor (Lecarpentier et al., 2003). The effect of the following isotopes was investigated: ^{103}Rh, ^{115}In, ^{177}Hf, ^{151}Eu and ^{167}Er. This could be done by inserting rods containing the isotopes in the graphite structure. According to the results, the last two isotopes are effective in reduction of the feedback coefficient but material evolution calculations show that the rods containing Eu or Er have to be renewed every year. In principle, it is not difficult but it means that the reactor has to shut down every year to replace neutron poison rods. Another approach is the modification of the geometry of the salt-graphite lattice and/or the composition of the salt. In earlier studies mostly the effects of geometry variations were investigated and it was concluded that the lattices which provide good breeding performance have intolerable feedback coefficients (Mathieu et al., 2006, 2009). The lattices can be modified so that the feedback is sufficiently negative but the breeding performance of those lattices is poor.

The limited lifespan of the graphite moderator is a problem which can not be eliminated completely (unless the graphite is eliminated from the core) but it can be increased if the power output of the reactor is reduced. The damage of the graphite depends on the fluency of the high-energy neutrons so the lifespan of the graphite is determined by the lifespan of the piece of graphite in the highest power density region of the core. Therefore, a more sophisticated way of increasing the lifespan is the flattening of the power peak in the reactor. A good example of this solution is the FUJI-U3 reactor (Mitachi et al., 2007),

which employs a three-region core in the radial direction in order to achieve a flat radial flux profile in the thermal and in the fast neutron energies. This core, combined with a low power output, provides 24 years of graphite lifespan at full power operation.

Finally, the development of a reasonable processing scheme instead of the quick scheme of the MSBR has to be addressed in the field of fluoride chemistry and no realistic scheme is widely used in the literature. However, the efficiencies of the removal of different FPs is an input parameter for any material evolution calculation regarding the MSRs. As a result, a different processing scheme is assumed in the calculation of different MSR designs which makes the comparison of different designs even more difficult. The impact of the reprocessing time on the breeding performance was investigated (Mathieu et al., 2006) but the processing scheme itself was not changed.

1.3.2   Modeling

The MSR is a unique reactor design and it has some characteristics which can not be found in other reactor types. First, the delayed neutron precursors move in the core and in the whole primary loop due to the circulation of the fuel salt. As a result, the delayed neutrons are emitted at a different location than the fission event and a part of the precursors decay outside the reactor core. Thus, the kinetics of the MSR is different from other types of reactors. Second, the heat transfer phenomena are different as well. Most of the heat is directly deposited in the salt which acts as coolant of the reactor. Furthermore, in a moderated system a part of the fission heat is deposited in the moderator by gamma and neutron heating. This heat is removed from the core by the salt as well. Therefore, the moderator is at a higher temperature than the salt during operation. For these reasons, the modeling of the MSR differs from other reactors and the development of dedicated tools is important.

First, the basic reactor physics problems were introduced (Lapenta and Ravetto, 2000) and later the neutronics of fluid fuel systems were investigated using a point-kinetics model (Lapenta et al., 2001) or the quasi-static method (Dulla et al., 2004; Dulla and Ravetto, 2007). It is common in these studies that the calculations used a prescribed one-dimensional velocity field. The first coupled neutronics and thermo-hydraulic calculations were performed on one channel (that is the fuel channel and the surrounding graphite) of the moderated MSRs. This approach was employed for the AMSTER reactor (Lecarpentier and Carpentier, 2003) and for the MSBR (Krepel et al., 2005; Cammi et al., 2011). Full core coupled calculations, which incorporate 2-D or 3-D reactor physics and 3-D heat transfer calculations, were reported as well, applied to the MSRE (Kophazi et al., 2009) and to the MSBR (Krepel et al., 2007, 2008). Even in these calculations, the flow field is paralell with the channels in the entire primary loop which includes the plena below and above the core and the loop outside the reactor vessel. Thus, the mixing of the precursors in the plena was not incorporated in the calculations although it was demonstrated to have an impact on the kinetic behavior of the reactor (Kophazi et al., 2007).

1.4 Objective and outline of this thesis

This thesis deals with the graphite-moderated MSR that aims to reach self-breeding. Both the dynamics of its fuel cycle and the dynamics of the reactor itself are investigated.

Several reactor designs offer self-breeding or breeding, but the salt processing strategies envisioned for them differ widely. The first objective of this thesis is to determine which processing strategy is necessary to reach self-breeding. Closely connected to this, it was found that the existing breeding gain definitions are not suitable for the MSR. Therefore, an effort is made in this thesis to introduce a new definition which allows for the quantification and comparison of the breeding performance of different MSRs.

The use of a graphite moderator introduces some problems in the reactor design. These are the possibly positive temperature feedback of the core and the short lifetime of the graphite. Although a fast reactor design completely eliminates these, the solid moderator gives an important advantage on the mass of the uranium inventory compared to non-moderated reactors. For this reason, the moderated reactor is an attractive option and the possibility of designing a moderated MSR core which has a negative feedback and is capable of self-breeding is investigated in this thesis.

The graphite moderator changes the spectrum in the region of the core where it is installed and the magnitude of this change can be controlled by the amount of the graphite. This is a great advantage because it allows to tailor the neutron spectrum in different regions of the core. Using this, the reactor core can be split into zones in which the amount of graphite is different. In this thesis, the benefits of dividing the reactor in two zones, namely the increase in the breeding performance of the reactor and the increase of the lifespan of the graphite, are investigated. Keeping in mind a self-breeder reactor, the final aim is to demonstrate if a two-region reactor can operate at a higher power density or can provide longer graphite lifetime than a one-region reactor.

In a more complex reactor design not only the moderator is different in the zones but the salt as well. This way a separate driver and breeder (blanket) volume is established in the core which are separated by a graphite or metal barrier. The two salt streams can employ different purification processes. If the driver and blanket salt differ in composition, especially if only the blanket salt contains thorium, simple processing schemes can be utilized compared to the one-fluid designs. The fuel regeneration capability of such systems is evaluated as well.

The safety of the moderated MSR is investigated in this thesis by simulating the transient behavior of a moderated MSR. In order to do this, several computer programs were developed which are able to model an MSR. Although such coupled code systems were developed before, the first aim was to establish more general codes than the existing ones. The neutronics and heat transfer calculations were coupled with a flow field calculation. The domain of this calculation is not only the core but the plena as well; thus, the mixing of the salt below and above the core is incorporated in the calculations. These models need the physical properties of the salts as an input but these properties (heat capacity, viscosity, thermal conductivity) are often not well known for the different salt mixtures. Thus, one of the objectives of the thesis is to show the impact of the substance properties on the nominal operating conditions and the feedback coefficients of the reactor.

Seven chapters form this thesis, the first one being this Introduction and the last one summarizing the most important results and conclusions. It is followed by several appendices which give the detailed description of the computer codes developed specially for MSR calculations. The second chapter gives an overview of the history of the MSR research programs. This chapter is not stricktly necessary for the understanding of the other chapters. In the other chapters the following subjects are investigated:

- In Chapter 3 the different salt processing strategies are compared. These are the once through, the batch-wise, the continuous, and finally the continuous with protactinium removal and storage. The dynamics of the thorium fuel cycle is presented for each strategy, together with the code system for the simulation of the neutronic behavior and material evolution of the MSR. In the next step, the different strategies are compared in order to determine which one is necessary to reach self-breeding in a moderated MSR. The possibility to change the fuel composition during operation is a unique feature of the reactor and it has to be specially addressed when the breeding performance of the system is quantified. In the last part of this chapter, an improved definition for the breeding gain is given which treats the inventory of the core and external stockpiles separately. The connection between this definition and the ones used earlier is discussed as well.
- The design of the graphite-salt lattice is optimized in Chapter 4. Based on the previous chapter, on-line salt processing and protactinium removal is chosen for the optimization. The temperature feedback of the core is used as a constraint for the optimization. The goal is to reach self-breeding at high power densities. Not only the dimensions of the graphite structure, but also the amount of thorium concentration is altered in order to get a full comparison. Several graphite-salt lattices reach breeding and long graphite lifetime at low power densities. The breeding gain of these is suppressed by raising the power density. The search for this was performed for each lattice separately. This way the specific power of the reactor is increased. Lattices with high specific power are accepted as optimal designs.
- All the breeder MSR designs have more complicated cores than a single zone. These more complex core designs are investigated in this chapter. First, the zoning of the graphite, forming an undermoderated zone on the outside of the reactor, is addressed. The other option is to use two different salt mixures in two separate loops. Based on an optimized lattice from the previous chapter, the effect of using an undermoderated region or blanket salt is calculated. The breeding gain definitions given in Chapter 3 are modified here to incorporate the blanket salt. These modifications further increase the breeding gain of the reactor and affect the flux distribution in the core. Thus, the reactor can operate at higher power density while the graphite lifetime is extended and self-breeding is preserved. Finally, the possibility of the use of vacuum distillation for FP removal is investigated. This can be done in a two-salt system, where the driver salt contains no thorium.
- Chapter 6 presents the coupled code system for the steady-state and transient simulation of the moderated MSR. It is applied to a power reactor which uses the graphite lattice and power density determined in Chapter 4. After the steady-state calculations,

which determine the temperature distribution in the core and the temperature feed-back of the reactor, several transients are analyzed. These include pump-driven and temperature induced transients. The substance properties of molten salts are not well known in the whole range of steady state operation and accident scenarios. Thus, it is important to know the effect of the assumptions made. The impact of the choice of substance property correlations on the calculated feedback coefficients is discussed. All these calculations aim to demonstrate the safety of the core design derived in Chapter 4.
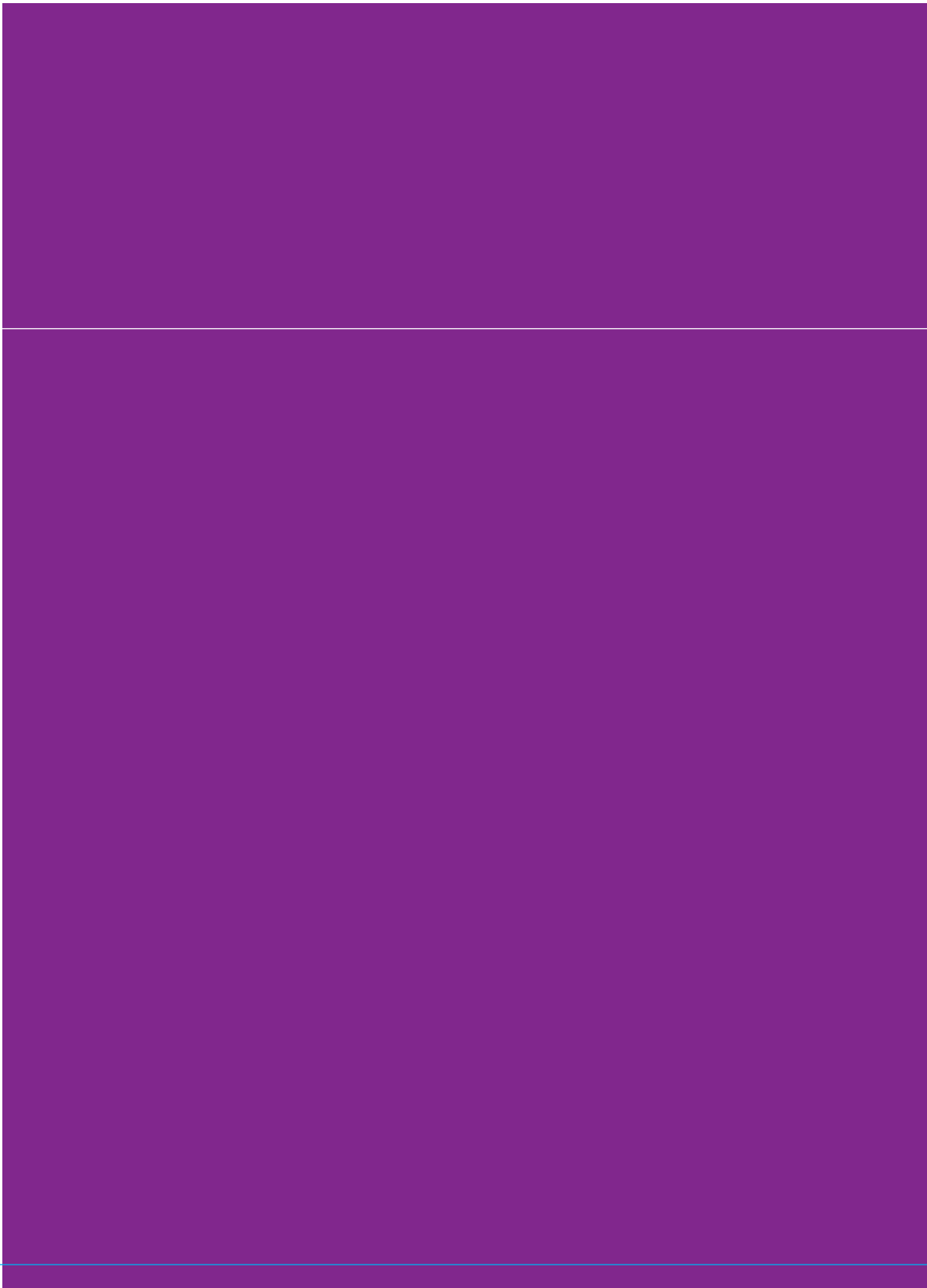
Chapter 2

History of the MSR development

An overview is given of the various MSR programs from the 1950s in this chapter. This is not a complete overview as it focuses only on the moderated MSR designs. In the last part of this chapter the different FP and actinide removal methods are explained.

2.1 History of the MSR research program at ORNL

The most extensive MSR research program was conducted at the ORNL from the early 1950s to the 1970s. The first MSR was intended to be used as propulsion for jet bombers, but after the rapid developments in rocket science the focus of the project moved to civilian applications (MacPherson, 1985). Two experimental reactors were built and operated, both of those employed solid moderator. This is the so-called heterogeneous design. In order to test material compatibility, structural and moderator materials were irradiated in molten salt environment. Finally, several ways of salt purification processes (U, FP and MA removal) were developed and tested. After preparing the conceptual design of a high breeding ratio MSR, the program was cancelled in favor of liquid metal cooled reactors.

2.1.1 The Aircraft Reactor Experiment

A group of researchers started design work on a sodium cooled reactor at ORNL. The fuel was ^{235}U (as UO_2) in a lattice of pins and the reactor was moderated by BeO blocks. The design of this reactor proceeded to the point of purchase of the BeO blocks. A relatively high power output was planned for the reactor, but a positive temperature coefficient of reactivity arose (Bettis et al., 1957a). This was associated with the cross section of ^{135}Xe at high (1000K) temperatures and the caused instability was serious enough to abandon the solid fuel design.

The solution for the xenon instability was the introduction of stagnant liquid fuel. The density change of the liquid fuel for a change in temperature stabilizes the reactor if a portion of the fuel can be made to leave the critical lattice. By that time, a considerable amount of work had been done on molten fluoride salts for use in preparing fuels in liquid form by the Materials Chemistry and Metallurgy Division of ORNL.

It was already known that fluoride salts of alkali metals have very low vapor pressure at elevated temperatures, have a wide range of uranium and thorium solubility, and have no radiolytic gas production. The physical properties of fluorine salts are of the same order of magnitude as for water while fluorine has low neutron absorption cross section but also a small average logarithmic energy loss per collision (Briant and Weinberg, 1957). As a cation, beryllium would be highly desirable for its slowing-down power, but the high viscosity of molten beryllium fluoride limits its permissible concentration. Thus, reactors moderated entirely by fluorine salts have high critical masses and to reach a thermal neutron spectrum a heterogeneous design with other moderator material is required.

The first design used the only fluoride fuel available at that time, a mixture of sodium, zirconium and uranium fluorides in which the uranium was enriched to 93.4% ^{235}U. In this design the fuel was stagnant and the core consisted of a cylindrical moderator matrix made up by the original BeO blocks. The reactor was supposed to be cooled by liquid sodium which flew through the holes of the moderator blocks. The design incorporated a

slab of boron carbide at the top of the lattice in which the fuel tubes would extend. The fuel level in the tubes would be above the boron carbide, but not completely filled at operating temperature and zero power. This system of control circumvented the solid-fuel control problem and gave an inherent stabilizing effect to the reactor control, as any expansion of the fuel due to a rise in temperature would expand more of the fuel above the lattice and into the boron carbide block.

This design had its major drawbacks as well, which necessitated another change in design. The primary difficulty was the indicated high temperature in the center of the fuel tube. In order to obtain high power output at manageable coolant flow rates the center fuel temperature would have been dangerously near the boiling point of the fluoride salt. Another problem was the fuelling of this type of reactor.

The stagnant-fuel design was abandoned and work was begun on a high temperature circulating fuel reactor. This gave a solution for the drawback of the stagnant fuel design as the mechanism for removing the heat from the fuel does not rely only on the thermal conductivity of the fluoride fuel. The piping of the fuel loop outside the pressure vessel provided access for the fuel loading as well.

In the final design the molten fluoride salt was pumped through the 66 passes of the core, through the heat exchangers and back to the core in a closed loop. The heat generated in the moderator and reflector BeO blocks was removed by liquid sodium which was pumped through the interstices of the moderator blocks and the coolant passages of the reflector blocks. The power level of the reactor was to be in the 1-3 MWt range and the mean temperature was to be 980 K. The entire system was made of Inconel, a nickel based alloy. This was chosen due to the low thermal absorption cross section of nickel.

The ARE reached criticality on November 3, 1954 and was operated for 9 days at different power levels before the experiment was terminated (Bettis et al., 1957b). Experimental data on reactor operation, temperature coefficients, critical mass, xenon poisoning and response to changes in operating conditions was obtained. It was observed that the fluoride fuel does not retain xenon; thus, no poisoning was measured (Savolainen, 1955). Irradiation tests of the fuel suggested that other volatile fission products leave the molten salt as well. During the approach to criticality, it was first noticed that liquid slugs of fuel retained their identity for several passes through the reactor and the external circuit (Cottrell et al., 1955). The effect of the loss of delayed neutrons due to the flow was also investigated (Ergen et al., 1957). It was found that reactivity insertion results in a shorter reactor period if the fuel is circulated. This happens because some precursors decay in the primary loop outside the core; thus, those are lost compared to the stationary fuel case. On the other hand, the short lived delayed neutron precursors, which have time to decay in the reactor, are quite effective and large excess reactivity has to be added to override them and bring the reactor on a very short period, even at high flow rates. The MSR can be operated safely even though some of the stabilizing delayed neutrons are lost from the core.

2.1.2 Homogeneous breeder designs

In the late 1950s, almost all proposed MSRs used fluorides as the salts because of their properties, such as low absorption cross section, low average logarithmic energy loss per

collision, and acceptable chemical properties. Due to this average logarithmic energy loss, reactors moderated entirely by fluorine would have very high critical masses. The cations considered for the salts were usually beryllium and lithium. Beryllium has low absorption and high scatter cross section, but the high viscosity of molten beryllium fluoride limits its permissible concentration in the compound. The scatter cross section of lithium is exceptionally small. Furthermore, the ^{6}Li content of the lithium has to be suppressed from the natural 7.5% to 0.0035% to have the same contribution to the absorption from as ^{7}Li (Ergen et al., 1957). Still, the LiF-BeF$_2$ mixture (often referred as FLiBe) has superior resonance escape probability and slowing-down power to salt mixtures containing other alkali metals.

The first power station designs from ORNL were homogeneous reactors, either simple converters or breeders on the thorium cycle. No solid moderator was used in the simple, sphere within sphere two region design (MacPherson, 1958a). The salt central core contained fissile and some fertile material (^{7}LiF-BeF$_2$-^{233}UF$_4$-ThF$_4$ mixture) while the surrounding blanket contained only thorium in the carrier salt. The heavy metal content of the salt determined the spectrum in the reactor, from epithermal to hard through a wide range. The barrier between the regions was made of INOR-8. The total thermal power of the reactor was assumed to be 640 MW. The large diameter of the vessel allowed less than 100 MW/m^3 power density. Chemical processing of both the driver and blanket salts was envisaged. Only the produced uranium was removed from the blanket salt, but FP removal was assumed for the driver salt. Depending on the thorium concentration in the core, the reactor could have reached a breeding ratio of 1.09 according to the original calculations.

2.1.3 The Molten Salt Reactor Experiment

The ARE program continued for a couple of years, but the interest in nuclear plane propulsion began to fall. The expertise in the molten fluoride salt technology was adapted to civilian power reactors. For a short while the emphasis was put on two regions and two salts, non-moderated, sphere within sphere designs which could operate as converter or breeder reactor. It was known from the ARE program that heterogeneous reactors (reactors with solid moderator) can reach smaller size and higher breeding ratio than homogeneous ones; thus, bare graphite samples were irradiated to test the compatibility of graphite with fluoride salts. After positive results were obtained, the focus of the project moved to heterogeneous reactors with high breeding ratio.

The Molten Salt Reactor Experiment (MSRE) (Haubenreich and Engel, 1970) was an extension of the program conducted at ORNL in the investigation of molten fluoride mixtures and structural materials for circulating fuel reactors. The objectives of the MSRE were to demonstrate the safety and feasibility of a molten salt reactor and to obtain experience about graphite in an operating MSR.

The MSRE (Robertson, 1965a) consisted of a cylindrical vessel in which a graphite matrix constituted about 78% of the volume. The fuel entered the vessel around the top of the cylinder and passed down between the graphite structure and the vessel wall. This downcomer flow was needed to cool the vessel. The core was an assembly of graphite bars 5 cm square by 166 cm long, as shown on Figure 2.1. Fuel salt circulated in direct contact with the graphite, no cladding was used. All structural parts were made of INOR-8

(sometimes called Hastelloy-N), a nickel-molybdenum-iron-chromium alloy. Three control rods operated in thimbles and a channel was provided for irradiating graphite and metal specimens. The flow turned in the dividing plenum and moved up through the rectangular passages of the graphite. The rectangular passages were chosen because the hot-spot temperature is lower than with cylindrical fuel passages. The fuel left the vessel at its top and returned through the pump and the heat exchanger. A part of the pump output was recirculated in the pump bowl to facilitate the release of entrained or dissolved gases from the salt. These gases, containing xenon and krypton, were carried to the off-gas disposal system by helium flowing through the gas space of the pump bowl. The helium also protected the oxygen-sensitive fuel from contact with air or moisture. The MSRE had a secondary fluoride salt loop and a radiator to dissipate the produced heat. The planned power production of the reactor was 10 MWth, but only 7.3 MWth was reached (Briggs, 1967). The mean temperature in the reactor was 923 K. The mixture of molten salt was LiF, BeF_2, ZrF_4 and UF_4. The MSRE was operated with enriched ^{235}U-^{238}U mixture, ^{233}U, and ^{239}Pu. The ^{233}U originated from the thorium fuel rods of the Indian Point reactor (Chandler and Bolt, 1969). Its successful operation from 1965 to 1969 demonstrated that molten fluoride salt fuelled reactors can be operated safely for a long time. The MSRE served as a material test for fuel, moderator and structural materials under real operating conditions.

After the reactor first became critical with ^{235}U fuel, zero power tests (Prince et al., 1968) were conducted in order to obtain control rod worths and reactivity coefficients (Briggs, 1965). Later, dynamic tests at several intermediate power levels (kilowatt to megawatt range) were performed. Thereafter, the reactor was operated at full power or near full power until its shutdown in 1968. The MSRE was critical with ^{233}U later that year (Rosenthal, 1969b), and zero power and dynamic tests were performed with the new fuel (Rosenthal, 1970). Just before its permanent shutdown in December 1969, a small amount of PuF_3 was added to the fuel to obtain experience with plutonium in a molten salt reactor.

The operation of the MSRE provided information about the reactor physics of circulating fuel reactors, material compatibility, and chemistry of fluoride based fuels. Although it was considered a successful experiment, some problem arose during the operation of the reactor. First, high energy neutrons produce tritium from ^{7}Li. This tritium penetrates metals at the high operating temperature of the reactor and needs to be captured, otherwise it reaches the atmosphere. After some development, an intermediate coolant salt, a mixture of sodium fluoride and sodium fluoroborate, was found, which captures the tritium. This tritium can be removed and isolated in a gas purge system. Second, cracks were discovered on the inside surface of the piping after the shutdown of the reactor. Later work showed that the cracks were caused by the fission product tellurium and that this attack could be controlled by keeping the fuel on the reducing side. This can be done by introduction of some UF3 to the salt. The necessary 2% of UF_3 can be maintained by adding some metallic beryllium, which robs some of the fluoride ions from the uranium (Haubenreich and Engel, 1970). Last, the INOR-8 alloy hardens under irradiation due to helium embrittlement from (n,α) reaction in nickel and in contaminants. Modified alloys, which have fine carbide precipitates within the grains, were developed. The migration
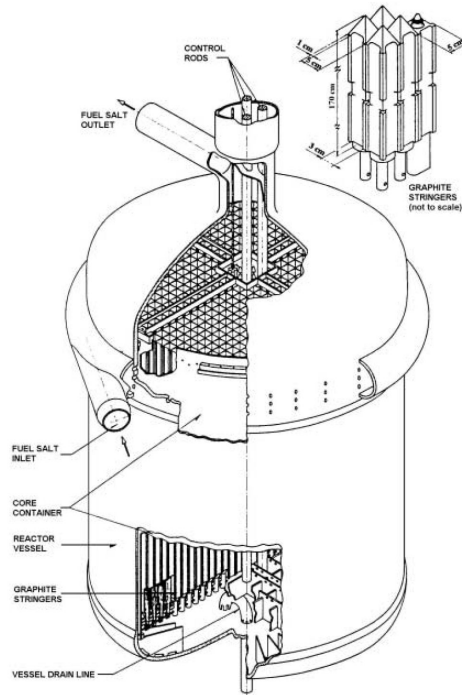
Figure 2.1: The internals of the MSRE vessel and the bars of the graphite structure.

of helium to the grain boundaries is restrained and helium is held in the grains in these alloys (McCoy et al., 1970). This effect would have limited the lifetime of the reactor in the homogeneous two-region designs discussed earlier.

2.1.4 Graphite moderated breeder designs

Parallel to the design and operation of the MSRE, the design of a heterogeneous breeder MSR was conducted at ORNL. The first designs were two-region two-fluid graphite moderated and reflected thermal reactors (Kasten et al., 1966). The two fluids were separated by the graphite structure in the core. The carrier salt for the driver and the blanket zone was a mixture of LiF and BeF_2. The designed cores were relatively large to reduce the flux damaging the graphite. Continuous processing of the driver and blanket salts was planned. The off-gas system removed the fission-product gases while the Fluoride Volatility Vacuum Distillation process was used for the driver salt. The formed ^{233}U was removed by the fluoride-volatility process. (The different chemical processes are discussed later in the introduction). The driver fuel contained only UF_4 while the blanket salt contained only ThF_4. The driver salt entered and left the reactor (Robertson et al., 1970) through

four concentric pipes which communicated with plenum chambers in the bottom head of the reactor vessel. The driver salt entered the outer plenum chamber and flew upward through the salt passages to the top of the reactor and downward to the inner plenum chamber. The blanket salt circulated around the graphite assemblies. The basic design of the reactor had the advantage of low neutron losses to structural materials other than the graphite; there was almost no neutron leakage through the thick blanket. A power of 2114 MW was produced in the driver zone and 111 MW in the blanket. The breeding ratio of this design was 1.05.

Attempts were made to find a process to efficiently remove protactinium from the blanket salt. Removing ^{233}Pa from the reactor increases the amount of produced ^{233}U because there is no loss due to neutron capture in the protactinium. Two processes were tested. One involves oxide precipitation of protactinium, while the other one treats the molten blanket salt with a stream of bismuth containing dissolved thorium metal. According to the design calculations, the two-region reactor with protactinium removal could have reached a breeding ratio somewhat higher than 1.07. Several preliminary designs were made, such as a single stream core breeder reactor and molten salt converter reactor. In the first design, the driver salt contained fertile material as well and a metallic wall separated the blanket fluid. For this reactor protactinium removal was assumed. The latter design was a single-region and single fluid reactor with fertile material in the salt. This design had a single pass core to reach exceptionally low operating and capital costs. First, no salt processing other than the off-gas system was planned, later the vacuum distillation process was suggested.

Several reasons led finally to a single-fluid breeder design (Bettis and Robertson, 1970). Throughout this thesis, this design will be referenced as Molten Salt Breeder Reactor (MSBR). Experiments showed that the removal of protactinium is possible from fluoride salts containing thorium and uranium. Thus, salts containing both fertile and fissile material can be processed, although with more difficulty than if separate driver and fertile fuel is used. Calculations showed that breeding is possible in a single fluid reactor if the outer region of the reactor core is undermoderated. Other serious problems were associated with the graphite of the two-fluid design. The graphite has a limited lifetime in the reactor due to its volume change under irradiation. In the two fluid designs the replacement of graphite was not possible, which limited the lifetime of the reactor vessel with the internal structure. The single fluid design permitted easier access through the top head, so it was possible to replace only the moderator graphite. Furthermore, the two-fluid concept depended upon the integrity of the graphite structure in the vessel to keep the driver and blanket salts separated. Finally, the design of the single fluid core could easier accommodate the dimensional changes of the graphite.

The MSBR primary system (Robertson, 1971) consisted of the reactor core, primary heat exchangers to the coolant salt and pumps. The reactor vessel was about 6.7 m in diameter and 4.5 m high with 5 cm thick wall and 7.5 cm thick dished heads at the top and the bottom. The reactor had a central zone in which 13% of the volume is salt and an outer, undermoderated region having 37% salt. These zones were made up of 10.2 cm x 10.2 cm x 4 m long graphite elements. Figure 2.2 shows a detailed plan view of the core. Ridges on the sides of the graphite elements separated the pieces and furnished flow
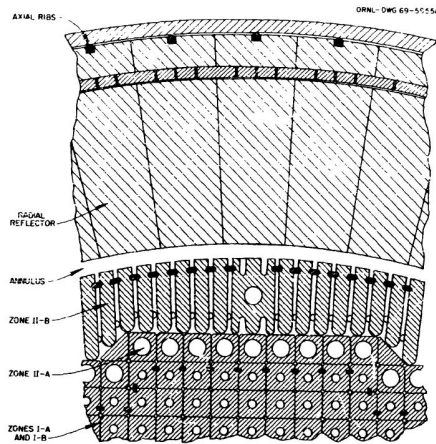
Figure 2.2: Detailed view of the MSBR graphite moderator and reflector structure.

passages. The main flow passage was the hole through the center of the blocks. The ends of the graphite elements were machined to a cylindrical shape for about 25 cm on each end to provide the undermoderated 37% salt region at the top and bottom of the reactor. There was a 5 cm wide annulus between the removable core and the reflector blocks to provide clearance when removing and inserting the core assembly. The undermoderated regions reduced the neutron leakage. Salt entered the central manifold at the bottom at about 839 K and flowed through the lower plenum and upwards through the passages of the graphite to exit at the top at about 978 K through four nozzles. The reactor produced 2250 MW heat.

The centrifugal fuel pumps forced the salt through the shell and tube primary heat exchangers. Each of the pumps had a bypass in which about 10% of the total discharge flow was circulated. This loop contained a gas bubble injection section, where sparging helium was introduced in small bubbles. The loop contained a gas separator which removed the helium and its burden of fission products with nearly 100% efficiency. Both the primary and secondary salt loops were provided with tanks for storage of the salt for emergency or maintenance. The fuel salt storage tank was connected to the primary loop by a drain line and it was separated by a freeze plug. The plug was made of solid fuel salt cooled by air. The plug can thaw in the event of overheating of the salt, loss of power, failure of the cooling system or by intervention by the operator. The salt was returned to the primary loop by pressurization of the tank. Soluble fission products and protactinium was removed from the fuel salt by Liquid Bismuth Reductive Extraction. The whole core was processed in 5 days. Protactinium was entirely removed in 5 days and the rare earth FP in about 50 days. The breeding ratio of the reactor was 1.06.

2.2 Research programs on the MSR after the MSBR

After the research program finished at ORNL, the MSR design was abandoned. The interest raised again in the 90s and all of these research projects were based on the MSBR desing initially.

2.2.1 The AMSTER

The Actinides Molten Salt TransmutER (AMSTER) design is a graphite-moderated molten salt reactor for actinide incineration (Vergnes and Lecarpentier, 2002). The design was changed to be a breeder on the thorium cycle, optimized to minimize the amount of long life nuclear waste. The design was derived from the MSBR. The lattice of the fuel channels was triangular, rather than square in the MSBR, and the graphite stringers were hexagonal. The core consisted of a well-moderated inner zone, an under-moderated outer zone and a final moderated zone adjacent to the graphite moderator. The core produces 2250 MW heat with only a very low production of transuranic elements, and it does not take Pu and MA as feed as the original incinerator. An important change in the salt processing was that protactinium was not removed, only the FP. The fuel salt was reprocessed in 300 EFPD and the reactor was supposed to reach self-breeding.

2.2.2 Japan: FUJI

Since the 1980s several small MSR reactors were designed, as a part of a symbiotic system based on the thorium cycle, the Thorium Molten-Salt Nuclear Energy Synergetic Systems (THORIMS-NES) (Furukawa et al., 2008). The ^{233}U is produced in Accelerator Molten-Salt Breeders (AMSB), while the produced fissile material is used in the FUJI critical reactors. The conceptual design of FUJI was established in 1985 based on the ORNL studies. The design is simplified in comparison with the MSBR (Furukawa et al., 1992). Several different versions of the reactor were published during the years which were designed in the 150 - 200 MWe power range. The graphite moderator does not need replacement during the lifetime of the reactor. This is achieved by low power density and high graphite volume ratio in the reactor core. On the other hand, the lifetime of the moderator - thus, the whole plant - is significantly lower than it is expected from a power plant. Continuous chemical processing of the salt is not envisaged for the FUJI reactors but those can reach a high conversion ratio. The latest design, the FUJI-U3 reaches 30 years of graphite lifetime at 75% load factor while it can achieve high conversion ratio (0.95) during its full life (Mitachi et al., 2007).

2.2.3 Up-to-date evaluation of MSR designs: the MOST project

In November 2001 the MOST project started as part of the EURATOM 5th Framework Programme (Renault et al., 2005). The objective of the project was a state-of-the-art review of the molten salt technology. The MOST project addressed the main aspects of the MSRs, such as the reactor physics, systems and components, safety, chemical aspects and fuel processing, structural materials, and economical aspects. Several MSR conceptual designs were considered, several incinerator reactors together with the MSBR and the AMSTER.

During the project, the computational tools of several participants were benchmarked against documented MSRE transients. Reactivity coefficient calculations showed that, in contrast to the original ORNL calculations (Perry and Bauman, 1970), the global temperature coefficient of the MSBR was slightly positive (Kophazi et al., 2003). This coefficient is the sum of the contribution of the salt and the graphite. While the first one is strongly negative and immediate, the slow positive effect of the graphite can make the reactor unstable on long time scales. Solutions exist by optimizing the core zoning or modifying the amount of graphite. Also the addition of erbium burnable poison in the graphite was considered in this study. According to the conducted transient calculations, the initial phase of a transient is always dominated by the negative reactivity coefficient of the salt and sufficient response time is provided for the operators. Thus, these reactors can be characterized as safe.

It was considered that the high fuel processing performance required by the outstanding breeding ratio of the MSBR may be difficult or impossible to reach in-line (Uhlir et al., 2003). The process leads to very large thorium losses. New calculations showed that the AMSTER concept can not be a breeder because the protactinium extraction was eliminated from its envisaged fuel processing scheme. According to parameter studies, breeding is achievable with a reduced on-site processing and low power density.

2.2.4 The Thorium Molten Salt Reactor

Based on the contribution of CNRS to the MOST project, a conceptual design of a thermal MSR was investigated. The design benefited from the results of the MOST project; thus, assumed slow purification of the salt and low power density (Mathieu et al., 2003). The standard system was a graphite moderated reactor, in which the moderator was made of a lattice of hexagonal elements with 15 cm sides. The radius of the fuel channel in every graphite block was 8.5 cm. The diameter and the height of the moderator matrix was 3.2 m. A blanket containing thorium surrounded the core. A binary salt, LiF-(Ac)F$_4$ (where Ac stands for actinides, mostly thorium and uranium in this case), was used. The proportion of (Ac)F$_4$ was 22%, which provided low melting point. The specific power was about 250 W/cm^3 for the salt in the core. The standard off-gas system was employed, while the further processing of the driver and blanket salt was delayed, a small amount of salt was removed from the reactor frequently. The total salt volume was assumed to be processed in 6 months with removal and storage of Pa and complete extraction of FP and TRU.

For the TMSR, the chemical processing scheme of the MSBR was considered too complex and hardly feasible at the envisioned large flow rates, and the focus moved from high breeding ratios. Thus, the impact of slower processing was investigated, and an inverse proportional relationship was found between the processing time and the breeding ratio (Merle-Lucotte et al., 2008). The above mentioned 6 months total volume processing provided a breeding ratio of 1. The other weaknesses of the MSBR design - positive total temperature feedback and short graphite lifetime - were addressed by a parameter study. The effects of changing several parameters were investigated.

First, the radius of the fuel channels was altered while the outer dimensions of the graphite blocks were not changed. According to the results, small channel diameters (low

salt and high graphite volume) provide high graphite lifetime, but positive feedback, while bigger radii perform well in terms of breeding ratio and total feedback coefficient (Mathieu et al., 2006). On the other hand, the lifetime of the graphite is only 2 years in the latter case. Thus, all fuel channel radii have a major disadvantage in this reactor. The effect of changing the specific power was also investigated by changing the size of the reactor while keeping the total power. The increase of the salt volume does not change the temperature feedback coefficient significantly, and it increases the breeding ratio and graphite lifetime but the uranium inventory increases with the size of the core. The influence of the composition of the driver salt was addressed by the change of the actinide content. For high breeding ratios, high heavy nuclide content is preferred, but all the salt compositions can result in positive total feedback coefficients, depending on the amount of graphite in the core.

Later, the size of the graphite hexagons was altered. It was hoped that a better homogenized core can provide negative temperature feedback and it was found that increasing the number of hexagons while keeping the graphite and salt volume results in negative feedback (Mathieu et al., 2009). Although some results were promising, the project continued with the non-moderated version of the reactor. This provides negative temperature feedback, small core size and high breeding ratio while has no problem arising from the graphite moderator.

2.2.5   The Generation - 4 initiative

Two different MSR designs are linked to the Gen IV initiative, one breeder design, the non-moderated version of the TMSR (TMSR-NM, lately referred to as MSFR) (Merle-Lucotte et al., 2009; Mathieu et al., 2009) and an incinerator design, the MOlten Salt Actinide Recycler and Transmuter (MOSART) (Ignatiev et al., 2007). Neither of these reactors have solid moderator, but some research goals associated with these designs (MA solubility, molten salt chemistry, fuel processing, material compatibility …) are important for the moderated MSR designs as well.

2.3   Processing of the fuel salt

2.3.1   Removal of non-soluble fission products

One of the major observations of the ARE operation was that gaseous fission products are not retained in the molten salt (Savolainen, 1955). The salt pumps of the MSRE and MSBR were specially designed with an off-gas system to remove gaseous and noble metal FPs (Robertson, 1971). The removal of noble gases is important, not only because of the high thermal absorption cross-section of ^{135}Xe, but because xenon is partly absorbed by graphite. Generally, it is easier to remove non-soluble FPs before they decay to a soluble element. The off-gas system chosen for MSBR involves circulation of helium bubbles. Non-soluble elements in the salt migrate readily to any available gaseous interface. The small circulating helium bubbles soak up the xenon together with other FPs, and these bubbles are separated from the salt and expelled to the off-gas system. 10% of the fuel salt from the pump discharge is bypassed through a bubble separator to remove the bubbles, then through a bubble generator to replenish the helium bubbles.

33

Small sized noble metal particles are simultaneously removed. The removed gas enters a particle trap and a decay tank. Later, the gas passes to activated charcoal traps. The average void fraction in the fuel loop was 0.2% in the plans of the MSBR. These helium bubbles make the salt compressible; thus, pressure has an influence on the reactivity of the reactor. During the operation of the MSRE with ^{233}U fuel, small increases in nuclear power were observed and these occurred with a low frequency. The explanation of the transient was the change of gas volume in the core, most likely caused by release of some gas that was collected in the core. All MSR designs incorporate an off-gas system to remove non-soluble FPs.

2.3.2   Removal of uranium

The fluoride volatilization process (Cathers et al., 1959), which was used successfully for recovery of the uranium from the ARE fuel mixture, was further tested in the ORNL laboratories to confirm that fluorination of FLiBe salts results in good recovery of the uranium (MacPherson, 1958b). This process is accomplished by bubbling fluorine gas through uranium containing salt. The UF_4 content of the salt is converted to volatile UF_6. This gaseous product is collected and converted back to UF_4. Other elements with high gaseous oxidation states are also removed, such as Np, Pu, Nb, Ru, Te, I, Mo, Cr and Tc. Successive NaF and MgF_2 traps at different temperatures are used to separate and recover the different elements. The uranium is recovered with 99.9% efficiency and 90% of plutonium removal was demonstrated as well. The decontamination factor for the FPs is higher than 10^5. The fluoride volatilization process is the first step of the on- or off-line chemical processing of the fuel and blanket salt.

2.3.3   Removal of lanthanides and actinides

First, the vacuum distillation method was developed (Rosenthal, 1967) to clean the salt from soluble FPs. After the fluorination step, LiF-BeF$_2$ is recovered simultaneously by volatilization of these components (Scott and Carter, 1966). Fortunately, the separated fission products are primarily rare earths, the most serious neutron absorbers. During the process, the fuel salt is distilled in vacuum. Only a modest vacuum (1 Hgmm), but high temperature (1300 K) is required. This process is possible because the solubility of rare-earth fluorides increases rapidly in LiF and BeF_2 as the temperature increases and the vapor pressure of the rare-earth FPs is much lower than either LiF or BeF_2 (Hightower and McNeese, 1971; Hightower et al., 1971). This method is very attractive, since it involves only a physical operation. The decontamination factor for the FPs is 10^2 to 10^3. The FPs are concentrated in the still residue, primarily LiF. The drawback of this process is that it does not differentiate between thorium and the rare earth fission products. On the other hand, it removes the UF_4 residual. Thus, the uranium losses can be further minimized.

Later, the liquid bismuth reductive extraction (Rosenthal, 1969a) was developed, which could differentiate between thorium and FPs. This opened the way of the single fluid breeder MSR designs, like the MSBR. The process involves the selective distribution of materials between salt and bismuth containing reducing agents such as thorium and lithium. The extraction of protactinium from the salt is straightforward since its chemical

behavior is different than the other components of the salt (Rosenthal, 1969b). First, a bismuth stream containing lithium and thorium removes the residual uranium and the protactinium from the salt. The bismuth stream then is contacted with an HF-H$_2$ mixture and uranium and protactinium is removed from the bismuth to molten salt. Uranium is removed by fluorination and the protactinium is sent to a tank where it is collected. Formed uranium can be removed from this tank by fluorination.

The remaining actinides and fission products are finally extracted by reductive extraction in liquid bismuth with metallic thorium (Savage and Hightower, 1977; Delpech et al., 2009). The separation between rare earths and actinides is established by the modification of the metallic pool composition. Its potential value can be changed by changing the thorium concentration. After some steps the di- and trivalent ions are removed. The back extraction is done to a chloride salt. After the salt is completely purified, uranium is added to it and it is sent back to the reactor.

2.3.4   Processing strategies

The simplest fuel processing strategy - batch-wise or off-line - employs only the off-gas system during the operation of the plant while removal of soluble FPs is done only during scheduled outages of the reactor. The FUJI reactors are planned to operate according to this strategy. In more advanced schemes soluble FPs are removed regularly - in a continuous stream or small portion processed daily/weekly - from the salt. In this case, first the uranium is removed by the fluoride volatilization process and it is send back quickly to minimize the fissile inventory of the reactor. Then, the FPs left in the salt are removed by the vacuum distillation or extraction to liquid bismuth. The breeding performance of the reactor can be enhanced if protactinium is removed from the salt and it is stored outside of the neutron flux. The strategies are discussed in detail in Chapter 3.

It is possible to run an MSR without removing the soluble FPs from the salt, or to clean the salt once in several years. The equilibrium concentrations of FPs in the case of this - batch wise - clean up might affect the physico-chemical properties, fluorine potential, corrosion of structural materials and deposition of FPs in the loop. Thus, the removal of FPs is not only necessary to reach high breeding ratios, but to maintain long-term operation of any MSR power station.

2.3.5   Non-proliferation

The different processing strategies and cycle times have a strong effect on non-proliferation because some processing steps increase the accessibility of the fissile material. While the salt is in the reactor, the fissile material is protected by the high temperature and intense radiation. On the other hand, the removal of soluble fission products is always preceded by the removal of uranium from the salt. This step separates the uranium from the salt and the core in an easily accessible form of UF$_6$ gas. If thorium is added to the salt, which is the case in breeder reactors, there is always some [232]U generated. The protection mechanism of this isotope was discussed in Section 1.2.

There are some concerns associated with the removal of protactinium. This can be applied in breeder systems to enhance uranium production. If protactinium is separated from the salt, it decays to uranium producing almost pure [233]U. This uranium is contained

in a high-temperature tank filled with molten salt and it is removed by the same fluoride volatilization process as the uranium from the core. The uranium separated from the tank can be diluted with the uranium removed from the core before the FP removal. This way the ^{232}U from the core protects the uranium formed outside the core. The uranium mixture can be sent back in to the core or stored in a separate tank depending on the criticality control.

Chapter 3

Comparison of processing schemes and breeding gain definitions for the MSR

The choice of the salt purification processes has a big influence on the fuel cycle perform-ance of the MSR. The critical mass of the reactor and the fissile feed depend strongly on it. In this chapter, the methodology of the code system used for modelling the fuel cycle and the different processing schemes of the MSR are presented first. The code system can be split into two parts, the time-dependent material evolution calculations and the other taking care of the static calculations to provide the spectrum data and the criticality of the reactor. The processing schemes are embedded in the material evolution code as the Bateman-equations are modified according to those.

The processing scheme of the MSBR was found to be impossible at its proposed high flow rates in the MOST project (Renault et al., 2005). This scheme was investigated and compared with similar but slower schemes (Merle-Lucotte et al., 2008; Mathieu et al., 2006). This approach focuses on one scheme but most of the reactors have their own proposed schemes. In this chapter, several schemes - from simple ones allowing only converter operation to the complex scheme of the MSBR - are defined and then compared for a range of lattice geometries.

Breeding ratio (BR) and breeding gain (BG) definitions are widely used to quantify and compare different breeder reactor designs (Ott and Borg, 1980). Based on a simple definition used in past studies, new BG definitions is introduced in this chapter which treat the core and the external fissile stockpile separately. As it is shown, this division is necessary in order to properly compare breeder MSR designs.

3.1   Processing schemes

Several processing schemes were considered for the different MSR designs, ranging from a simple once-through scheme to the complex process of the MSBR. These can be practically divided into 4 groups:

- Once through: During operation, only the non-soluble FPs, that is noble gases and noble metals, are removed by an off-gas system. This removal is quick, less than a minute for gaseous elements and up to a few hours for noble metals. After a certain burnup, the whole salt is unloaded and fresh salt is loaded into the reactor to start a new campaign.
- Batch-wise processing: This processing scheme does not differ from the once-through in the applied salt purification processes during operation but the fuel salt is cleaned regularly off-line, when the reactor is shut down. Only the non-soluble FPs are continu-ously removed by an off-gas system and the soluble FPs and MAs accumulate in the salt during operation. These are removed from the salt regularly by chemical processes when the concentration of soluble FPs is too high. This is done in a separate processing plant every 5-15 years of operation. This scheme is attractive for power plants with many units as the utilisation of the processing plant can be high. The processing of the salt can be delayed in this case: after the uranium is removed, the reactor can be started using a previously processed salt of another unit (and the removed uranium). The salt of the re-started unit is then set to cool down and it is processed later, before it is used to start another reactor.

- Continuous processing: In this scenario both soluble and non-soluble FPs are removed. This scheme includes the off-gas system which removes the non-soluble FPs and the quick removal and re-introduction of uranium from the processed salt via fluorination. This process must be as quick as possible and the extracted uranium must be returned into the core immediately in order to keep the fissile inventory low. The soluble FPs are removed in a chemical processing plant. This plant is either connected to the primary loop of the reactor through a small salt stream or a small amount of salt is often (i.e. daily) taken out from the loop and processed in a stand-alone plant. Depending on the capacity and the efficiency of the plant, the mean residence time of the soluble FPs ranges from a few years to a few months (Rosenthal, 1969a; Delpech et al., 2009). Because the salt contains thorium, the salt is purified by the Liquid Bismuth Reductive Extraction process. Plutonium and minor actinides can be removed with the same process, if necessary.
- Protactinium removal and storage: This scenario is the extension of the continuous processing scheme which includes the removal and storage of protactinium. This can be done in the same way as soluble FPs are removed. The protactinium is stored in a tank from which the formed uranium is removed by fluoride volatilization. This uranium can be stored or used to fuel the reactor.

3.2 Calculational tools

The time evolution of the fuel salt of the MSR was calculated employing an in-house developed scheme which is based on the SCALE5.1 code system (SCALE, 2005). Criticality calculations were performed with XSDRN, which is a 1D S_n solver, assuming a cylindrical fuel channel surrounded by an annular moderator region. A white boundary condition was used on the outer surface of the moderator. Thus, the reactor was modelled as an infinite core made of molten salt channels surrounded by a graphite moderator. In order to provide resonance-corrected and self-shielded cross-sections for the code, the CSAS sequence of SCALE was used. This sequence runs the BONAMI and CENTRM code, which prepare the temperature and problem dependent cross-sections. A 238 group ENDF-BVII cross-section set was used as the input of the sequence, which was provided with the SCALE5.1 system.

Since the criticality calculations were performed on a unit-cell, its results apply to an infinite core. To give a prediction about the k_{eff}, the non-leakage probability was calculated for a non-reflected cylindrical core with 98 m^3 volume on the basis of the diffusion length L and geometrical buckling B of the core (see Eq. 3.1). The non-leakage probability was very close to unity (>0.99) for all the moderation ratios taken into account in this study.

$$P_{NL} = \left(1 + L^2 B^2\right)^{-1} \qquad (3.1)$$

The XSDRN is a static code and does not take into account the flow of the fuel of the MSR. In reality, a part of the delayed neutron precursors leave the core with the flow and decay in the primary loop. These neutrons are lost for the chain reaction. The delayed neutron fraction is 0.003 in a reactor fuelled with ^{233}U. In this chapter, the volume of the salt outside of the core is assumed to equal the salt inside the core and a homogeneous distribution of the delayed precursors is assumed. The true distribution was calculated and used in Chapter 6. The assumptions listed here result in an absolute discrepancy of 0.0015 in the calculated eigenvalues which had to be substracted from the results. In reality, this number is even smaller since the concentration of short-lived precursors is higher in the core than in the primary loop.

An in-house developed code was used to solve the Bateman equations which were modified to describe the continuous processing of the fuel of the MSR (see Appendix A). The code is capable of incorporating the removal and feed of elements in the equations and keeps track of isotopes outside the core. The cross-sections for the calculation were prepared by the COUPLE code. A 3 group cross-section library of nearly 1500 isotopes was provided with the program which was collapsed into one group using the neutron spectrum obtained from the criticality calculation. The problem-dependent 238 group cross-section set, which was used in the criticality calculation, was further processed by COUPLE and collapsed into one group. More than 100 isotopes were handled this way (thus, used in the criticality calculation), the isotopes of the salt and their activation products, important fission products and heavy nuclei. The one-group cross-section coming from the two sources were finally merged into one set which is used in the fuel evolution calculation.

Figure 3.1: Calculation procedure.

The calculation scheme was started by the preparation of the isotopic composition of the salt. This can be done in several ways, in a form of fresh salt with set molar composition, a saved full isotopic list of the core or a fresh salt without setting the uranium concentration. In the latter case the calculation scheme started with a search for the critical load. In each step of the time-dependent calculation, a uranium feed rate was assumed and used in the fuel evolution calculation. At the end of the time step, the criticality of the core was calculated. If the k_{eff} was within the pre-set margins, the time step was accepted, a new cross-section file was prepared for the burn-up code and a new feed rate was estimated based on the old one and the calculated k_{eff}. If the k_{eff} did not meet the requirements, a new feed rate was estimated and the time step
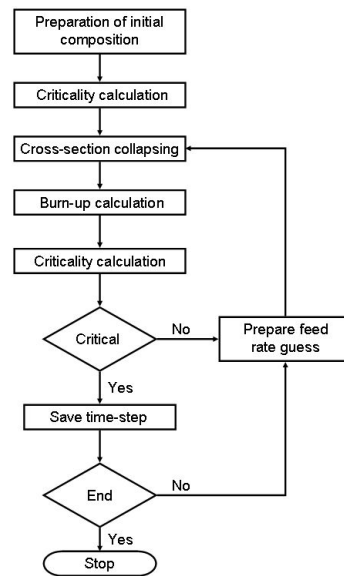
was repeated. In the calculations, all the uranium used to refuel the reactor was assumed to be extracted from the external stockpile and all the uranium produced by the decay of the extracted protactinium was placed in the stockpile. Furthermore, the thorium mass was kept constant by continuous feed in each calculation. No predictor-corrector method was implemented in the calculation scheme. In order to overcome this drawback, short time steps were used throughout the calculations. The calculation procedure discussed above is shown in Figure 3.1.

3.3 Comparison of the processing schemes

The four processing schemes were compared on a range of core configurations because the actual core geometry has a big influence on various parameters of the reactor, such as the critical mass, the neutron capture rate of thorium and protactinium and the neutron aborption rate of fission products, as was shown by (Mathieu et al., 2009). All these parameters effect conversion (or breeding) performance of the MSR. Both the size of the graphite blocks and the diameter of the fuel channels were varied in this study. This way the amount of graphite in the core and the diameter of the fuel channels could be changed independently. The number of fuel channels was set in each case to fill the volume of the reactor core.

The core was 5 m in diameter and in height which makes a volume of 98 m^3. The size of the core was kept constant in all the calculations. This core consisted of hexagonal graphite blocks with fuel channels at the center of each block. The volume of the fuel salt in the loop was assumed to be equal to that in the core. The volume ratio of the core, that is the volume of graphite over the volume of salt in the core, was varied from 1 to 9 while the fuel channel diameters ranged from 2 to 10 cm. Two different average power densities of the core were used in the calculations, 5 and 22 MW/m^3. The density of the graphite was set to 1.84 g/cm^3 and the mean operating temperature of the reactor was 1000 K. For this study the operation time of the reactor was set to 50 full power years.

In a breeder molten salt reactor the fuel consists of UF_4 as fuel and ThF_4 as fertile isotope. The fluorides of these actinides are dissolved in a mixture of LiF, BeF_2, NaF, KF or ZrF_4. For the moderated self-breeder MSR in the scope of this study the 2 to 1 mixture of LiF and BeF_2 (FLiBe) was chosen because of its low neutron capture cross-section. To reach this good neutron economy the lithium has to be enriched to 99.995% in ^{7}Li. The available enrichment processes are the Colex (column extraction) process, ion exchange chromatography and vacuum distillation (Symons, 1985). The theoretical efficiencies of these processes vary, but a multi-stage process may be used to achieve higher degrees of separation. The concentration of thorium was 12 mol% throughout this chapter and the concentration of the uranium, which makes the reactor critical, varied for every case. These are listed in Table 3.1. Criticality was maintained by a continuous feed of $^{233}UF_4$ while the concentration of thorium was kept constant during operation.

The applied mean residence times in the different processing schemes are summarized in Table. 3.2. The batch-wise processing scheme does not differ from the once-through in the applied salt purification processes during operation but the fuel salt is

Table 3.1: The initial load (kg) of ^{233}U of the studied core geometries.

Volume ratio	Channel diameter (cm)				
	2	4	6	8	10
1	8007	6485	5570	4998	4613
3	1421	1220	1135	1089	1061
5	746	675	646	632	626
7	509	474	460	455	454
9	390	369	362	361	363

Table 3.2: The applied mean residence times of different elements for the processing schemes

Once-through and batch-wise processing			
Gaseous	Non-soluble	Soluble	Protactinium
50 sec	2.4 hours	-	-
Continuous processing			
Gaseous	Non-soluble	Soluble	Protactinium
50 sec	2.4 hours	1 year / 3 years	-
Protactinium removal and storage			
Gaseous	Non-soluble	Soluble	Protactinium
50 sec	2.4 hours	1 year	3 months / 1 year

cleaned regularly off-line, when the reactor is shut down. Two different intervals were considered in this study, 10 and 5 years. The reactor was shut down for 30 days for each off-line chemical processing. During this time, all fission products were removed from the salt. This assumption was made because either the salt might go through a multi-stage purification process, or the actinides might be extracted from the used salt and transferred to a clean or previously purified salt to start the reactor. In case of the continuous processing scheme, two different mean residence times, 1 year and 3 years, were considered for the soluble FPs. Finally, two different mean residence times of Pa, 3 months and 1 year, were chosen for the protactinium removal and storage scheme while the mean residence time of soluble FPs was set to 1 year. Only these two residence times were chosen because cases with more different mean residence times were compared for this scheme in (Merle-Lucotte et al., 2008; Mathieu et al., 2006).
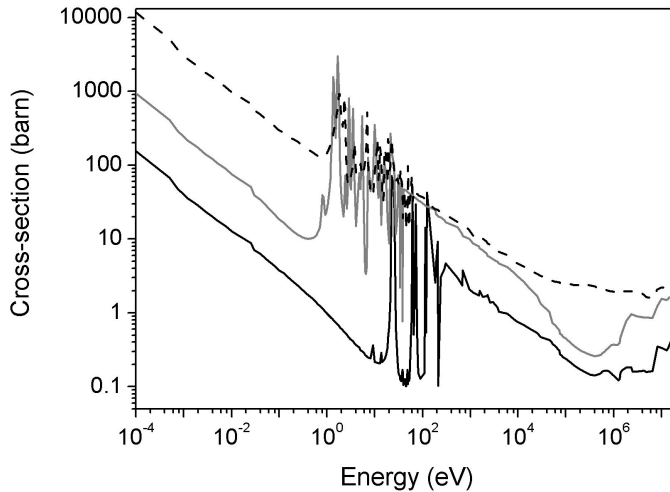
Figure 3.2: The microscopic cross-section of ^{232}Th (black), ^{233}Pa (gray), and ^{233}U (dashed). The cross-section of thorium is low in the epithermal range except a few resonances. Those resonances are located at higher energies than the resonances of protactinium.

3.4   Results

The amount of the graphite moderator influences the neutron spectrum, which can range from epithermal to thermal. Thorium, protactinium and uranium have resonances in the epithermal range and the spectrum determines whether the thermal or the epithermal neutrons have important contribution to the absorption rate of those isotopes. The positions and the amplitudes of the resonance peaks of the key isotopes of the thorium fuel cycle differ (see Figure 3.2) so the choice of the amount of the graphite in the core (thus, the spectrum) can increase the neutron capture rate of ^{232}Th and decrease that of ^{233}Pa. Similarly, the amount of graphite has an influence on the critical load and the feed rate.

The mean free path of neutrons in a moderated MSR is usually 2-3 cm, depending on the actual core geometry. On the other hand, this is mainly due to scatter; the neutrons can travel long distances before getting absorbed. The mean value of the distance a neutron travels until it is absorbed is shown in Figure 3.3. This distance is more than 10 cm, or even more than 100 cm, for every neutron energy except for three peaks. The energy of those peaks correspond to the positions of the three main resonances of ^{232}Th. The distances the neutrons with an energy corresponding to the peak values travel until absorption are comparable with the diameter of the channel so the neutron flux at the energy of the resonances of ^{232}Th is seriously depressed in the fuel channels. An example is presented in Figure 3.4. This is a limiting factor for the diameter of the fuel channels
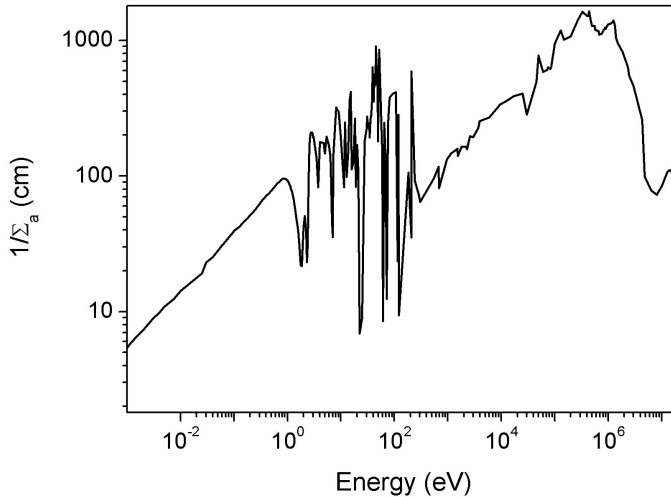
Figure 3.3: The mean value of the distance a neutron travels in the fuel salt until it is absorbed as a function of the energy of the neutron. The example is calculated for FLiBe, with 12 mol% ThF4 in a fuel channel of 10 cm in diameter. The mean value of the travelled distance drops at the resonances of ^{232}Th.

because those resonances have an important contribution to the neutron capture rate of ^{232}Th and ultimately to the uranium production.

The amount of fissile material fed into the core during the 50 full power years of operation is used to compare the different geometries. This is a part of the total need of fissile material, the other part is produced in the reactor from thorium. The share between these two processes differ for each case. The more efficient a core produces uranium, the less is needed from an external stockpile; but this comparison is true only for cases with the same power density. Smaller channel diameters and lower volume ratios increase the neutron capture rate in ^{232}Th but the initial load increases for these geometries as well and it implies a higher uranium feed rate during operation. Furthermore, the power production and the flux level increase in the channels as the volume ratio increases since the same power density is applied for the different geometries. Thus, the smallest channel diameter and volume ratio might not be the optimum case.
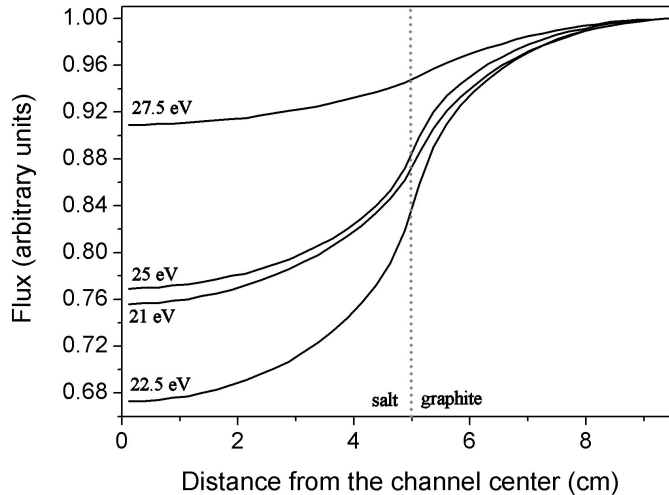
Figure 3.4: The radial distribution of the neutron flux around the centerline of a fuel channel of 10 cm in diameter. The energy range incorporates the first resonance of ^{232}Th at 22.5 eV. The fluxes at the various neutron energies are normalized to the value on the side of the graphite block. The neutron flux is depressed at the resonance energy.

3.4.1 Once through processing scheme

The results of the calculations are summarized in Table 3.3. High volume ratios result in higher total uranium feed at both power levels and the feed is increasing as the channel diameter increases. These effects are due to the lower neutron capture rate in thorium and the high power density in the salt which leads to higher fission product concentrations. At large channel diameters (6 to 10 cm) the optimum is at a volume ratio of 3 which is a balance between the decreasing critical mass and decreasing uranium production. On the other hand, the optimum differs at small channel diameters in case of the two different power levels, cores with a harder spectrum require less feed at high power density but better moderated cores are advantageous at low power density. The geometry with the smallest channel diameter and volume ratio performs the best at high power density, and core geometries built of large channels and small volume ratios result in a relatively low total feed due to the combination of modest uranium production and low critical load.

Table 3.3: The total mass (kg) of uranium fed during 50 years of operation at power densities of $22MW/m^3$ and $5MW/m^3$ (left/right) without chemical processing

Volume ratio	Channel diameter (cm)				
	2	4	6	8	10
1	12239/3829	13096/3897	13479/3768	13599/3574	13575/3378
3	14125/1630	13547/1420	13193/1343	12910/1302	12659/1274
5	14076/1351	14228/1382	14263/1407	14233/1428	14180/1449
7	15285/1524	15746/1625	15912/1683	15988/1731	16043/1780
9	16710/1786	17185/1905	17394/1982	17461/2052	17492/2125

3.4.2 Batch-wise processing scheme

Table 3.4 summarizes the results of the calculations for the batch-wise processing. The general observations of the previous section are true for these results as well; namely, that the small channel diameters are advantageous in case of high volume ratios and that larger fuel channel diameters are beneficial only at low volume ratios. Furthermore, the removal of FPs is effective and significantly reduces the necessary uranium feed during operation. On the other hand, the difference is modest between the effect of the long and the short cycle time. The difference between the masses of the fed uranium in case of once-through and batch-wise processing increases as the cores get more thermalized and better homogenized.

3.4.3 Continuous processing scheme

This scenario is essentially different from the previous ones because the soluble FPs are removed during operation in this case. This is expected to enhance the uranium production by reducing the neutron loss to the FPs. The results of the calculations are presented in Table 3.5. The continuous removal scheme results in less uranium feed during operation than the batch-wise scheme due to the shorter residence times of the absorbing FPs. In case of the high power density cases, a considerable amount of uranium is necessary to maintain criticality but it is less than half the total mass of uranium feed of the once-through scheme. The cores which have better fuel reproducing capabilities and need less feed (the ones with a volume ratio of 3 or 5) provide an even higher gain, less than a quarter of the feed of the once-through scheme. For some cases with low power density operation the mass of the fed uranium is close to zero. In these cases the reactor produces almost enough uranium for self-breeder operation or the addition of uranium is not necessary during operation after the initial start-up phase. However, these cores do not reproduce the amount of ^{233}U which was fed during the start of the thorium fuel cycle. The continuous scheme is sufficient for the operation of a self-breeder reactor or a converter close to break-even as the necessary addition of uranium in 50 years is less than the initial load of ^{233}U.

Table 3.4: The total mass (kg) of uranium fed during 50 years of operation at power densities of $22MW/m^3$ and $5MW/m^3$ (left/right) with batch-wise processing

Volume ratio	Channel diameter (cm)				
	2	4	6	8	10
10 years cycle time					
1	7095/2356	7795/2389	8064/2259	8101/2089	8012/1919
3	7576/579	7254/477	7097/445	6961/429	6872/419
5	7736/472	7993/511	8082/540	8101/564	8089/588
7	8988/638	9252/719	9424/773	9521/821	9604/871
9	10034/855	10510/959	10741/1032	10909/1102	11086/1176
5 years cycle time					
1	5839/2046	6481/2079	6697/1958	6692/1799	6567/1636
3	5636/307	5384/221	5273/197	5172/186	5067/181
5	5841/218	6106/259	6210/289	6242/314	6252/339
7	6904/374	7306/451	7484/504	7589/553	7688/603
9	8059/575	8519/675	8743/747	8930/812	9113/894

Table 3.5: The total mass (kg) of uranium fed during 50 years of operation at power densities of $22MW/m^3$ and $5MW/m^3$ (left/right) with continuous processing

Volume ratio	Channel diameter (cm)				
	2	4	6	8	10
3 years cycle time					
1	5415/1954	6048/1970	6259/1845	6257/1688	6140/1532
3	5274/201	5146/118	5114/102	5064/93	4993/89
5	5830/124	6250/174	6425/217	6500/253	6534/285
7	7177/312	7700/416	7929/483	8070/541	8183/599
9	8514/553	9072/680	9343/764	9550/843	9747/924
1 years cycle time					
1	4406/1726	4956/1725	5105/1600	5052/1443	4896/1294
3	3250/58	3089/33	3048/29	3003/28	2943/27
5	3531/28	3898/36	4055/41	4093/48	4119/53
7	4705/55	5192/120	5422/186	5572/246	5703/306
9	5931/243	6454/359	6730/443	6952/524	7172/609

Table 3.6: The total mass (kg) of uranium fed during 50 years of operation at power densities of $22MW/m^3$ and $5MW/m^3$ (left/right) with protactinium removal

Volume ratio	Channel diameter (cm)				
	2	4	6	8	10
1 year Pa cycle time					
1	4355/1714	4896/1716	5040/1587	4984/1431	4825/1283
3	3108/31*	2949/117*	2911/139*	2870/147*	2815/148*
5	3377/156*	3758/99*	3931/57*	4022/21*	4081/14
7	4549/12	5036/109	5272/176	5433/236	5575/297
9	5767/231	6287/348	6576/432	6801/514	7006/600
3 months Pa cycle time					
1	4213/1699	4738/1697	4867/1568	4800/1413	4633/1262
3	2758/64*	2603/142*	2573/164*	2540/171*	2495/172*
5	2958/183*	3338/116*	3520/72*	3619/38*	3695/1*
7	4250/0	4771/92	5161/158	5345/219	5485/283
9	5421/212	6165/328	6412/413	6507/492	6758/583

*   surplus production

3.4.4   Protactinium removal processing scheme

The protactinium removal and storage further reduces the amount of fed uranium compared to the continuous removal case, but in cases where the mean residence time of Pa is longer than the half-life of [233]Pa, this reduction is small, only a few hundred kilograms. This is due to the fact that only a small portion of [233]Pa is removed and stored outside the reactor, most of it is still in the core. At high power densities this scheme does not offer much gain because the capture of neutrons in [233]Pa scales with the amplitude of the flux while the decay of [233]Pa is independent of that. On the other hand, this scheme with a long Pa residence time is enough to make some reactor cores breeder at low power density.

3.5   Evolution of fissile fuel in the MSR

3.5.1   Distinction between converter and breeder MSR

Long-term reactivity control is realized without burnable poisons because it is possible to add fissile nuclides to the core of the MSR during operation. To compensate for the build-up of FPs, non-fissile uranium isotopes and trans-uranium elements, fuel is added regularly to the salt. First, a reactor without protactinium extraction is considered. The reactor is a converter if uranium has to be added to maintain criticality and is a breeder if reactivity is increasing in the core. In the latter case some uranium has to be removed by fluorination

to reduce reactivity. This removed uranium is the bred fuel. In all the calculated cases in the previous section, the reactors without the protactinium removal scheme operated as converters.

If a part of the protactinium is removed from the salt, uranium is produced both in the core and in the stockpile by decay. The ^{233}U produced in the core may not be enough to compensate for the increased absorption. This produced uranium has to be left in the core and more needs to be added from the stockpile. If the amount of the uranium produced in the stockpile exceeds the needs to maintain criticality, the remainder is the gain which is considered as bred fuel. On the other hand, if the amount of uranium produced in the core and the stockpile together is not enough to maintain criticality, addition of fuel from an independent source is necessary. Although the reactor produces more fissile material than it consumes, it is a converter in this case because it needs a growing fissile invertory to compensate for FP and MA buildup.

3.5.2   Burnup calculations

As an illustration, the time variation of the mass of ^{233}U was calculated for three different cases, a converter with high conversion ratio, a self-breeder and a breeder reactor. In order to realize this different behavior, only the volume ratio of the cores was changed. The results presented here - using three different volume ratios, 7, 5 and 3, respectively - were chosen from the set of the results presented in Table 3.6. Each case was calculated using FLiBe as carrier salt with 12 mol% ThF$_4$. The reactor was started with ^{233}U and UF$_4$ was added continuously to maintain criticality. In all cases the diameter of the fuel channels is 8 cm. The number of channels was different in each case but the total volume of the salt was kept the same. The processing scheme was the same as well, namely the protactinium removal scheme with 1 year mean residence time for Pa. The power density was 5 MW/m^3.

3.5.3   Discussion

The results are shown in Figure 3.5 for the three reactor types (converter, self-breeder, breeder) and the important points of the figure are compared in Table 3.7. The mass of ^{233}U is continuously increasing in the core to keep the reactor critical. This increase is necessary because of the build-up of absorbers in the salt. The build-up of FPs is slow because the mean residence time of those is 1 year (see Table 3.2) and the actinides take decades to reach equilibrium in the core even at higher power densities (Nuttin et al., 2005). The flux decreases when the power production is kept constant. This decreases the ^{232}Th capture rate while the hardening of the spectrum increases it. The net effect is still negative, the capture rate is around 14% lower after 50 years of full power operation compared to the initial core for all the three cases. Different amounts of graphite in the core result in spectrum differences which cause the differences in the mass of the initial load and all the subsequent loadings. The amount of ^{233}U in the stockpile shows different behavior in the three cases but all can be separated in three stages. At the startup, there is no ^{233}Pa; thus, there is no uranium production in the reactor.

First, the ^{233}Pa in the core has to reach its equilibrium concentration in order to produce ^{233}U in the core. This takes around 3 months, depending on the efficiency of the
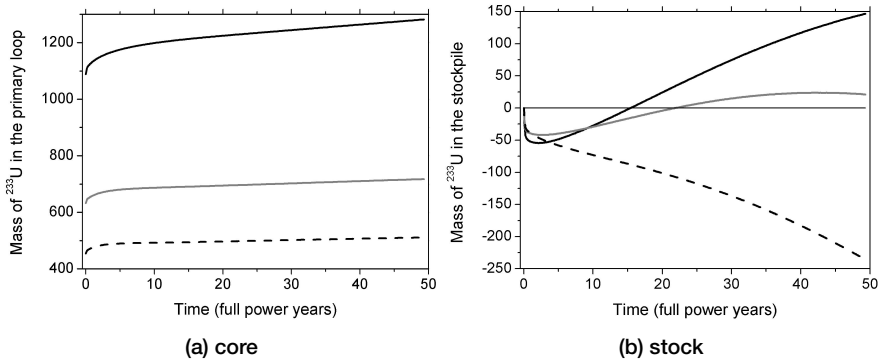
Figure 3.5: Evolution of the mass of ^{233}U in the core (left) and in the stockpile (right) for the three studied cases. The inventory is determined by criticality control. Black, gray and dashed lines show the breeder, self-breeder and converter cases, respectively.

Table 3.7: Comparison of the three cases presented in Figure 3.5

Volume ratio of graphite and salt	3	5	7
Initial load of ^{233}U (kg)	1089	632	455
Load after 50 years (kg)	1281	717	511
Minimum of the stock (kg)	-55	-42	-236
Stock after 50 years (kg)	147	21	-236

protactinium removal. During this time the reactor needs a high feeding rate compared to the later stages. Second, because the residence time of protactinium is longer than its half-life, the protactinium reaches its equilibrium mass in the external stockpile much slower than in the core. During this time only the core produces ^{233}U at the maximal possible rate. This takes around 1 year with the applied residence time. Once the protactinium reaches equilibrium in the stockpile, the reactor (the core and the stockpile together) is producing ^{233}U at its maximal capacity. After this point, depending on the amount of ^{233}U needed to maintain criticality, the reactor may turn to a breeder while it was a converter before. As the necessary feeding rate decreases with time the transition from a converter to a breeder may happen after a long time of operation.

The mass of ^{233}U in the stockpile is set to a starting value of 0. As the fuel loadings during operation are assumed to be taken from this pile and the ^{233}U produced by the decay of the extracted protactinium is placed here, negative values note that more uranium was extracted from the stockpile than produced. Similarly, positive values show the excess

fissile material. The case with a volume ratio of 5 is close to self-breeding. Although the reactor produces enough ^{233}U in 33 years to replace the uranium used in the first period of operation but the amount of uranium slowly stabilizes in the stockpile. The reactor with a volume ratio of 7 is a converter, the mass in the stockpile is monotonously decreasing. In the case of a volume ratio of 3 the reactor is a breeder. It turns to breeding after 2.5 years and it reproduces the uranium used in the converter phase in 15 years after the start-up. After this time the reactor produces excess fissile fuel.

3.6 Equilibrium breeding ratio

The different concepts for breeding quantification have developed together with the breeder reactor designs (Ott and Borg, 1980). Generally, these concepts compare the production of the fissile material to the consumption of those. This is usually done by forming the ratio of the production to the consumption: BR=FP/FC, where FP and FC stand for production and consumption of fissile materials. First, only ^{235}U and ^{239}Pu were considered but more fissile isotopes got involved with the development of the closed fuel cycles. The production and destruction are expressed either as reaction rates or as (produced or lost) masses of the fissile material. These approaches result in two different groups of breeding ratio definitions. The first is differential in nature because the reaction rates can be calculated of every moment during the cycle while the latter is based purely on time integrated quantites as total produced and lost material. Recent integral definitions compare the reactivity weighted isotopic masses of actinides at two different times during the cycle (Van Rooijen et al., 2007). The irradiation and cool-down cycles of the solid fuel reactors give intrinsic reference points in time and the amount of the fuel is usually calculated at the beginning and at the end of the cycles. These cycles do not exist in a breeder MSR as the fuel is continuously processed. Thus, integral definitions developed for solid fuel reactors do not suit the MSR.

3.6.1 Definition of breeding ratio at equilibrium
In several studies, the breeding ratio of the MSR is calculated in the following way:

$$BR = \frac{R_c^{02} - R_c^{13}}{R_f^{23} + R_c^{23}} \tag{3.2}$$

Here R stands for reaction rate and the type of reaction is noted in the subscript, c for capture and f for fission in this case. Throughout the thesis, the two digit superscripts denote the actinides with the last digit of their atomic and mass number ($90 \leq A < 100$), respectively. Reaction rates are calculated as it is given below:

$$R_i^j(t) = V w^j N^j(t) \int \sigma_i^j(E)\phi(E,t)dE \qquad (3.3)$$

Here N, σ_i^j and $\phi(E,t)$ represent the atomic density and the cross-section of isotope j and the flux, respectively. The correct treatment of the problem would be to integrate over the volume of the reactor and the stockpile. The simple multiplication with the volume (denoted as V in Eq. 3.3) is sufficient since the flowing fuel continuously mixes in the primary loop and the plenums of the core. Correspondingly volume-averaged cross-sections are used. The flux is averaged over the volume of the core and weighted according to the residence times in the core and the loop. For the time being, all w weights equal 1.

In Eq. 3.2 the production rate of [233]U is calculated as the capture rate of thorium minus the capture rate of protactinium. Since [233]U is produced by the decay of [233]Pa, this BR definition holds only for equilibrium. Only 2 key nuclides of the thorium fuel cycle, [232]Th and [233]U, are considered in the equation because the concentration of [233]Pa can be calculated on the basis of the thorium content of the core. After the substitution the equation reads as:

$$BR = \frac{R_c^{02}(1 - (\int \sigma_c^{13}(E)\phi(E)dE + 1)/\lambda^{13})}{R_f^{23} + R_c^{23}}, \qquad (3.4)$$

where λ denotes the decay constant. It is assumed in Eq. 3.4 that [233]Pa is directly produced by neutron capture in [232]Th because the half-life of [233]Th is short. This equation shows that the production term depends on the flux. In other words, the [233]U production and breeding can be increased by decreasing the power density.

3.6.2 Comparison of different geometries with the equilibrium breeding ratio

The equilibrium breeding ratio (Eq. 3.2) was calculated for two different cases: the continuous processing scheme with 1 year of mean residence time and the protactinium removal scheme with 1 year of residence time, both at the power density of $5 MW/m^3$. Theoretically, this breeding ratio holds in equilibrium, however, none of the reactors have reached the equilibrium state of the thorium fuel cycle in 50 years of full power operation. Uranium is slowly but continuously added to the salt and the neutron spectrum of the core shifts slowly with the changing material composition of the salt. On the other hand, the denominator of Eq. 3.2 is constant during the whole operation as the total produced power is fixed and the concentration of thorium is kept constant as well. This way, only the amplitude and the shape of the flux change slowly as Eq. 3.2 is evaluated at different points of time. Therefore, the breeding ratio was calculated for every month of the operation of the cores and the time-average of those was taken. The first year of operation after the startup was skipped in the averaging because the cores contain initially no protactinium

Table 3.8: Comparison of the breeding ratio of the continuous and the protactinium removal schemes

Volume ratio	Channel diameter (cm)				
	2	4	6	8	10
1 year mean residence time continuous removal scheme					
1	1.05062	1.04402	1.04101	1.03985	1.03970
3	1.02966	1.02502	1.02182	1.01996	1.01871
5	1.01020	1.00187	0.99597	0.99154	0.98760
7	0.98461	0.97203	0.96432	0.95782	0.95151
9	0.95713	0.94224	0.93295	0.92444	0.91574
1 year mean residence time protactinium removal scheme					
1	1.05090	1.04441	1.04139	1.04027	1.04015
3	1.04624	1.04372	1.04175	1.04028	1.03908
5	1.03600	1.02724	1.02182	1.01749	1.01346
7	1.01360	1.00215	0.99468	0.98808	0.98146
9	0.98876	0.97568	0.96644	0.95766	0.94851

and it takes around three months for the ^{233}Pa to build up in the core. This process results in rapid changes compared to the later operation of the core. The results are summarized in Table 3.8.

First, the calculated BR is always higher for the protactinium removal case than it is for the continuous removal. This was expected as a part of the ^{233}Pa is removed from the core. This part of the Pa cannot absorb neutrons; therefore, more uranium is produced. This effect is incorporated in Eq. 3.2 as the concentration of the Pa in the core is lower in these cases. For both processing schemes, the BR is higher for low volume ratios and for small channel diameters. The low volume ratio of graphite results in a more epithermal spectrum which favors the neutron capture in thorium (see Fig. 3.2) and the small channel diameter causes less shielding in the fuel channels at the resonance energies (see Fig. 3.4). The difference of the BR between the two processing schemes increase as one moves to higher volume ratios. This is due to the increasing capture in ^{233}Pa in the better moderated cores. However, the BR predicts that half of the investigated cores, the ones with harder spectrum, are breeding surplus uranium but the actual calculations show that these cores are converters (see Table 3.5). Similarly, the BR calculation predicted more cores to be breeders with the protactinium removal scheme than the ones which are breeders according to the burnup calculations (see Table 3.6). Furthermore, the cores with a volume ratio of 1 are not breeders and have a higher BR than the cores which are breeders (volume ratio of 3 and 5).

The equilibrium breeding ratio describes the ^{233}U production capacity of the cores. Since the power density and thus the denominator of the expression is fixed for each

core and processing scheme, it shows only the change in capture rate of fertile material but does not take into account the continuous feed of ^{233}U which is necessary to keep the cores critical. It is clear from the results above that this description is not sufficient to predict the converter or breeder operation of a reactor and that another method should be used which incorporates the feeding of ^{233}U.

3.7 Breeding gain definitions

First, the mass change rates in the core and in the stockpile are defined and discussed. These help to understand the time variation of the fuel mass in both volumes. Two mass change rates are defined for the core, one for the increase needed for criticality and one for the actual production of the core. These two almost never equal during the operation of the reactor. The difference is important because it gives the amount of the fissile material to be fed to the core. This way three different mass change rates are introduced (two for the core and one for the stockpile). Breeding gains are defined on the basis of each of those by scaling the mass change rates by the total consumption rate of fissile isotopes in the reactor.

3.7.1 Mass change rates of the core

Even if an MSR is started up purely on ^{233}U, the ^{235}U will build up significantly during the operation. The whole uranium vector changes because of neutron capture even after the fission products have reached their equilibrium. The uranium composition reaches its equilibrium only after decades of full power operation and the weight of ^{233}U is only two third of the uranium mass in the core. The rate of consumption of the fissile isotopes in a reactor can be defined as:

$$C(t) = R_a^{23}(t) + R_a^{25}(t) \tag{3.5}$$

The reaction rates are calculated according to Eq. 3.3. There are more ways to define the weights, w^j, in the reaction rate, depending on the choice the rate can count the number of atoms, the mass or the ^{233}U equivalent mass of fissile isotope. In the first case, the weight is 1 for every isotope, while in the second case the weight equals the mass of the isotope. In the last case, the weight is the mass of the isotope multiplied by a factor which accounts for the contribution of the isotope to criticality or to fuel production. The weight of the product is used for any production term. This last approach is used in the thesis; thus, the weights are defined by the following formula:

$$w^j = \frac{\sigma^j - \sigma^{02}}{\sigma^{23} - \sigma^{02}} \cdot M, \tag{3.6}$$

where M denotes the mass of the isotope. The σ^j for a certain nuclide is defined as the traditional reactivity weight (Salvatores, 1986):

$$\sigma^j = \nu^j \sigma_f^j - \sigma_a^j \tag{3.7}$$

The mass change rate of fissile uranium (^{233}U and ^{235}U) in a critical core is given as:

$$\left(\frac{dm(t)}{dt}\right)_{critical} = R_d^{13}(t) + R_c^{24}(t) + R_{fe}^{23}(t) - C(t) \tag{3.8}$$

where the subscript d denotes decay and the integral term in Eq. 3.3 is replaced by the decay constant of the isotope. The ^{233}U is produced by the decay of ^{233}Pa and a part of the ^{233}U produced in the stockpile is sent back to maintain criticality. This "feed" from the stockpile to the core is noted as fe in the subscripts. ^{235}U is produced by the neutron capture rate of ^{234}U. This expression counts all the production processes occurring in the core and an extra one, namely the mass change due to the feeding of the core from the stockpile. This term does not explicitly depend on the amplitude of the flux, only on the decrease rate of reactivity in the core and it is set to reach the necessary mass growth rate to keep the reactor critical. Without this term the mass change rate counts only the production and consumption processes in the core:

$$\left(\frac{dm(t)}{dt}\right)_{core} = R_d^{13}(t) + R_c^{24}(t) - C(t) \tag{3.9}$$

3.7.2 Limitations of the mass change rates defined for the core

These definitions are not useful for direct comparison of completely different cases of MSR because the efficiency of the chemical removal processes is incorporated in them. For a simple demonstration two identical MSRs with different efficiency of the removal processes will be considered.

If the removal of protactinium is quicker in one reactor, less ^{233}U will be produced in the core by decay; thus, the right hand side of Eq. 3.9 is smaller than in the case of slow removal. On the contrary the value of Eq. 3.8 does not differ for the two reactors because the decay of ^{233}Pa and the ^{233}U feed are supposed to cover the needed increase of uranium mass in order to maintain criticality. The mass of the uranium stockpile is different for the two reactors but it is not included in these definitions.

The removal efficiency of fission products can be different as well. In this case the value of Eq. 3.9 does not differ for the two reactors but the right hand side of Eq. 3.8 does. If the efficiency is low, the higher amount of absorbers in the salt has to be compensated by uranium, thus the feed rate is higher. This results in a smaller uranium stockpile as well but the stockpile is not included in the definition.

Based on these considerations it is concluded that these definitions can be used for direct comparison only if the efficiencies of the removal processes are the same for each case.

3.7.3 Mass change rate of the stockpile

It is an obvious choice to extend the growth definitions to the stockpile, defining the net gain in the uranium stockpile as:

$$\left(\frac{dm(t)}{dt} \right)_{stock} = R_d^{13stock}(t) - R_{fe}^{23}(t) \tag{3.10}$$

where the first term denotes the decay rate of ^{233}Pa in the stockpile while the latter term is the mass transfer from the stockpile to the core. This expression contains the effect of different removal processes. The decay rate of ^{233}Pa in the stockpile is connected with its removal efficiency, and the mass transfer depends in the increase of absorption in the core and thus on the removal efficiency of fission products.

3.7.4 Breeding gain definitions

Differential breeding gain calculations count the balance of nuclear reactions increasing and decreasing the amount of fissile material in the reactor. Based on the mass change rates defined in equations 3.8, 3.9 and 3.10, breeding gains can be defined. Generally, the total consumption rate as described in Eq. 3.5 is used in the differential BG definitions as a scaling factor. In this particular case, the stockpile is considered to be part of the reactor where the flux is negligible. This way, the consumption rate is the sum of the consumption in the reactor core and in the stockpile. This assumption allows to use the same consumption rate for the core and the stockpile. The breeding gains are defined as the mass growth rate over the consumption rate:

$$BG_{critical} = \frac{R_d^{13}(t) + R_c^{24}(t) + R_{fe}^{23}(t)}{C(t)} - 1 \tag{3.11}$$

$$BG_{core} = \frac{R_d^{13}(t) + R_c^{24}(t)}{C(t)} - 1 \qquad (3.12)$$

$$BG_{stock} = \frac{R_d^{13stock}(t) - R_{fe}^{23}(t)}{C(t)} \qquad (3.13)$$

The first definition contains the feed term, and this term is adjusted to keep the reactor critical. Therefore Eq. 3.11 is the BG in the core needed to maintain criticality. Eq. 3.12 describes the amount of fuel the reactor core produces. This can not be directly observed in a real reactor. The last definition is the BG connected to the available fuel as all the excess from the core and the stockpile is supposed to be placed here. The mass change rates defined above can be expressed as the product of the corresponding breeding gain and the consumption rate.

Based on the BG definitions the doubling time of the reactor can be estimated. The reactor (core and stockpile together) needs a feed of fissile fuel until the stockpile reaches a minimum value; thus, the doubling time is time dependent (Harms, 1978). The first identical reactor can be started when the amount of ^{233}U in the stockpile equals the initial ^{233}U mass in the core:

$$m = \int_0^{DT} \left(\frac{dm(t)}{dt} \right)_{stock} dt = \int_0^{DT} BG_{stock}(t)C(t)dt, \qquad (3.14)$$

where m is the initial load of the reactor and DT denotes the doubling time. The integral is necessary because of the time variation of the BG after start-up. After the initial period the BG may be considered as constant and the equation can be simplified to calculate the equilibrium doubling time.

The presented BG in Eqs. 3.11, 3.12 and 3.13 are differential BG definitions and not suitable to support the comparison of different cores. Integral definitions are more useful in this sense but the ones used for fast breeder (solid fuel) reactors cannot be used in this case (Nagy et al., 2010). The proposed BG definitions averaged over the operation time give integral BG definitions. These averages directly relate to the change of fissile mass in the core or in the stockpile through the consumption rate (Eq. 3.5) of the reactor.

As the breeding gain of the stockpile describes the evolution of the available fissile fuel, this definition is used in the following optimization study. In order to form an integral value which describes the whole lifetime of the reactor, the time average of Eq. 3.13 is calculated in each case. The relation between the BG definitions presented here and the BR definition used in 3.6 is discussed in Appendix B .

3.7.5 Time behavior of the breeding gain definitions

Figure 3.6 shows the time behavior of the three BG definitions at start-up and at the transition from converter stage to breeder operation for the reactor described in Section 3.5.3 with a volume ratio of 3. The fissile uranium isotopes are weighted to get ^{233}U-equivalent masses as described in 3.7.1. The $BG_{critical}$, Eq. 3.11, describing the growth rate of the mass in the core, is always positive as fissile fuel is continuously added to balance the decrease of reactivity due to the initial build-up of FPs and the build-up of absorber actinides. On the other hand, this definition does not distinguish between the growth due to breeding or feeding while the BG_{core}, Eq. 3.12, counts only the fuel production in the core. This is negative during the whole time of operation meaning that the core alone is a converter. The BG of the stock starts from large negative values since the large amount of ^{233}U needed to maintain criticality at the start-up of the reactor is assumed to be extracted from the stockpile. After the protactinium reaches its equilibrium level both in the core and in the stockpile, more uranium is produced than consumed and the stockpile starts to increase. As the reactor shifts to breeding from conversion the value of BG_{stock} turns to positive.
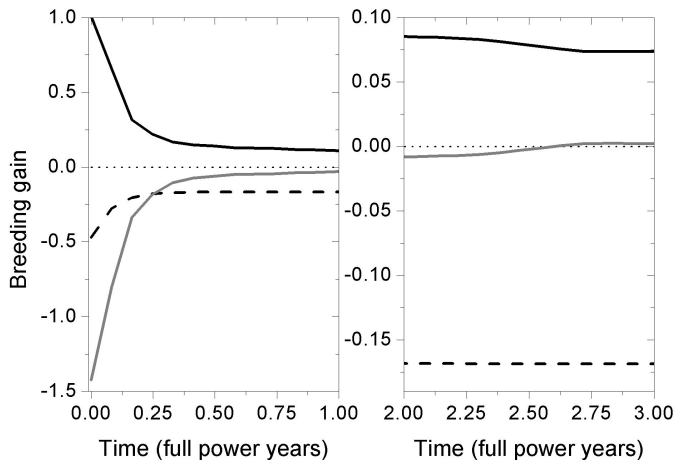
Figure 3.6: Time variation of the three breeding gain definitions at startup (left) and during the transition from converter to breeder operation (right). The black, gray and dashed lines represent the critical, the stock and the core breeding gain definitions, respectively (Eq. 3.11, 3.12 and 3.13)

3.8 Summary and conclusions

In this chapter the following questions were answered: what does a moderated MSR need to be a breeder employing the thorium fuel cycle and how can be this breeding performance quantified. After the identification of the different possible salt processing schemes and the definition of key parameters of the reactor, a set of different core geometries was chosen on which the different processing schemes were compared. Furthermore, this approach allowed to compare the different core geometries as well. First, it was found that neither the cores with minimal nor maximal amount of graphite are the best in terms of conversion or breeding. Although the ^{233}Pa production increases as the spectrum hardens in the cores, the initial load of the cores and the mass of the subsequent feed behaves the same way. Therefore, hard spectrum cores produce the most uranium but require the most as well, while soft spectrum cores require a low amount of uranium to operate but offer low uranium production. The two extrema of the investigated range of cores perform poorly for different reasons but there is an optimum range of cores which ultimately perform well despite of their modest uranium production and load. The comparison of the cores was performed at two different power densities. The results show that self-breeding or breeding is only possible at a low power density if the proper processing scheme is applied.

It is expected that the more complex processing schemes result in better thorium conversion or even breeding but the difference between the schemes is sometimes small. Even the protactinium removal scheme is not sufficient to operate a self-breeder reactor at the high power density of the MSBR, unless the mean residence times of the FPs and the Pa are comparable with the ones in the MSBR. Furthermore, batch-wise processing offers a strong reduction of the uranium feed but the gain of the more complex schemes is not so attractive. Therefore, one may consider to use only batch-wise processing if the reactor is operated at high power densities. On the other hand, the batch-wise offers a high conversion ratio operation at a low power density of 5 MW/m^3 while self-breeder and breeder operation is possible employing the continuous or the protactinium removal scheme at this power level.

Finally, a new set of breeding gain definitions was proposed for the MSR. It was shown that the current definition does not adequately describe the full problem; therefore, it can give wrong prediction about the breeding performance of the reactor. The proposed definitions - both differential and integral - describe the different actinide-containing volumes of the reactor with separate equations which can be summed to obtain the total breeding gain of the reactor. The equations also count for the transfer of the nuclides of the thorium fuel cycle between the different volumes. As it is shown, the simplified form of the proposed definition is equivalent with the previously used definition. The unique behavior of the MSR such as the transition from a converter to a breeder reactor and the increase of the critical load during operation can be described using these definitions.
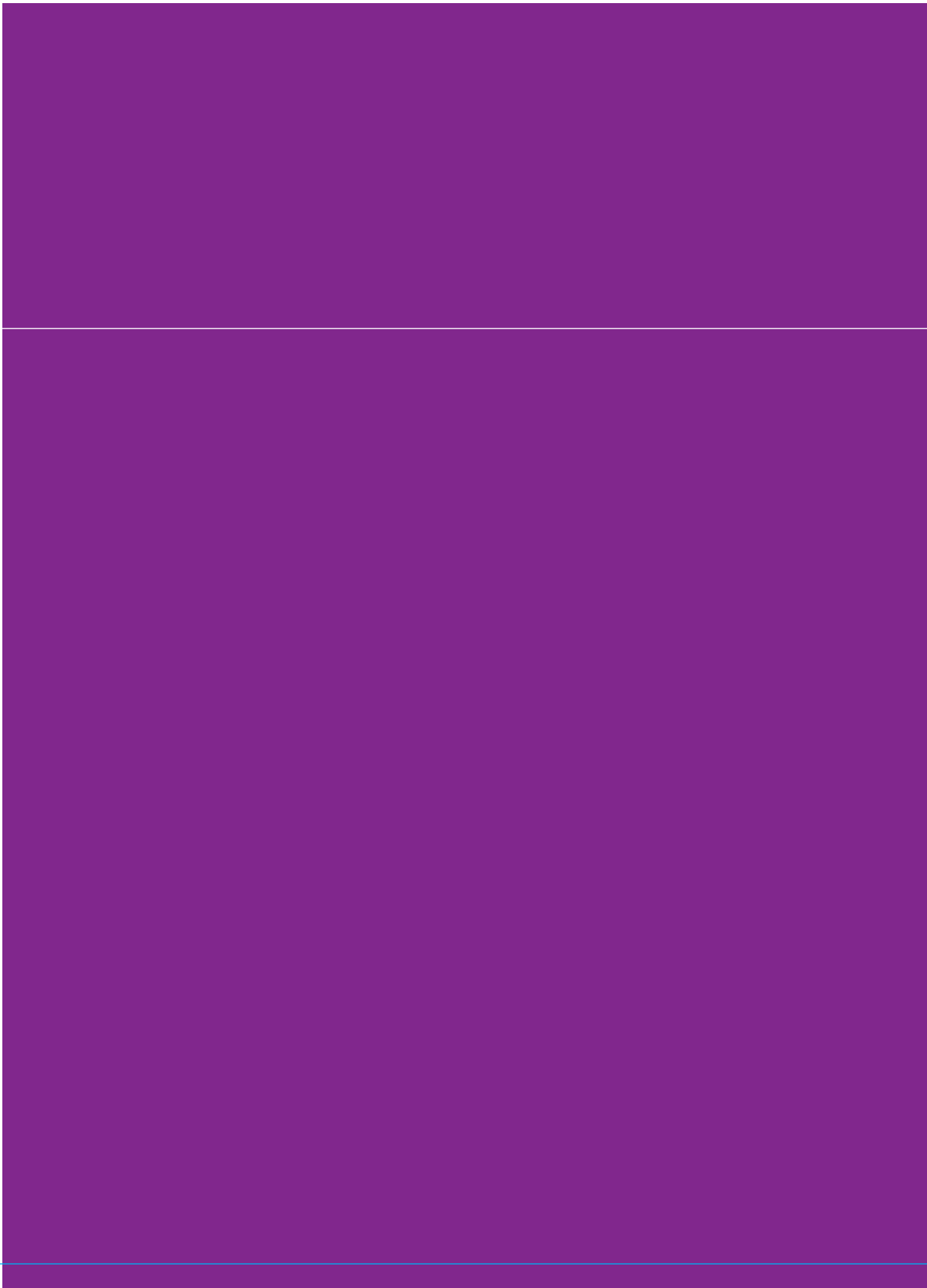
Chapter 4

Optimization of the graphite - salt lattice

As it was shown in the previous chapter, the graphite moderator reduces the critical load of the reactor and the geometry of the graphite lattice has a big influence on the neutron spectrum of the core. However, graphite has other than beneficial properties in the MSR core, like a positive temperature feedback coefficient and a limited lifespan. In this chapter, the graphite-salt lattice is optimized with regards to these effects while the goal of the optimization is a self-breeder core with high power density.

Some studies have already focused on these properties of the graphite - salt lattice. In an earlier study (Mathieu et al., 2006), the radius of the fuel channels was varied while the outer dimensions of the graphite blocks were not changed. This way, the amount of salt in the core and the ratio of moderator to fissile nuclei was altered simultaneously. According to their results, small channel diameters (low salt and high graphite volume) enable a high graphite lifetime, but a positive feedback, while larger radii perform well in terms of breeding ratio and total feedback coefficient. On the other hand, the lifetime of the graphite is only 2 years in the latter case. Thus, all fuel channel radii have a disadvantage in the reactor, so a compromise has to be sought. Later, the size of the graphite hexagons was altered and the diameter of the fuel channels was scaled with it (Mathieu et al., 2009). This way the moderator to fissile nuclei ratio was kept constant. It was expected that a better homogenized core can provide a negative temperature feedback and it was found that increasing the number of hexagons while keeping the graphite and salt volume fixed results in a negative feedback. The influence of the power density was also investigated by increasing the size of the reactor while keeping the total power fixed. This change increases the breeding ratio and graphite lifetime but the uranium inventory increases with the size of the core. The influence of the composition of the driver salt was addressed by the change of the actinide concentration. For high breeding ratios, high HN content is preferred, but all the salt compositions can result in positive total feedback coefficients, depending on the amount of graphite in the core.

In this chapter, the physical processes causing the temperature dependency of the criticality and the limited lifespan of the moderator graphite are explained first. Then, the effect of changing four parameters, namely the fuel channel diameter, the volume ratio, the thorium concentration and the power density, are discussed. These four parameters are altered in the optimization study of the graphite-salt lattice. The temperature feedback coefficients and the lifespan of the moderator are used constraints in the optimization process. The goal of the optimization is to maximize the power density of self-breeder cores.

4.1   Drawbacks of the graphite moderator

4.1.1   Temperature feedback

The temperature feedback coefficient of the core, which is the derivative of the variation of the multiplication factor with the temperature of a part or of the entire core, is an important safety parameter and a reactor can only be considered safe if this coefficient is negative. This total feedback of the core can be split into the effect due to the salt and the effect
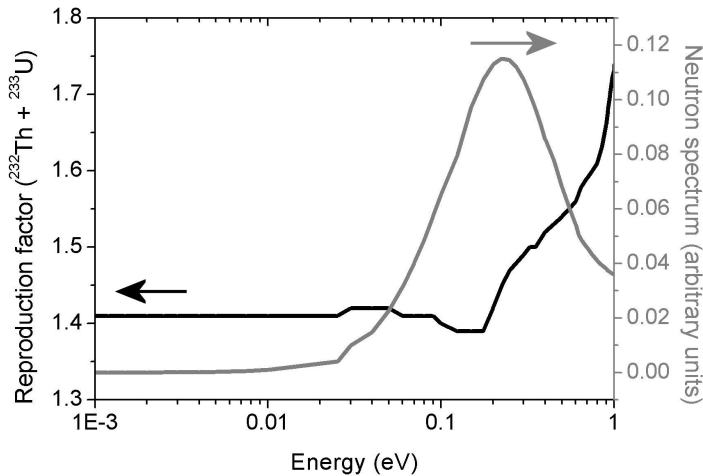
Figure 4.1: Neutron reproduction factor of the thorium - uranium mixture and the neutron spectrum at 1000K in the core.

due to the graphite. The salt itself has usually a negative feedback coefficient and this has to compensate for the positive effect of the graphite.

The positive feedback of the graphite is caused by the temperature-dependency of its scatter cross-section. As the temperature of the graphite increases, the thermal peak of the neutron spectrum shifts towards higher energies. The η value (the average number of fission neutrons produced per neutron absorbed in the fuel) of the thorium and uranium mixture is increasing above 0.2 eV because of the first resonance of the ^{233}U fission cross-section (see Figure 4.1). As the temperature increases, the hardening of the thermal spectrum results in higher neutron production because of the increasing η and causes an increase of reactivity. The magnitude of this effect can be influenced by adjusting the neutron spectrum. The smaller the spectrum changes in the 0.1-1 eV range as the temperature increases, the lower is the magnitude. This positive feedback effect of the moderator temperature probably exists in every type of reactor fuelled with ^{232}Th-^{233}U mixture.

To achieve a core with a negative temperature feedback, the temperature effect of the salt must be strongly negative to compensate for the positive contribution of the graphite. This effect of the salt is the sum of two different phenomena, the Doppler-broadening and the effect of the density change of the salt. The effect of the Doppler-broadening may be positive or negative for the different nuclides in the salt as it is a combination of different contributions of the various interactions. The change of the capture cross-section results in a negative feedback but this effect is weak for most of the nuclides. A change in the scatter cross-section of the light nuclides has a postive effect on the fuel temperature feedback, for the same reason as for the graphite. In case of a fissile nuclide, the change of the

Table 4.1: Summary of the different contributions of the salt components to the temperature feedback. The first three rows refer to the Doppler-broadening while the last one refers to the density change of the salt.

	Light nuclides	Heavy nuclides	Fissile nuclides
Capture	-	-	-
Scatter	+	0	0
Fission	0	0	+
Dilatation	0	+	-

fission cross-section implies a positive reactivity change. Summing up these effects, light nuclides have a positive contribution to the Doppler-effect of the salt because the feedback due to the change of their scatter cross-section exceeds the negative contribution of their absorption cross-section. The effect due to the fission cross-section change makes the contribution of the fissile isotopes positive as well. Only the heavy non-fissile nuclides have a negative effect because the total cross-section of these is dominated by their capture. The low-energy resonances of these nuclides have a strong negative contribution to the feedback. In case of the fuel salt of a breeder MSR, the contribution of the first resonance of the thorium capture cross-section makes the Doppler coefficient negative for the whole salt.

The composition of the molten salt strongly affects the temperature feedback coefficient of the fuel salt since nuclides with high absorption cross-section have strong positive effect on the feedback due to the change in their atomic density. The sum of the two contributions has to be negative in order to have a fuel salt with negative temperature feedback. If the magnitude of this feedback is larger than the effect of the graphite, the whole core has a negative temperature feedback. The different contributions of the components are summarized in Table 4.1.

4.1.2 Graphite lifespan

The behavior of graphite under radiation damage is of prime importance because it is the principal material other than the salt in the core of the MSR. Under the fluences and temperatures which may occur in the reactor core, the radiation induces structural deterioration and dimensional changes of the graphite. This means that the graphite moderator in the core may not last as long as the expected lifetime of the reactor and either only the graphite structure or the whole reactor vessel has to be replaced regularly.

The primary effect of neutron irradiation on graphite is to create cristal lattice defects (Kelly, 1982). Radiation damage is a macroscopic term describing dimensional changes and changes of the material properties caused by these lattice defects. The simplest defects are point defects, vacancies and interstitials, referred to as a Frenkel pair. Most of these pairs recombine as the interstitials move into the vacant sites. The mobile interstitials that do not recombine form a small interstitial group of a stable size of 2 to 6 atoms and

Table 4.2: The applied mean residence times of different elements

Gaseous	Non-soluble	Soluble	Protactinium
50 sec	2.4 hours	1 year	3 months

grow as the neutron fluence increases until a new graphite plane is built. Similarly, random atomic displacements can produce a linear group of vacancies and these can collapse parallel to the basal planes of the graphite lattice. These two processes have opposite effects, one increasing and the other one decreasing the volume of the graphite. During the irradiation the sum of these two processes can be observed. First, the graphite shrinks as the collapse of the displacement groups is superior to the formation of new basal planes. This turns around at a certain neutron fluence, which depends on the temperature and the material, and the graphite starts to swell. This effect of the radiation does not saturate (Brocklehurst and Kelly, 1993).

The growth of the graphite is unwanted in an MSR because the pores of the graphite start to grow. The prevention of molten salt and xenon from getting into the open pore volumes is one of the requirements on the graphite. Any significant penetration of the fuel salt into the graphite would create a local hot spot which enhances the radiation damage of the graphite and could cause local boiling of the salt. Since the salt is nonwetting to the graphite, this requirement is met if the diameter of the pores is small enough. Usually the point at which the graphite returns to its original volume is used to define the useful life. Considering this, the fluence the graphite can absorb was calculated as $3 \cdot 10^{22} n/cm^2$ for neutrons above 50 keV for the MSBR reactor (Robertson, 1971). This limit is used in recent publications (Mitachi et al., 2007) as well and in this thesis.

4.2   Description of the optimization study

The power density of the reactor investigated in Chapter 3 is low compared to other MSR designs (MSBR, FUJI, TMSR) and other reactor types. Therefore, an optimization study was carried out to maximize the power density of the reactor. In order to reach this goal, the graphite-salt lattice is optimized. Two constraints were applied: the core has to achieve self-breeding and has to be passively safe. The limits set on these parameters are: $\overline{BG_{stock}} = 0$ and $-1.5 pcm/K$ total temperature feedback coefficient. The reactor core was assumed to have only one region. The parameters calculated for each case are the breeding gain defined in eq. 3.13 averaged over 50 years of full power operation, the graphite lifetime and the temperature feedback coefficients for the graphite and the salt; while the fuel channel diameter, the volume ratio of the core (volume of graphite over the volume of the salt) and the amount of thorium in the salt were varied.

4.2.1 Reactor model

The reactor core consisted of hexagonal graphite blocks with fuel channels at the center of each block. Both the size of the graphite blocks and the diameter of the fuel channels were varied in the optimization process. This way the amount of graphite in the core and the diameter of the fuel channels were changed independently. The core was 5 m in diameter and in height which results in a volume of 98 m^3. The volume of the fuel salt in the loop was assumed to be equal to that in the core. During the optimization the overall size of the core was kept constant. The mean operating temperature of the reactor was set to 1000 K.

Graphite is a suitable moderator for the MSR; its low absorption helps to achieve a good neutron economy. No metals are used in the core because the salt does not wet the graphite and does not penetrate its pores. The density of the graphite was 1.84 g/cm^3 in the calcualtions. For the moderated self-breeder MSR in the scope of this study the two to one mixture of LiF and BeF$_2$ (FLiBe) was chosen because of its low neutron capture cross-section. To reach this good neutron economy the lithium has to be enriched to 99.995% in ^{7}Li. In the optimization study the concentration of ThF$_4$ was varied between 12 mol% and 30 mol%. In the range between 22 and 30 mol% the melting point of the LiF-ThF$_4$ mixture is sufficiently low (850 K) (Benes and Konings, 2009). Substituting the beryllium with lithium does not significantly change the results of this study. Continuous processing of the fuel salt together with Pa removal is assumed. The residence times of FP and Pa are listed in Table 4.2. During the calculations all uranium fed to the core was taken from the stockpile.

4.2.2 Calculation procedure

The search for optimal self-breeder lattices was performed in three steps. The first step was to find the graphite-salt lattices which have a feedback coefficient of $-1.5 pcm/K$ at startup. This was needed because the reactor cores which provide good breeding performance usually have unacceptable feedback coefficients. In the next step, the graphite lifetime and the breeding gain were calculated for these cores at an average power density of 5 MW/m^3. This results in the total thermal power production of the core of 490 MW. Finally, the power density was increased for each of these lattices to suppress breeding to self-breeding, resulting in a higher power density. This is possible because the absorption rate of ^{233}Pa is proportional to the flux while its decay rate does not depend on the flux (see eq. 3.4). The lifespan of the graphite is re-calculated as well.

4.3 Effects of the parameter variation

The various parameters, channel diameter, volume ratio, thorium concentration and power density are not changed independently in the optimization scheme. Thus, the effect of varying a single parameter cannot be observed in the optimization calculations. In order to overcome this drawback, these effects were calculated separately from the optimization calculations and are discussed here. The parameter used for the evaluation of all the cases is the breeding gain of the stockpile, averaged over 50 years of full power operation.
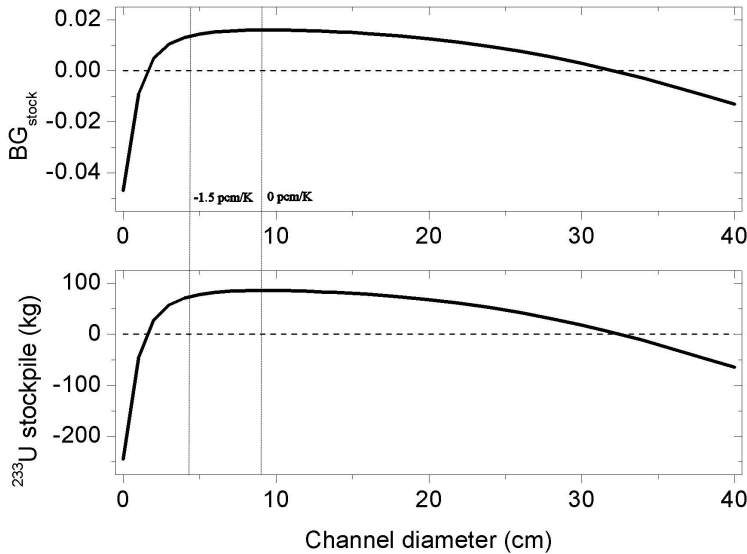
Figure 4.2: Effect of the variation of the channel diameter on the breeding gain. Th concentration: 12 mol%, power density: 5 MW/m^3, volume ratio: 3. The temperature feedback coefficient of the core increases as the channel diameter increases. The -1.5 pcm/K and 0 pcm/K points are shown in the figure.

4.3.1 Channel diameter

First, the effect of the channel diameter on the BG of the reactor is demonstrated here. As the channel diameter was varied, the volume ratio (the volume of the graphite moderator over the volume of the salt) was fixed at 3. The concentration of the ThF$_4$ in the salt was 12 mol% and the results were evaluated for a core of 98 m^3 which produced a thermal power of 490 MW. The results are shown in Figure 4.2. There is one maximum of the BG and the position of the maximum is the sum of two converse effects. First, the Pa production has its maximum at zero channel diameter (simulated as a homogeneous reactor) and decreases as the channel diameter increases. Second, the critical load decreases with the increase of the channel diameter as well to its local minimum at 20 cm. The balance of these two effects is optimal at 9 cm channel diameter. This maximum is in the region where the reactor has a near zero temperature feedback coefficient.

4.3.2 Volume ratio

In the calculation of the effect of the volume ratio the channel diameter was kept constant at 6 cm and the concentration of the ThF$_4$ at 12 mol% in the salt. Each case was calculated for a core of 98 m^3, so the number of fuel channels was varied, and the thermal power of the core was set to 490 MW. The results of these calculations are shown in Figure
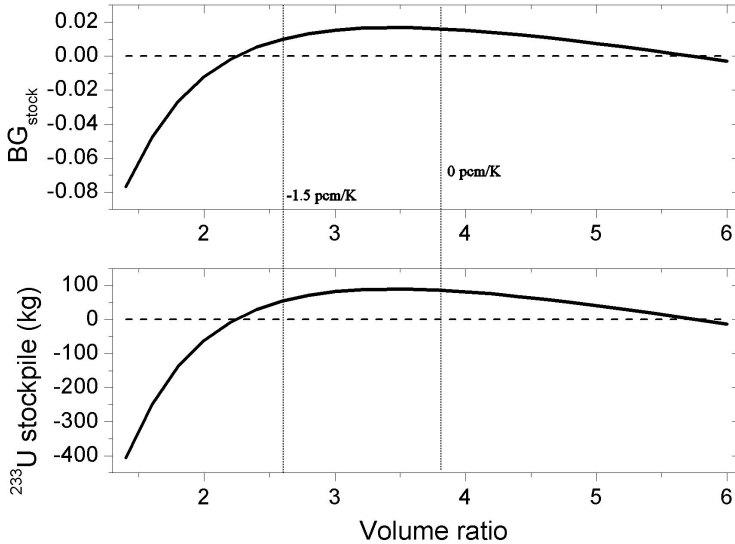
Figure 4.3: Effect of the variation of the volume ratio on the breeding gain. Th concentration: 12 mol%, power density: 5 MW/m^3, channel diameter: 6 cm. The temperature feedback coefficient of the core increases as the volume ratio increases. The -1.5 pcm/K and 0 pcm/K points are shown in the figure.

4.3. There is a clean maximum of BG around the volume ratio of 3.5. The variation in the BG is caused by the changes in the spectrum, the production rate of uranium and the needed feeding rate changes as volume ratio is altered. At low volume ratios both the Pa production and the critical load are high and both are decreasing as the volume ratio increases and the spectrum in the core becomes softer. The maximum is located in the region where the reactor has a near zero temperature feedback coefficient. This observation is valid in general, the best breeder lattices for different channel diameter or volume ratio have a temperature feedback which is positive or close to zero. The possible channel diameter - volume ratio combinations, which are breeders and have sufficient negative feedback, are limited.

4.3.3 Thorium concentration

The effect of the thorium concentration was calculated for a core in which the diameter of the fuel channels was 6 cm and the volume ratio was fixed at 3. Each case was calculated for a core of 98 m^3 with thermal power of 490 MW. The molar concentration of ThF$_4$ was varied between 6 and 30 mol%.

The results of these calculations are shown in Figure 4.4. The increase of thorium in the salt mixture removed some moderator nuclides from the system as the thorium
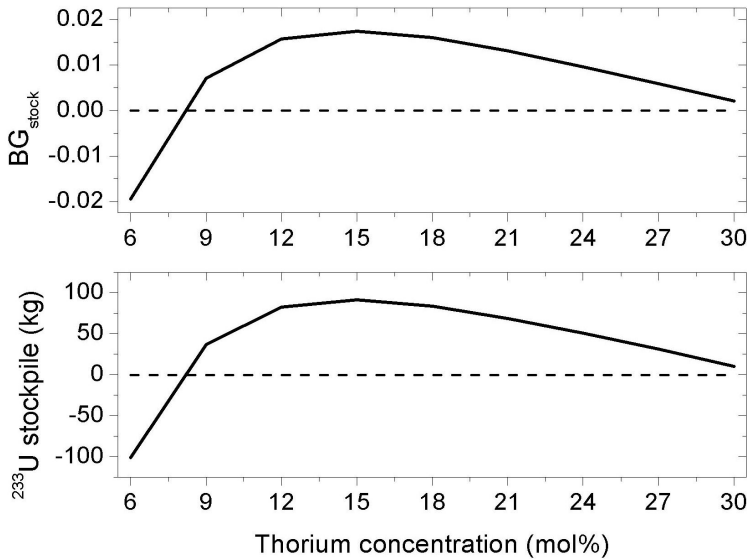
Figure 4.4: Effect of the variation of the thorium concentration on the breeding gain. Channel diameter: 6 cm, power density: 5 MW/m^3, volume ratio: 3.

substitutes lithium and beryllium in the salt. Furthermore, the uranium concentration had to be increased as well in order to keep the reactor critical, so the ratio of the moderator to fissile nuclei decreased rapidly as the thorium concentration was increased. The BG has a maximum at 15 mol%. Further raise of the thorium concentration results in a harder spectrum and a higher critical load of the reactor. The effect of these is a decrease of BG. At low concentration the amount of the produced uranium is not enough to supply the reactor.

4.3.4 Power density

Finally, the effect of varying the power density is presented. The calculations were performed on a core which was 5 m tall and 5 m in diameter. The fuel channel diameter, volume ratio and thorium concentration was set to 6 cm, 3 and 12 mol%, respectively. The power density of the cores was varied between 0.5 and 15 MW/m^3. The results of these calculations are shown in Figure 4.5. It was expected that the BG decreases monotonously as the power density increases. This can indeed be seen above the power density of 2 MW/m^3. This power density corresponds to the maximum value of the BG and below that BG decreases with the decreasing power density. The maximum of the BG and the uranium mass is at a different position because in the BG calculation the uranium production is weighted with the consumption (see Eq. 3.13), while the uranium mass is the absolute excess production for each case.
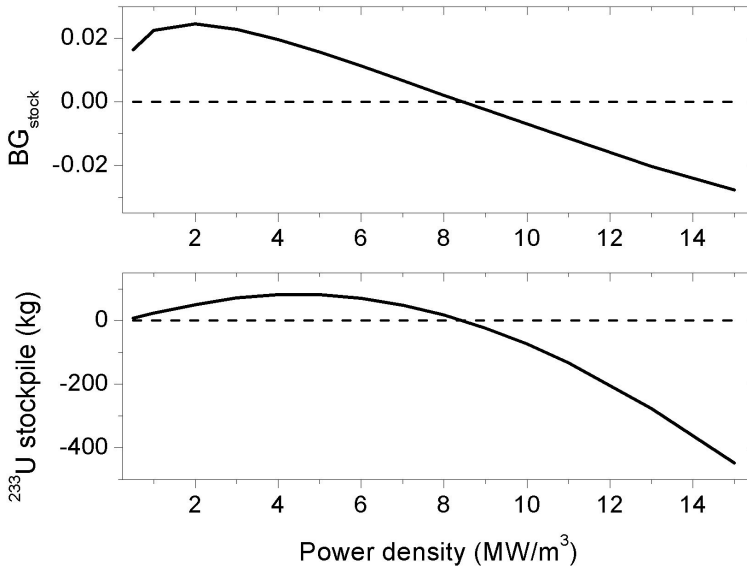
Figure 4.5: Effect of the variation of the power density on the breeding gain. Th concentration: 12 mol%, channel diamter: 6 cm, volume ratio: 3.

4.4   Optimization

In the rest of this chapter the full optimization procedure is described, following the steps which were listed in Chap. 4.2.2.

4.4.1   Temperature feedback

The first step in the optimization is to determine the range of lattices providing a sufficiently large negative feedback. In order to do this, the temperature feedback coefficient of different critical lattices had to be calculated. The varied parameters were the volume ratio, channel diameter and Th concentration. The uranium concentration which results in a critical reactor was determined for every case separately. First, the k_{eff} for a temperature of 1000 K was calculated then it was calculated again at a higher (1100 K) reactor temperature. The thermal expansion of the salt was taken into account as it follows. Densities at different temperatures were calculated based on the temperature-dependent molar volume of the components assuming an ideal mixture, as it is explained in (Williams et al., 2006). The raw data of the component salts were taken from (Williams et al., 2006) and (Konings and Van der Meer, 2003). Thus, the dilatation coefficient differs for every salt mixture. This approach gives a dilatation coefficient of $6 \cdot 10^{-4}/K$ for FLiBe which contains 12 mol% ThF_4 and 0.24% UF_4. This value corresponds with the literature (Robertson, 1971). Dilatation of the graphite was neglected.

Figure 4.6 shows the results with the margin of $-1.5pcm/K$ for four different Th concentrations, 12, 18, 24 and 30 mol%. This margin limits the possible channel diameter and volume ratio combinations. All the varied parameters, channel diameter, volume ratio and thorium concentration have effect on the temperature feedback. More homogenized cores - small fuel channels or less graphite volume - provide stronger negative feedback coefficients, as it was shown in the literature (Mathieu et al., 2009). Higher thorium concentrations result in stronger negative coefficients in the same graphite structure. Changing the thorium concentration in the core changes the amount of berillium as well; thus, the spectrum hardens in the core if the thorium concentration is increased. This results in a less positive contribution of the graphite because the thermal peak is closer to the resonances. The feedback of the salt becomes more negative as well. This is the sum of the Doppler and the dilatation effect and the decrease of the first to stronger negative values overrules the more positive effect of the thermal expansion. During the burnup the feedback coefficient changes, first it increases to $-1.2pcm/K$ and then starts to slowly decrease to stronger negative values.

4.4.2 Calculations with constant power density

Unfortunately, the best breeder configurations do not meet the safety criteria. As it was shown in Figures 4.2 and 4.3, the lattice configurations on the -1.5 pcm/K margin give the highest possible BG. In the second step of the optimization, the volume ratio resulting in a -1.5 pcm/K feedback coefficient at startup was determined for every channel diameter between 1 and 9 cm. Then, the graphite lifetime and the breeding gain of these cores were calculated with a constant power density of 5 MW/m^3. The peak power density is significantly higher than the average because there is only one region in the reactor and the graphite blocks in the center have higher fluence than the ones at the side of the core. This can be overcome if the graphite blocks are reshuffled when the reactor is shut down for maintenance. This way the whole volume of graphite reaches the irradiation limit at the same time. The lifetime of the graphite is calculated for both cases.

Table 4.3 shows the results of the calculations. All the studied cases are breeders at a power level of 5 MW/m^3. Small channel diameters correspond to larger volume ratios as it was shown in Chapter 4.4.1. These channel diameters offer a higher breeding gain due to their more thermalized spectrum and due to their higher Pa production rate. The lifespan of the graphite is longer in a better moderated core. The initial load of the reactor decreases together with the channel diameter and this increases the breeding performance as well because less uranium feed rate is also lower for those cores. Based on these results, it is concluded that a core built of small channels is superior to a similar sized core which consists of fewer but larger channels. As the thorium concentration increases, the amount of graphite allowed by the safety margin increases too; thus, compensating for the loss of the moderating components, Li and Be, in the salt. Higher fertile material content results in better breeding performance and lower initial load but the decrease of the initial load is the effect of the increased volume ratio. The lifetime of the graphite is comparable in every case, ranging from 19 to 22 years. On the other hand, the lifetime of the power plant is expected to be longer, so replacement of the moderator is necessary once or twice during the lifetime of the reactor.

Table 4.3: Results with constant power density of 5 MW/m^3

Th	(mol%)	Channel diameter (cm)								
		1	2	3	4	5	6	7	8	9
12	Volume ratio	4.7	4	3.5	3.1	2.8	2.6	2.4	2.25	2.1
	BOL load (kg)	955	977	1067	1172	1273	1347	1445	1527	1628
	BG ($\cdot 10^{-2}$)	1.96	1.84	1.66	1.43	1.19	1.00	0.73	0.51	0.20
	Lifetime (PP)	22.5	22.3	22	21.9	21.8	21.6	21.5	21.3	21.2
	Lifetime (AP)	36	35.5	35.2	35	34.8	34.6	34.4	34.2	34
15	Volume ratio	5.5	4.6	4	3.5	3.15	2.85	2.65	2.45	2.3
	BOL load (kg)	918	1011	1112	1242	1356	1484	1580	1702	1805
	BG ($\cdot 10^{-2}$)	2.56	2.41	2.24	1.99	1.73	1.40	1.17	0.84	0.57
	Lifetime (PP)	22.1	21.8	21.5	21.4	21.2	21.1	21	20.8	20.6
	Lifetime (AP)	35.3	34.7	34.4	34.1	33.9	33.8	33.5	33.3	33
18	Volume ratio	6.35	5.25	4.4	3.8	3.4	3.05	2.8	2.6	2.45
	BOL load (kg)	908	1006	1159	1317	1451	1608	1742	1869	1976
	BG ($\cdot 10^{-2}$)	2.97	2.86	2.65	2.35	2.06	1.66	1.33	1.01	0.76
	Lifetime (PP)	21.8	21.3	21.1	21	20.9	20.8	20.6	20.5	20.2
	Lifetime (AP)	34.7	33.9	33.7	33.5	33.3	33.2	33	32.7	32.3
21	Volume ratio	7.05	5.75	4.7	4.1	3.6	3.25	3	2.75	2.6
	BOL load (kg)	891	1021	1215	1364	1541	1696	1826	1995	2101
	BG ($\cdot 10^{-2}$)	3.23	3.19	2.93	2.67	2.28	1.92	1.65	1.22	1.03
	Lifetime (PP)	21.4	21	20.9	20.6	20.5	20.4	20.1	20	19.7
	Lifetime (AP)	34	33.4	33.3	33	32.8	32.5	32.2	32	31.6
24	Volume ratio	7.7	6.1	5	4.3	3.8	3.4	3.1	2.9	2.7
	BOL load (kg)	898	1055	1251	1432	1605	1790	1961	2088	2247
	BG ($\cdot 10^{-2}$)	3.50	3.43	3.17	2.85	2.50	2.09	1.70	1.47	1.13
	Lifetime (PP)	21.2	20.8	20.6	20.5	20.3	20.1	20	19.6	19.5
	Lifetime (AP)	33.8	33	32.8	32.5	32.3	32.1	31.9	31.4	31
27	Volume ratio	8.3	6.5	5.3	4.5	3.95	3.55	3.25	3	2.8
	BOL load (kg)	894	1065	1272	1481	1677	1860	2029	2202	2364
	BG ($\cdot 10^{-2}$)	3.68	3.63	3.40	3.03	2.64	2.25	1.92	1.57	1.27
	Lifetime (PP)	21	20.5	20.4	20.2	20.1	19.9	19.6	19.4	19.2
	Lifetime (AP)	33.5	32.6	32.4	32.2	32	31.7	31.4	31	30.7
30	Volume ratio	8.8	6.75	5.55	4.7	4.1	3.65	3.35	3.1	2.85
	BOL load (kg)	897	1098	1298	1516	1733	1948	2120	2293	2516
	BG ($\cdot 10^{-2}$)	3.84	3.79	3.57	3.20	2.79	2.33	2.02	1.70	1.24
	Lifetime (PP)	20.9	20.4	20.1	20	19.8	19.7	19.5	19.2	19.1
	Lifetime (AP)	33.1	32.5	32.1	31.8	31.6	31.4	31.1	30.7	30.4

PP - Peak Power
AP - Average Power
Lifetimes are given in full power years

(a) 12 mol%

(b) 18 mol%
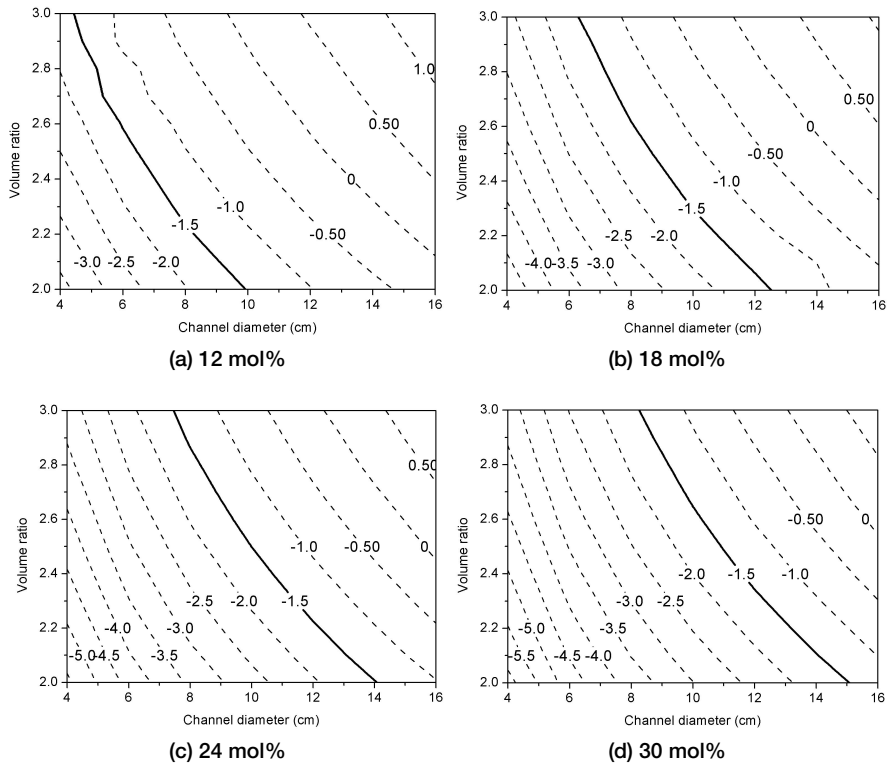
(c) 24 mol%

(d) 30 mol%

Figure 4.6: Temperature feedback coefficient (pcm/K) as a function of channel diameter, graphite volume and thorium concentration

4.4.3 Self-breeder reactors

The aim of this study is to find a core configuration which combines self-breeding, long graphite lifetime and passive safety. As it was shown, all the different reactors are breeders at 5 MW/m^3 average power density. Therefore, the breeder reactors from the last section were shifted to self-breeders in the last step of the optimization. In this thesis a reactor is considered self-breeder if it reproduces all the fuel used to keep the reactor critical after startup. Numerically this means that the lifetime-average of the BG_{stock} has to be 0. This shift was realized by increasing the power density in the core. The power density resulting in a self-breeder core was calculated for some cases in Table 4.3. The lifetime of the graphite is shown in Table 4.4 for the cases with low thorium concentration. The lifetime drops as the power density increases and at higher thorium concentrations the lifetime is too short for the scope of this study. A lifetime of 10 to 20 years of the graphite

Table 4.4: Power density and corresponding graphite lifetime for self-breeder cores

Th	(mol%)	Channel diameter (cm)						
		3	4	5	6	7	8	9
12	Volume ratio	3.5	3.1	2.8	2.6	2.4	2.25	2.1
	BOL load (kg)	1067	1172	1273	1347	1445	1527	1628
	Power density (MW/m^3)	8.52	8.22	7.84	7.55	7.04	6.55	5.8
	Flux level($\cdot 10^{14}$/cm^{2}s)	2.02	1.89	1.75	1.65	1.51	1.38	1.20
	Lifetime (PP)	13.1	13.5	14.1	14.5	15.4	16.4	18.3
	Lifetime (AP)	20.9	21.5	22.4	23.1	24.6	26.2	29.4
15	Volume ratio	4	3.5	3.15	2.85	2.65	2.45	2.3
	BOL load (kg)	1112	1242	1356	1484	1580	1702	1805
	Power density (MW/m^3)	9.75	9.5	9.19	8.71	8.25	7.71	7.11
	Flux level($\cdot 10^{14}$/cm^{2}s)	2.28	2.13	2.00	1.84	1.74	1.56	1.42
	Lifetime (PP)	11.2	11.4	11.7	12.2	12.7	13.6	14.6
	Lifetime (AP)	17.8	18.2	18.7	19.6	20.2	21.8	23.3

PP - Peak Power
AP - Average Power
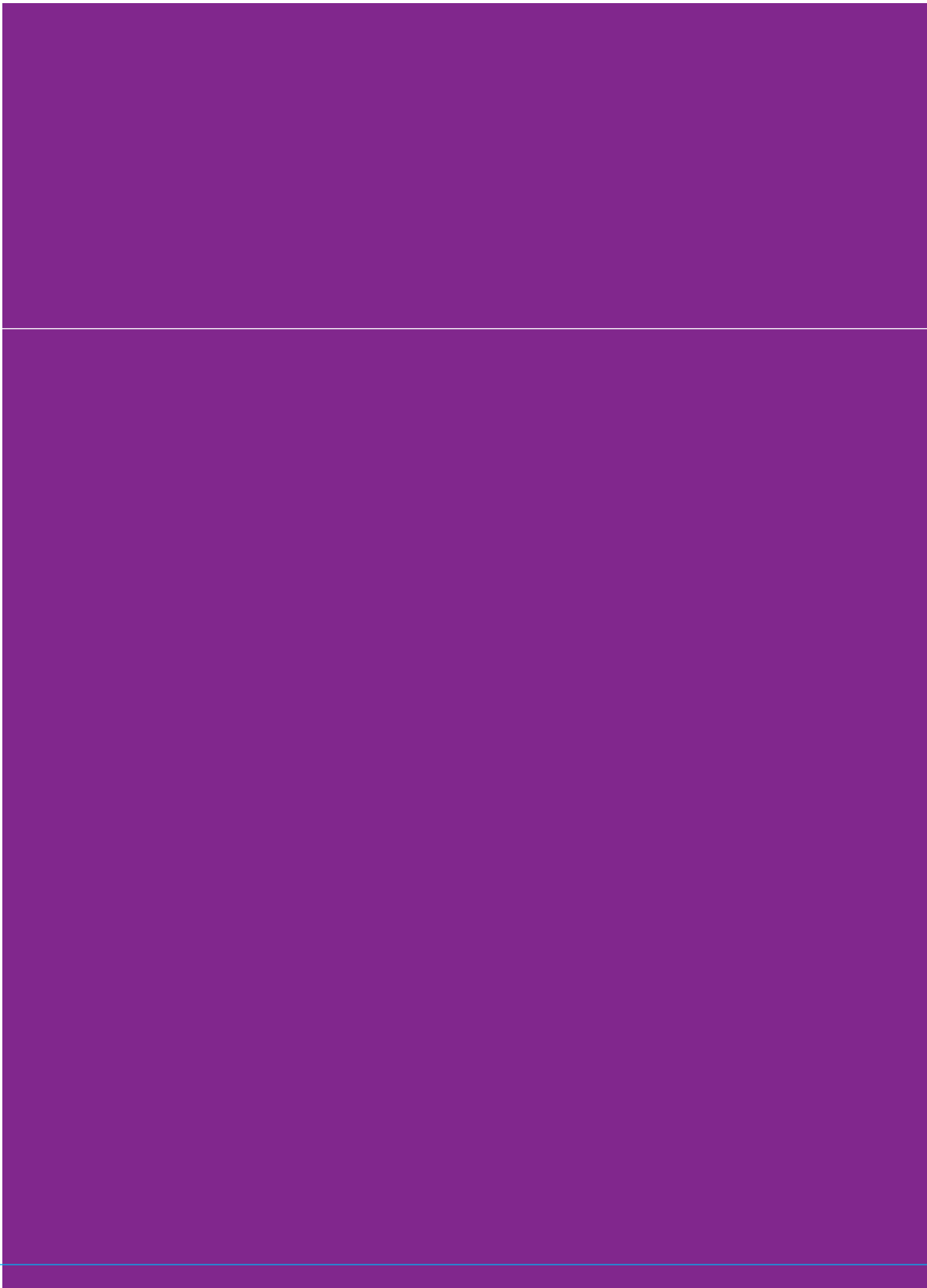Lifetimes are given in full power years

can be achieved in the range of 5 - 10 MW/m^3 power density. This is true for one region throughout the core. Further increase of the lifetime can be attained by dividing the core into more regions. This way the fast flux peak can be reduced in the center of the reactor. As a limiting case, a completely flat power distribution in the core was considered and the corresponding lifetime is presented in the tables as well. Although the lifetimes with average power are significantly longer, these still do not meet the lifetime of a power plant.

4.5   Conclusions

In the first step of the optimization, both the fuel channel diameter and the graphite to salt volume ratio were varied. It was found that the temperature feedback coefficient of the core depends strongly on these variables and that the possible lattice configurations are limited by the restrictions on negative feedback. Furthermore, the lattices providing the best breeding performances have positive feedback and there is a small range of lattice configurations which are breeder and have a negative feedback coefficient. These lattices were compared for a wide range of thorium concentrations in the salt at a set power density. The results show that breeding is possible both at low and high Th concentration. The lifetime of the graphite moderator - around 20 years - is shorter than the expected lifetime of the reactor; thus, the replacement of the graphite is necessary even at low power

operation. Self-breeding was achieved by increasing the power density of the breeder configurations. This reduces the graphite lifetime further more. The graphite - salt lattices found in the optimization study combine passive safety, self-breeding and 10 to 20 years of graphite lifetime in the range of 5 - 10 MW/m^3 average power density. These cores consist of only one region of graphite and an increase of graphite lifetime can be achieved by core designs with two or more regions. This is studied in the next chapter.

Chapter 5

Advanced core designs: Non-uniform lattice and separate blanket salt

It is common in the MSR designs to divide the core into more regions. In fact, all the reactors discussed in this thesis have either a multi-zone core (MSBR, AMSTER, FUJI-U3) or a separate blanket salt (early reactor designs from ORNL, TMSR). The purpose of this blanket is to increase breeding. A breeder blanket is proposed for the fast systems as well. However, zoning a one-fluid core can lead to a flat power profile and a longer graphite lifespan. These zones may differ from each other only by the volume fraction of the graphite.

In this chapter, the different core designs, namely the two-zone one-fluid reactors and the two-fluid reactors are compared with each other and with a one-zone self-breeder reactor. The only difference between the graphite structure of these cores is in the outer zone of the core. Additionally, the salt composition of the two-fluid reactors is varied, together with the processing scheme of the two salt loops. The motivation for the comparison is to evaluate the achievable improvements in terms of BG, graphite lifespan or fissile loads. To be able to do this, the BG definition is extended for two-fluid reactors. Finally, the power densities of the two-zone cores are varied to achieve self-breeding in order to assess the variation of graphite lifespan and power output compared with a one-zone self-breeder reactor.

5.1   Advantages of complex designs

All the one-fluid breeder MSR designs used under-moderated regions near to the boundary of the core. The core of the MSBR (Robertson, 1971) consisted of regions both in radial and axial directions. Only a radial under-moderated region was proposed for the AMSTER breeder concept (Vergnes and Lecarpentier, 2002). These multi-zone core designs were employed because the neutron capture rate of ^{232}Th increases as the spectrum hardens (see Chap. 3.4) in the under-moderated regions and this effect results in an increase of the fissile material production. The zoning modifies the power distribution in the core as well and it can lead to an increase of the power production in the center of the core and to a drop of the power production in the under-moderated zone. This peaked power distribution results in a shorter graphite lifespan. On the contrary, the proper zoning of the graphite cores can help to achieve a long graphite lifespan as it was shown for the FUJI-U3 reactor (Mitachi et al., 2007). In this case, the zones are arranged in such a way that the resulted power density distribution is flat in the core.

Graphite moderated two-fluid breeder MSRs were considered at ORNL before the one-fluid MSBR design (Kasten et al., 1966). The separation of driver and blanket salts was necessary because no chemical process was available at that time to separate Th and Pa from the lanthanide fission products. The two salts were kept separate by the graphite structure which minimized the neutron capture rate of ^{233}Pa as it was effectively diluted in the much larger volume of blanket salt and the neutron flux in the blanket was low. Unfortunately, this complicated graphite core was the main drawback of the design since the two salts had to be separated properly otherwise leaks could cause reactivity-induced transients. Similarly, a separate radial breeder blanket was considered for the TMSR (Mathieu et al., 2003). In this design, the blanket was separated by a metal barrier

from the fuel salt. Thorium containing blankets were proposed for new fast reactor designs as well (Mathieu et al., 2009; LeBlanc, 2010).

5.2   Calculational tools

The computational scheme of the material evolution calculations presented in this chapter can be found in Chapter 3.2 together with the flowchart in Figure 3.1. Only some of the solver routines were exchanged to new ones which can incorporate the more complex geometries. The neutronic calculations were performed with the KENO-VI module of the SCALE6 code package (SCALE, 2009) and the full 3D model of the active core of the two-zone MSR was used in the criticality calculations. The details of the model are presented in Figure 5.1. The distribution of the produced power was calculated based on the fission source distribution in the KENO-VI model. In case of a single-fluid, two-zone system, the fuel channels of the different zones were filled with the same salt mixture while the outer zone was filled with the blanket salt for the calculations of two-fluid systems. The spectra of both zones were used to produce separate collapsed cross-section libraries for the burnup calculations. The material evolution code, which was used in the two-zone calculations, was a modified version of the one used for one-zone calculations. This version performs calculations on the two zones simultaneously and keeps track of the materials in the stockpile which is connected to both zones of the core. In case of the two-fluid system, two separated loops and stockpiles were considered.

5.3   Non-uniform lattice

In a one-zone self-breeder core, the graphite lifespan is shorter than the expected lifetime of a power plant, even at the applied power densities of 5-10 MW/m^3. It is known that a gain in BG (or in the power output at self-breeding operation) or in the graphite lifespan is possible with zoning but the increase of both the power output and the graphite lifespan would be beneficial for the self-breeder MSR.

First, the differences between the two-zone one-fluid designs and the one-zone designs were evaluated. For this study, a one-zone self-breeder core design was chosen from the previous chapter. The one-zone core was divided into two radial zones and the original salt-graphite lattice of the one-zone core was used as the design of the inner zone of the two-zone core. The hexagonal blocks of graphite were sized based on that one-zone design and were used in both zones. The dimensions of the blocks were not changed throughout the study, only the fuel channel diameter in the outer zone. Additionally, the boundary between the zones was varied radially. This way, the total volume of the reactor core, the number of the fuel channels and the total power production was kept constant in each case.

The breeding performance of the reactor cores was compared with the BG definition described in Chapter 3. The average value of the BG of the stockpile (Eq. 3.13), with a small modification for the two-zone core, was calculated for every case. The average fluxes
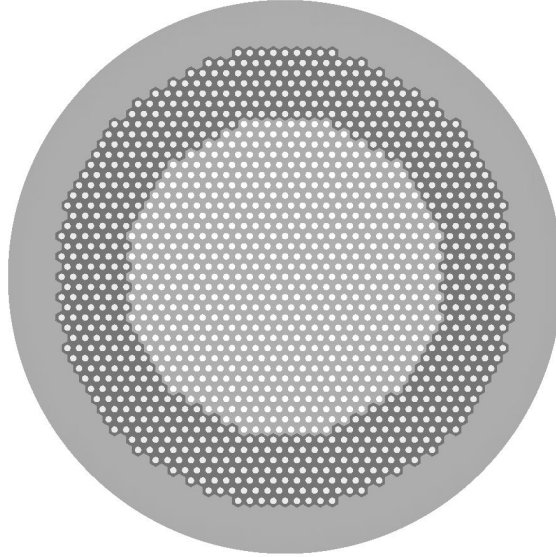
Figure 5.1: Top view of the two-zone MSR core. The two zones are separated radially. The same graphite blocks are used throughout the core and the fuel channel diameter of the outer zone is varied.

and cross-sections were calculated separately for the two zones so the total consumption rate was calculated as follows:

$$C(t) = \frac{V_1 \cdot (R_{a,1}^{23}(t) + R_{a,1}^{25}(t)) + V_2 \cdot (R_{a,2}^{23}(t) + R_{a,2}^{25}(t))}{V_1 + V_2}, \tag{5.1}$$

where the subscripts 1 and 2 refer to the inner and the outer zones of the reactor. This expression was substituted into Eq. 3.13 and averaged over the operation time of the reactor. The numerator of the equation was calculated in the same way as it was calulated for the one-zone cores since the reactor has one external stockpile.

5.3.1 Reactor model

The fuel salt, the corresponding core geometry and the power density was chosen from Table 4.4 which lists the self-breeder configurations of the one-zone cores. The basis of the core geometry was the graphite-salt lattice with a volume ratio of 2.65 and 7 cm fuel channel diameter (see Table 4.4). The salt mixture corresponding to this core geometry consisted of FLiBe with 15 mol% ThF_4 and this core configuration operates as a self-

breeder at $8.25 MW/m^3$ average power density according to the calculations performed in Chapter 4. The size of the hexagonal graphite blocks, which was kept constant, was calculated on the basis of this chosen volume ratio and channel diameter. The reactor was 5 meter in diameter and 5 meter in height while the thickness of the reflector was 0.75 meter. An example of the 3D model is shown in Figure 5.1. The total number of fuel channels was 1381. The uranium concentration was calculated separately for every case.

The density of the graphite was set to 1.84 g/cm^3 while the mean operating temperature of the salt was 1000K. Similarly to the optimization study in the previous chapter, the volume of the salt in the loop was assumed to be the same as the volume of that in the core and the continuous processing scheme was not changed as well (see Table 4.2). During the calculations all uranium fed to the core was taken from the stockpile. The reactor was operated for 50 full power years in every case.

The channel diameter in the outer zone was modified (both increased and decreased) with respect to that in the inner zone. An increase of the channel diameter results in a harder spectrum and that is expected to increase the uranium production rate, while the power production decreases in the outer zone and increases in the inner zone. Thus, the graphite lifetime is expected to decrease due to the higher power peak in the center. Similarly, the decreased channel diameter causes a softer spectrum which results in an increase of the power production in the outer region of the core. As the total power of the reactor is kept constant, the power produced in the inner zone decreases. This way, the fast neutron fluence is reduced in the high power density region. The channel diameter in the outer zone was increased to 8 and 9 cm, and decreased to 6 and 5 cm. The volume of the two zones was varied in four steps by changing the radius of the inner zone from 150 cm to 225 cm. In order to provide a reference point, the original one-zone core was re-calculated as a two-zone reactor by not changing the fuel channel diameter in the outer zone for all four inner zone radii. The number of fuel channels in the inner and in the outer zone, together with the volume of salt in the zones and the average power densities at startup and after 50 ful power years of operation are listed in Table 5.1 for all the core geometries.

5.3.2   Calculations with constant power density

The main results after 50 years of full power operation are shown in Table 5.2. Most of the results are repeated in Figure 5.2 to highlight the trends in the changes of the most important calculated parameters. The results of the reference one-zone reactor, which was calculated using four different position for the zone boundary, agree well and are not dependent on the radius of the inner zone. The BG of the one-zone reactor is $1.03 \cdot 10^{-2}$, which is higher than the BG calculated in the previous chapter (the calculated BG of the reference one-zone reactor was zero in the previous chapter). This difference comes from the different neutronic code. Previously, a 1-D transport calculation was used on an infinite lattice with a correction for the leakage while in this work a 3-D Monte Carlo calculation is employed. Since the leakage correction overpredicted the leakage compared to the results for a one-zone core presented here, the initial fissile load and the feed rate were also higher in the 1-D transport calculations. Furthermore, the neutron spectrum was slightly softer in the infinite lattice calculations than in the 3-D calculations. As a result of the higher

Table 5.1: The number of fuel channels, the volumes of different zones and the power densities in the considered cores.

Inner zone		Channel diameter (cm)				
radius (cm)		5	6	7	8	9
150	No. ch. inner / outer zone			475 / 906		
	Salt vol. inner zone (m^3)			9.14		
	Salt vol. outer zone (m^3)	8.89	12.81	17.43	22.77	28.82
	P. dens. i. z. BOL (MW/m^3)	9.41	9.39	10.97	14.44	17.30
	P. dens. o. z. BOL (MW/m^3)	7.63	7.65	6.82	5.01	3.51
	P. dens. i. z. EOL (MW/m^3)	7.49	8.06	10.72	15.09	18.04
	P. dens. o. z. EOL (MW/m^3)	8.65	8.35	6.96	4.67	3.12
175	No. ch. inner / outer zone			661 / 720		
	Salt vol. inner zone (m^3)			12.72		
	Salt vol. outer zone (m^3)	7.07	10.18	13.85	18.10	22.90
	P. dens. i. z. BOL (MW/m^3)	9.40	9.34	10.36	12.06	13.64
	P. dens. o. z. BOL (MW/m^3)	7.19	7.25	6.31	4.76	3.30
	P. dens. i. z. EOL (MW/m^3)	8.01	8.41	10.14	12.48	14.09
	P. dens. o. z. EOL (MW/m^3)	8.47	8.10	6.52	4.36	2.89
200	No. ch. inner / outer zone			859 / 522		
	Salt vol. inner zone (m^3)			16.53		
	Salt vol. outer zone (m^3)	5.12	7.38	10.04	13.12	16.60
	P. dens. i. z. BOL (MW/m^3)	9.55	9.30	9.73	10.45	11.18
	P. dens. o. z. BOL (MW/m^3)	6.10	6.53	5.81	4.62	3.53
	P. dens. i. z. EOL (MW/m^3)	8.63	8.80	9.45	10.53	11.29
	P. dens. o. z. EOL (MW/m^3)	7.63	7.35	6.27	4.49	3.24
225	No. ch. inner / outer zone			1111 / 270		
	Salt vol. inner zone (m^3)			21.38		
	Salt vol. outer zone (m^3)	2.65	3.82	5.20	6.79	8.59
	P. dens. i. z. BOL (MW/m^3)	9.14	8.98	8.94	8.98	9.15
	P. dens. o. z. BOL (MW/m^3)	4.60	5.25	5.41	5.25	4.55
	P. dens. i. z. EOL (MW/m^3)	8.91	8.77	8.86	8.99	9.15
	P. dens. o. z. EOL (MW/m^3)	5.54	6.12	5.73	5.21	4.55

feed rate, the BG was slightly lower than the BG calculated with the two-zone calculation scheme for the one-zone core.

The core configurations in the first row of the table (inner zone radius of 150 cm) differ the most from each other as the radius of the inner zone is the smallest in these cases. Therefore, the largest deviations from the BG and graphite lifespan of the reference core can be found in these cases and this row is discussed first. The critical load of the reactor increases as the channel diameter increases in the outer zone and as it is expected, the cores with harder spectrum in the outer zone have higher breeding gain. Although the critical load is higher for large channel diameters, the mass of the uranium fed to the core from the stockpile during the operation is the lowest then. This, and the high ^{233}Pa content of the large outer channel diameter cores is the reason of the higher BG. Furthermore, the power density and the flux level is reduced in the large fuel channels which gives an additional increase to the BG. Similarly, the power density and the total feed is relatively high in the small fuel channels while the ^{233}Pa content is low. Due to the reasons mentioned, the BG of these cores is negative. On the other hand, the reduced fuel channel diameter in the outer zone increases the lifespan of the graphite moderator because the power peak is reduced. In case of the smallest channel diameter, this suppression is so strong that the lifespan of the graphite in the outer zone is shorter than that of the inner zone. The lifespan decreases with the increasing channel diameter, which is due to the increasing power density in the inner zone of the core.

Next, all the results of the cores with increased channel diameter in the outer zone (channel diameter of 8 and 9 cm) are discussed. The BG has a maximum at the smallest inner zone radius and in case of 9 cm channel diameter it is almost four times the BG of the reference core. On the other hand, the initial load is higher than that of the reference core because the neutron spectrum is harder. The power production is low in the outer zone and this results in a high power density in the inner zone. Therefore, the graphite lifespan is shorter than for the reference core. The increase of the radius of the inner zone reduces the BG and increases the graphite lifespan to the values of those of the reference reactor. At the largest inner zone diameter, the BG of these cores is comparable or slightly lower than the BG of the reference one-zone core because the critical load of these cores is higher than the load of the one-zone core but the ^{233}Pa content is the same. Therefore, cores with a small and hard-spectrum outer zone perform similarly to a one-zone core.

Finally, the results of the core configurations employing a soft-spectrum outer core (channel diameter of 5 and 6 cm) are discussed. In case of a small inner zone radius, most of the power is produced in the small channels of the outer zone in these reactors. This, together with the low critical load impies a high flux level. The result of these are low ^{233}Pa content, high feed rates and ultimately a negative BG. These core configurations were intended to increase the lifespan of the moderator and indeed it is longer than the lifespan of the graphite in the reference core. As the radius of the inner zone is increased, the power density in the outer zone decreases and this results in an increasing BG while the graphite lifespan decreases. Finally, the cores with small outer zone have higher BG as the reference case due to the lower critical load, total feed and higher ^{233}Pa content

Table 5.2: Results of the calculations at a fixed average power density of $8.25 MW/m^3$.

Inner zone		Channel diameter (cm)				
radius (cm)		5	6	7	8	9
150	BOL load (kg)	927	1181	1528	1940	2383
	Breeding gain ($\cdot 10^{-2}$)	-2.29	-0.65	1.03	3.00	3.94
	Graphite lifespan (years)	12.1*	14.1	11.8	9.0	7.6
	Mass of ^{233}Pa in the core (kg)	29.4	30.0	30.7	31.4	31.7
	Mass increase (kg)	168	260	398	507	583
	Feed in 50 years (kg)	3480	3460	3360	3040	2960
175	BOL load (kg)	1055	1262	1528	1834	2163
	Breeding gain ($\cdot 10^{-2}$)	-1.51	-0.47	1.02	2.60	3.39
	Graphite lifespan (years)	13.3	13.2	11.8	10.1	9.0
	Mass of ^{233}Pa in the core (kg)	29.7	30.2	30.7	31.2	31.4
	Mass increase (kg)	213	295	400	477	523
	Feed in 50 years (kg)	3400	3440	3360	3120	3060
200	BOL load (kg)	1195	1348	1528	1744	1974
	Breeding gain ($\cdot 10^{-2}$)	0.003	0.22	1.03	2.01	2.58
	Graphite lifespan (years)	12.2	12.2	11.8	10.9	10.4
	Mass of ^{233}Pa in the core (kg)	30.4	30.4	30.7	31.0	31.2
	Mass increase (kg)	268	325	397	451	483
	Feed in 50 years (kg)	3260	3360	3360	3240	3140
225	BOL load (kg)	1366	1439	1528	1636	1754
	Breeding gain ($\cdot 10^{-2}$)	2.69	1.49	1.03	0.95	1.03
	Graphite lifespan (years)	11.6	11.8	11.8	11.8	11.6
	Mass of ^{233}Pa in the core (kg)	31.1	30.8	30.7	30.7	30.7
	Mass increase (kg)	354	374	395	426	440
	Feed in 50 years (kg)	3010	3280	3380	3340	3360

* Lifespan is limited by the outer zone

than those of the reference core. This gain in breeding is possible because the graphite-salt lattice in the inner zone is not optimized for breeding but it was chosen based on the limits on the temperature feedback coefficient. As it was shown in Chapter 4.3, the best breeder lattices have a higher volume ratio than the ones that fulfill the limit on feedback. Thus, the decrease of the channel diameter resulted in a core which has a better breeding performance than the one-zone core. This increase was achieved without the penalty of reduced graphite lifespan because of the power peak in the inner zone did not increase significantly.
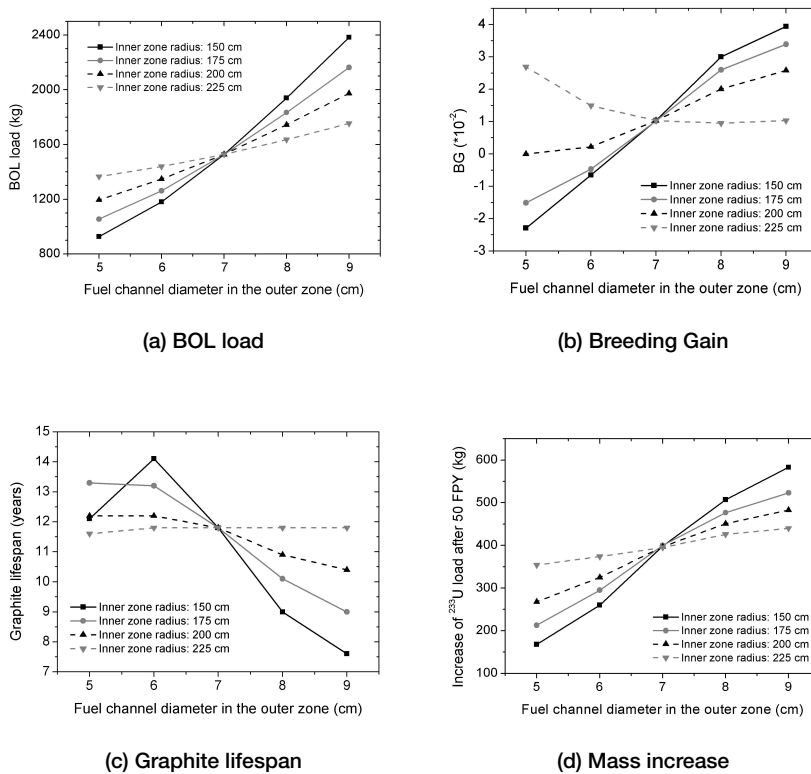
(a) BOL load

(b) Breeding Gain

(c) Graphite lifespan

(d) Mass increase

Figure 5.2: Selected results of the calculations at a fixed average power density of $8.25 MW/m^3$**. The deviation of the calculated parameters from the values obtained for a one-zone core increases as the inner zone radius decreases or as the fuel channel diameter in the outer zone deviates from that in the inner zone.**

5.3.3 Self-breeder reactors

As the aim in this study is to find self-breeder reactor configurations, the average power density was varied for each core. The power density was increased in case of breeder reactors (according to Table 5.2) and it was reduced otherwise. The reactor is considered a self-breeder if it reproduces all the fuel used to keep the reactor critical after startup. Numerically this means that the lifetime-average of the BG_{stock} has to be zero. The average power density resulting in a self-breeder reactor and the lifetime of the graphite is shown in Table 5.3 and in Figure 5.3 for all the cases. The power densities differ significantly and the cores which achieved high BG in the previous calculations can operate as a self-breeder at high power densities compared to the one-zone reference case. This high power density, which can be more than twice the value of the reference case, has a strong penalty on the lifespan of the graphite. This short lifespan is not only a result of the high

Table 5.3: Power density and corresponding graphite lifetime for self-breeder cores						
Inner zone		Channel diameter (cm)				
radius (cm)		5	6	7	8	9
150	Power density (MW/m^3)	4.1	7	10.8	17.25	23.25
	Graphite lifespan (years)	24.3*	16.6	9.1	4.3	2.7
175	Power density (MW/m^3)	5.57	7.25	10.8	15.8	20.25
	Graphite lifespan (years)	19.3	14.8	9.1	5.3	
200	Power density (MW/m^3)	8.35	8.65	10.8	13.75	16.25
	Graphite lifespan (years)	12.1	11.7	9.1	6.6	5.3
225	Power density (MW/m^3)	14.1	11.55	10.8	10.75	11.25
	Graphite lifespan (years)	6.8	8.5	9.1	9	8.7

* Lifespan is limited by the outer zone

overall power density but also of the skewed distribution of the power production. The core configurations which were not breeders in the previous calculations provide an extended graphite lifespan due to their lower power density needed to achieve the self-breeding operation. The average neutron spectrum in these cores is more thermal than it is in the reference case and this further increases the lifespan.

As it is expected, a significant gain can be achieved in the power production and in the graphite lifespan of the two-zone self-breeder MSR. However, the results show that the simultaneous increase of both the power production and the graphite lifespan is not possible. It is concluded that the separation of a self-breeder MSR core into two zones can increase can increase either one of the two parameters.

5.4 Separate blanket salt

Different salt processing can be applied to the fuel and to the blanket salt of a two-fluid reactor and as a result, the schemes for two-fluid MSRs can be different from the schemes of one-fluid MSRs. These different processing options are compared in this section. The blanket salt contains mainly fertile material, thorium. The useful product in the blanket is the fissile material, ^{233}U, which is regularly or continuously removed by fluorination. The fission density is low in the blanket due to the low concentration of uranium; therefore, no chemical separation other than the fluorination is applied to the blanket salt. It is possible to add thorium to the driver salt but this choice has an impact on the applicable salt purification processes. If the driver salt contains thorium, the same chemical processes are necessary as for the salt of the one-fluid reactors. On the contrary, the FPs can be removed by the vacuum distillation process from the fertile-free driver salt. A two-fluid reactor which contains fertile material only in the blanket salt can be operated without applying chemical
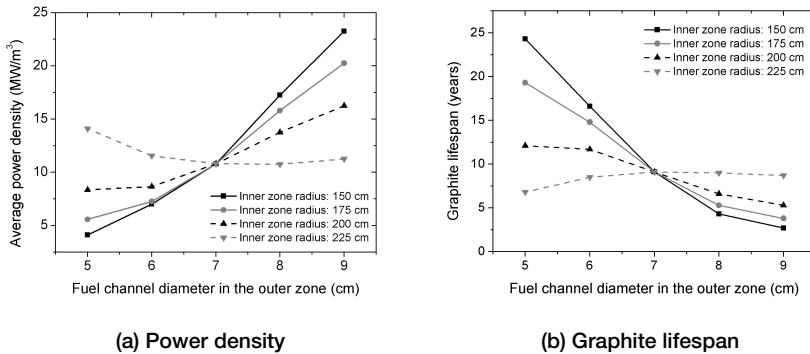
(a) Power density

(b) Graphite lifespan

Figure 5.3: The average power density and the corresponding graphite lifespan for self-breeder cores. The cores with smaller inner zone show larger deviation from the one-zone case. High power densities correspond to short graphite lifespan and vice versa.

separation processes to its diver salt, using the off-gas system to remove non-soluble FPs, the vacuum distillation to remove soluble FPs and fluorination to remove the uranium from the blanket salt. In this part of the thesis these options are compared with each other and with the one-fluid designs in terms of breeding.

5.4.1 Methodology and reactor model

Three different fuel cycle scenarios were investigated in this study. These differ not only in their processing schemes but in their salt compositions as well. The driver salt of the first two contained thorium and these differed only in the processing scheme of the driver salt: in the first case the protactinium removal scheme was applied while only the continuous removal scheme was used in the second one. The former was used to investigate the effect of the rate of uranium removal from the blanket salt while the processing scheme of the driver salt was not changed. The effect of the driver salt's thorium concentration on the BG was studied in the latter case. In the last case, the driver salt contained no thorium. This modification allows to use the vacuum distillation on the driver salt. This fertile free two-fluid MSR was compared with the fertile-containing scenario. The core geometry was not changed throughout the study.

One non-uniform reactor core was chosen from Chapter 5.3.1. The outer dimensions of the reactor core were 5 meter in diameter and 5 meter in height and it was surrounded by a reflector of 0.75 meter thickness. The graphite-salt lattice in the driver region had a volume ratio of 2.65 and 7 cm fuel channel diameter in each graphite block. The radius of the driver zone was 2 meter. The graphite blocks have the same outer dimensions in the blanket zone as in the driver zone but the diameter of the fuel channels was 9 cm. The total number of the fuel channels was 1381, 859 in the driver zone and 522 in the blanket zone. The volume of the driver salt was 16.53 m^3 and 16.6 m^3, respectively. The salt mixture was FLiBe in both loops, with 30 mol% ThF_4 in the blanket salt. This concentration was chosen

because it is the upper limit of thorium concentration based on the melting point of the salt (see Chap. 4.2.1). The uranium concentration of the driver salt was calculated separately for every case. This core was operated at $8.25 MW/m^3$ average power density, which allows for comparison with the original one-fluid calculations. The density of the graphite was set to 1.84 g/cm^3 while the mean operating temperature of the salt was 1000K. Similarly to the optimization study in the previous chapter, the volume of the salt in the loop was assumed to be the same as that in the core and the continuous processing scheme was not changed as well (see Table 4.2). During the calculations all uranium fed to the core was taken from the stockpile. The reactor was operated for 50 full power years in every case.

First, the concentration of ThF$_4$ was 15 mol% in the driver salt and the same processing scheme from the previous chapters (see Table 4.2) was applied to it. This reactor was used for the investigation of the U removal efficiency from the blanket. No soluble FPs and protactinium were removed from the blanket salt. Three different U removal rates were used, resulting in 1.5 months, 3 months and 6 months mean residence time of U in the blanket. In order to reach these residence times, 0.68 m^3, 0.34 m^3 and 0.17 m^3 of salt has to be treated by fluorination each day (assuming 99% efficiency), respectively.

In the fertile-containing scenario the thorium concentration of the driver salt was varied in three steps, 15, 21 and 30 mol% while the continuous processing scheme was applied to the driver salt. In case of the fertile-free scenario no thorium was added to the driver salt. The mean residence time of the FP was varied in both scenarios, namely 0.5 year, 1 year and 3 years. The mean residence time of U in the blanket was 0.5 years in each case.

5.4.2 Breeding gain definitions

The BG definitions were generalized for the evaluation of the breeding performance of the two-fluid reactors. The consumption rate in the driver and in the blanket zones are defined with the reaction rate and the notation used in Chapter 3 in the following way:

$$C_{dr/bl}(t) = R^{23}_{a,dr/bl}(t) + R^{25}_{a,dr/bl}(t) \qquad (5.2)$$

Here, the subscripts dr and bl refer to the driver and blanket loop of the reactor. The production rate of fissile material in the zones are calculated as it is given below:

$$P_{dr/bl}(t) = R^{13}_{d,dr/bl}(t) + R^{24}_{c,dr/bl}(t) \qquad (5.3)$$

One set of BG can be defined for both the two salt loops using these rates, assuming that both loops have a separate external stockpile, similar to Eq. 3.11, 3.12 and 3.13. In

these equations the mass growth rate of the loops is weighted with the total consumption rate of the reactor which is the sum of the consumption rates in the driver and the blanket zones:

$$BG_{critical,dr/bl}(t) = \frac{P_{dr/bl}(t) + R^{23}_{fe,dr/bl}(t) - C_{dr/bl}(t)}{C_{dr}(t) + C_{bl}(t)}$$

(5.4)

$$BG_{core,dr/bl}(t) = \frac{P_{dr/bl}(t) - C_{dr/bl}(t)}{C_{dr}(t) + C_{bl}(t)}$$

(5.5)

$$BG_{stock,dr/bl}(t) = \frac{R^{13stock}_{d,dr/bl}(t) - R^{23}_{fe,dr/bl}(t)}{C_{dr}(t) + C_{bl}(t)}$$

(5.6)

Here, the terms counting the mass transfer between the core and the stockpile have oppposite sign for the driver and the blanket loop as uranium is added to the driver loop but it is removed from the blanket. The BG describing the increase of fissile mass in the core is the sum of $BG_{critical,dr}$ and $BG_{critical,bl}$ while change of the excess fissile material in the stockpiles is characterized by the sum of $BG_{stock,dr}$ and $BG_{stock,bl}$:

$$BG_{critical,sum}(t) = \frac{P_{dr}(t) + R^{23}_{fe,dr}(t) + P_{bl}(t) + R^{23}_{fe,bl}(t)}{C_{dr}(t) + C_{bl}(t)} - 1$$

(5.7)

$$BG_{stock,sum}(t) = \frac{R^{13stock}_{d,dr}(t) - R^{23}_{fe,dr}(t) + R^{13stock}_{d,bl}(t) - R^{23}_{fe,bl}(t)}{C_{dr}(t) + C_{bl}(t)}$$

(5.8)

The time-average of the presented BG definitions are used for the comparison of the different cases in this section (for more explanation see Chapter 3.7).

Table 5.4: Comparison of U residence times in the blanket

Mean U residence time	1.5 months	3 months	6 months
BOL load (kg)	1008	1008	1008
EOL load of driver (kg)	1416	1412	1411
EOL load of blanket (kg)	1.2	2.5	3.7
EOL load of stock (kg)	-783	-779	-778
$BG_{critical,sum}$	0.0276	0.0276	0.0276
$BG_{stock,driver}$	-0.0553	-0.0553	-0.0553
$BG_{stock,blanket}$	0.0175	0.0175	0.0175
$BG_{stock,sum}$	-0.0378	-0.0378	-0.0378

5.4.3 Results

The results of the comparison of U mean residence times in the blanket are presented in Table 5.4. There are only slight differences in the masses of ^{233}U after 50 years of full power operation. The uranium mass in the blanket depends only on its removal rate because its production rate is the same in all cases. The U content decreases as the removal rate increases and this decrease is reflected in the increase of the U content of the driver salt which is determined by criticality control. For the further calculations the slowest removal rate is chosen as it has no effect on the uranium production in the range of practical removal rate values. The reactor is not a breeder, the BG of the stock is -0.0378; however, the one-fluid version of this core, which employed the same processing scheme as for the driver salt in this case, was a breeder with a BG of 0.0258 (see Table 5.2). This is due to the high power density in the driver zone. As this zone produces the total power output of the reactor, the power density is higher in this zone than it was in the one-fluid reactor. This decreases the uranium production in this zone which is only partially compensated by the blanket. This is why the $BG_{stock,driver}$ is negative while $BG_{stock,blanket}$ is positive. The uranium in the blanket (or removed from the blanket) is almost pure ^{233}U which contains 50 ppm ^{232}U and 540 ppm ^{234}U. This first isotope is responsible for the intrinsic proliferation resistance of the salt (see Chap. 1.2). For comparison, the driver salt contains 87 ppm ^{232}U but in the driver loop non-fissile isotopes build up as well. After 50 full power years only 60% of the uranium is ^{233}U and 10% is ^{235}U.

The main results are shown in Table 5.5 for the fertile-containing scenario. None of the calculated cases are breeder. The increase of ThF$_4$ concentration in the driver salt increases the load of the reactor and decreases the mass of U in the blanket due to the higher absorption in the driver zone. Even so, less uranium is needed to operate the converter cores as the Th content increases. This also means that the BG increases but remains negative. This effect of the increasing Th concentration is similar to that in one-fluid reactors (see Chap. 4). As the FP removal rate increases, less absorbers accumulate in the driver salt. This results in a lower uranium need to keep the reactor critical during operation and a higher U mass in the blanket. Both effects decrease the amount of U

Table 5.5: Results of the fertile-containing scenario

Mean FP residence time	6 months	1 year	3 years
ThF$_4$ concentration		15 mol%	
BOL load (kg)	1008	1008	1008
EOL load of driver (kg)	1393	1427	1554
EOL load of blanket (kg)	3.8	3.7	3.4
EOL load of stock (kg)	-658	-950	-1765
$BG_{critical,sum}$	0.0261	0.0278	0.0341
$BG_{stock,driver}$	-0.0481	-0.0611	-0.0971
$BG_{stock,blanket}$	0.0177	0.0173	0.0161
$BG_{stock,sum}$	-0.0304	-0.0438	-0.0810
ThF$_4$ concentration		21 mol%	
BOL load (kg)	1368	1368	1368
EOL load of driver (kg)	1913	1959	2113
EOL load of blanket (kg)	2.7	2.6	2.4
EOL load of stock (kg)	-600	-860	-1602
$BG_{critical,sum}$	0.0553	0.0571	0.0634
$BG_{stock,driver}$	-0.0404	-0.0519	-0.0848
$BG_{stock,blanket}$	0.0129	0.0126	0.0117
$BG_{stock,sum}$	-0.0275	-0.0393	-0.0731
ThF$_4$ concentration		30 mol%	
BOL load (kg)	1858	1858	1858
EOL load of driver (kg)	2615	2679	2848
EOL load of blanket (kg)	1.8	1.8	1.6
EOL load of stock (kg)	-588	-831	-1486
$BG_{critical,sum}$	0.0620	0.0647	0.0719
$BG_{stock,driver}$	-0.0358	-0.0466	-0.0756
$BG_{stock,blanket}$	0.0090	0.0088	0.0082
$BG_{stock,sum}$	-0.0268	-0.0378	-0.0674

fed from the external stockpile and result in a higher $BG_{stock,sum}$. In comparison with the previous case, the fastest processing option performs better than the cases with Pa removal from the driver salt. This result suggests that the removal of FP from the driver salt of a two-fluid MSR is more important than the removal of Pa to reach breeding operation.

For the fertile-free scenario, the results are presented in Figure 5.6. It is noticeable that the reactor needs only 62 kg of fissile material at the start-up. This is due to the low absorption in the driver zone. There is no uranium production in the driver zone, only the feed from the stockpile compensates for the losses and the absorption build-up. The

Table 5.6: Results of the fertile-free scenario

Mean FP residence time	3 months	6 months	1 year	3 years
BOL load (kg)	61.6	61.6	61.6	61.6
EOL load of driver (kg)	69.7	72.7	77.5	89.4
EOL load of blanket (kg)	45.6	43.8	41.7	36.6
EOL load of stock (kg)	-16085	-16263	-16469	-16963
$BG_{critical,sum}$	0.00247	0.00250	0.00258	0.00282
$BG_{stock,driver}$	-0.935	-0.936	-0.937	-0.938
$BG_{stock,blanket}$	0.193	0.186	0.176	0.158
$BG_{stock,sum}$	-0.748	-0.75	-0.761	-0.78

uranium produced in the blanket does not compensate for this and a total amount of 16 to 17 ton of ^{233}U is needed during the 50 years of full power operation. This is reflected in the breeding gain of the reactors as it is 20 to 30 times lower than the corresponding BG of the stock ($BG_{stock,sum}$, see Eq. 5.8) in the fertile-containing scenario. The change in the FP removal rate from the driver salt has an effect on the BG but this effect is weak. Compared with the one fluid and the other two fluid reactors, the fertile-free scenario has the worse performance in terms of breeding.

5.5 Conclusions

In this chapter the two-zone one-fluid moderated MSR cores were investigated. The cores were prepared by modifying the amount of moderator in the outer region of the core in the radial direction, and were compared with each other and with a reference one-zone core based on the lifespan of the graphite moderator and on the breeding gain. The comparison was performed both at a set power density and after changing the power density in each case to result in self-breeding operation.

A self-breeder graphite-salt lattice was chosen for the inner zone of the core while the amount of moderator was both increased and decreased in the outer zone of the core. Furthermore, the volume of the two zones was varied as well. It was found in the set power density calculations that zoning has a strong impact on the BG of the reactor as the BG of the best breeder configuration was four times higher than that of the reference one-zone core. On the other hand, the lifespan is reduced in these cases. Decrease of the BG is also possible, turning the originally breeder one-zone core into a converter. This modification of the core also increases the graphite lifespan; however, this increase is only up to 20% compared with the reference core. Generally, if the result of the zoning is an increase of one of the calculated parameters, the other one decreases. The only exceptions were the cases where the amount of moderator was increased in a small volume of the core near the radial reflector. In these cases the BG increased without decreasing the graphite lifespan.

Finally, the power density of each core configuration was varied to achieve self-breeding. The power densities, together with the graphite lifespan show a wide spread. A self-breeder can be operated for 24 full power years without changing the moderator at the cost of low power density of 4.1 MW/m^3 or can have a high power density (comparable to that of the MSBR) but very short graphite lifespan. This can be reached only by varying the diameter of the fuel channels in one region of the moderated core.

Generally, the two-fluid reactors considered in this chapter have a lower BG than the one-fluid cores. The two-fluid cores which operate with thorium in the driver salt have a BG slightly worse than the one-fluid core reactors. In fact, it was shown that the increase of the thorium concentration in the driver salt increases the BG of the system. Another main disadvantage of the two-fluid reactors is that the power production is limited to the driver zone; therefore, the occuring power densities are higher than in an one-fluid core, given that the same power output and core volume is used. This drawback can only be overcome by lowering the power output or increasing the size of the two-fluid core and these modifications would increase the BG as well. Finally, it is concluded that the best approach to design a two-fluid reactor which uses one of the salt processing scenarios is not to extend a one-fluid core but to start a completely new design which focuses on the specific problems of the two-fluid reactors.
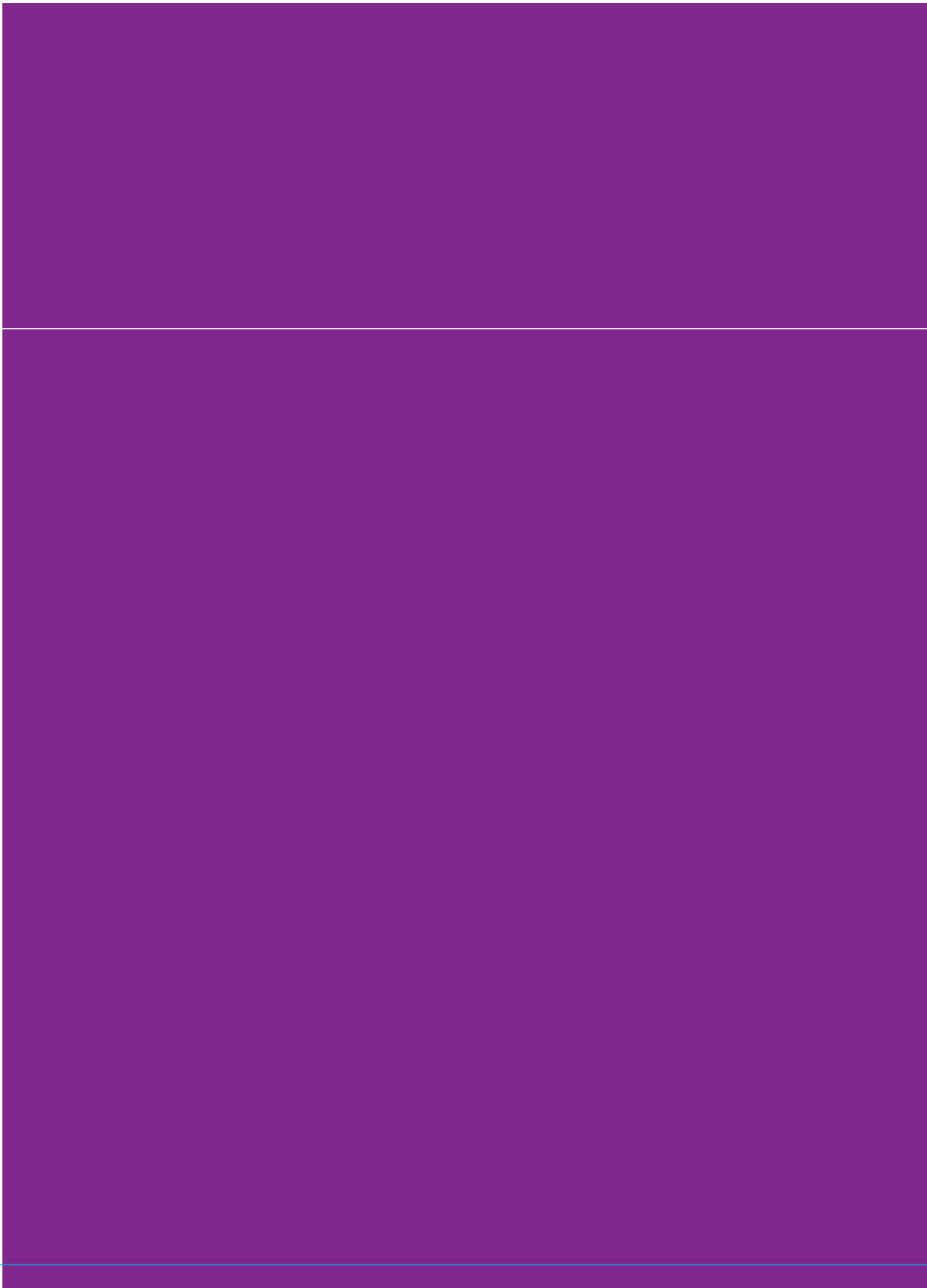
Chapter 6

Steady-state and dynamic behaviour of the moderated MSR

The kinetics of the MSR is fundamentally different from other types of reactors because the spatial distribution of the delayed neutron precursors is decoupled from the flux distribution. Most of the heat is deposited in the salt which acts as coolant of the reactor; therefore, the heat transfer phenomena are unique in this reactor. As a part of the fission heat is deposited in the moderator by gamma and neutron heating and this heat is removed by the salt, the moderator is at a higher temperature than the salt during operation.

In this chapter, a 3-D coupled neutronics-thermal-hydraulics code system is presented and used to evaluate the safety of moderated MSRs. This code system contains both static and time-dependent calculation routines. In the heat transfer calculations, all the fuel channels are modelled separately and the thermal coupling between those is realized by a 3-D heat conduction model of the moderator. The flow field is calculated in the reactor core and the plena, and this is used in the neutronics and heat transfer calculations. The steady-state calculations were used to obtain the nominal operating conditions of the reactor, and to study the feedback coefficients and the sensitivity of those to the uncertainty in the material property definitions of the salt. The influence of the fuel circulation on the reactor physics is shown on zero-power pump-driven transients. Several full power transients were calculated to demonstrate the stability of the reactor against positive reactivity insertion.

6.1   Overview of the existing code systems

Several publications have discussed the physical aspects of liquid fuel reactor systems, from basic reactor physics problems (Lapenta and Ravetto, 2000), to theoretical aspects of dynamic systems, which include the generalization of the quasi-static method for the MSR (Dulla et al., 2004), and dynamic space and frequency dependent response of MSRs to stationary perturbations (Pazsit and Jonsson, 2011). One-dimensional coupled neutronics and heat transfer programs were developed for time-dependent analysis (Krepel et al., 2005; Lecarpentier and Carpentier, 2003) and benchmarked against experimental data of the MSRE together with many other codes (Deplech et al., 2003) in the framework of the MOST project (Kophazi et al., 2003).

For the simulation of spatial transients of the MSR, a 3-D coupled model is necessary. One of the code systems which is capable of 3-D dynamic calculations of a moderated MSR is a modification of computational tools designed for pressurized water reactors (Krepel et al., 2007). It is based on the diffusion theory in two energy groups and an arbitrary number (1-6) of precursor families. The original thermal-hydraulic model was extended with a heat transfer model of the graphite moderator. The code was used for simulation of various reactivity- and pump-driven transients as well as accidents occuring at channel blockage of the MSBR (Krepel et al., 2008). Another coupled neutronics-thermal-hydraulics code was developed at Delft University of Technology (Kophazi et al., 2009). This code consisted of a diffusion code, which was modified to calculate the precursor drift, and a full 3-D heat transfer model of the salt and graphite in the reactor core of the MSRE. It was used in the analysis of power transients induced by debris left in the core and

by blockage of fuel channels. Both codes were validated against the natural-circulation experiment of the MSRE.

The development of coupled codes dedicated to fast MSRs has started as well. In these studies the Molten Salt Actinide Recycler and Transmuter (MOSART) reactor (Ignatiev et al., 2007; Rineiski et al., 2006) was considered. The SIMMER-III two-dimensional code was modified and the conducted research focused on fluid dynamics simulations and optimization of the MOSART core (Wang et al., 2006). The development of a 2-D coupled neutronics - fluid dynamics code was reported (Nicolino et al., 2008) and applied to the full core modelling of the MOSART reactor. Finally, a steady-state (Zhang et al., 2009b) and dynamic (Zhang et al., 2009a) code system was prepared which was used a simplified 2-D model of the MOSART and intended to provide more basic understanding of coupling of flow calculations to neutron kinetics and heat transfer.

6.2 Computational tools

The computational model developed at TU Delft consists of several parts specially developed for MSRs in order to investigate the behavior of such a system. Separate computer codes calculate the neutron flux and precursor distribution, the flow field in the reactor, and the temperatures in the fuel and in the moderator. The in-house developed neutron diffusion code DALTON was extended to incorporate the drift of the precursors. This code is described in details in Appendix D. DALTON performs its calculations using a 2-D or 3-D flow field of the fuel rather than only a slug flow. This velocity field is provided by the FLOW code which calculates the radial distribution of the axial velocities in the fuel channels and the flow fields in the plena. The interested reader is referred to Appendix C for the full description. The temperature field in the salt and in the graphite are calculated on the true geometry of the fuel channels and the moderator structure which thermally couples the fuel channels. The separate calculational routines are called SATE and GRAPHITE and these are described in Appendix E and Appendix F. The cross-sections for the neutronics calculations are provided by 1-D cell calculations of the SCALE code (SCALE, 2009).

6.2.1 Coupling scheme for steady-state calculations

In Figure 6.1, the schematic overview of the coupled code system for steady-state calculations is presented. First, a temperature and problem dependent cross-section set is built. This weighted and homogenized set describes the various parts of the reactor and is produced by the SCALE code system. The temperature steps are coarse in this set but the spatial dependence is taken into account through 1-D axial and radial cell calculations by XSDRN. Finally, the weighted cross-sections were collapsed to 21 energy groups. In this structure, the boundaries were distributed equidistantly on the lethargy scale. This process of axial and radial cell calculations was repeated for every temperature point in the set and the difference between the temperature points was 100 K. The density of the salt at different temperatures was calculated with the method described in Chapter 4.4.1.
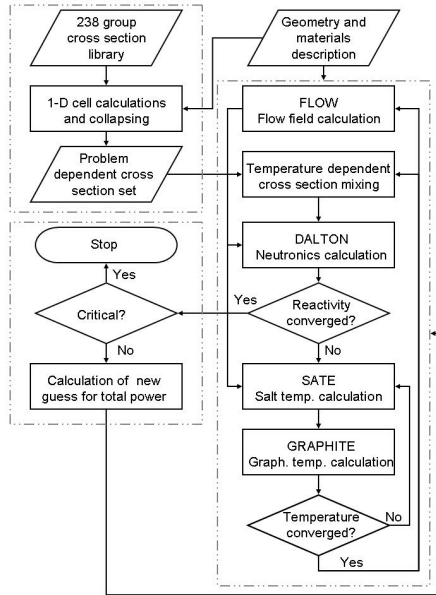
Figure 6.1: The calculation scheme for steady-state calculations. The top left block contains the cross-section preparation. These cross-sections are used in the calculation block (right). This block runs until the temperature and flux field have converged for a given total power production. The search block (bottom left) drives the calculation towards a critical configuration by changing the power production.

Density variations of the graphite were neglected. This cross-section set is used in the neutronics calculations.

Two loops are used in the calculation routine. The inner loop determines the temperature fields in the salt and in the graphite. This loop is nested in the main loop which finds the corresponding reactivity at a given total power. In the outer loop the temperature fields are used to calculate the flow field and prepare the temperature-dependent cross-sections for the neutronics calculation. For every element in the neutronics mesh, the cross-sections are taken either from a radial or axial set, depending on the position, and the cross-sections are linearly interpolated for the actual temperature in the element. The iteration in the outer loop continues until the neutron flux and the temperature fields converge.

The outermost loop in the scheme searches for the total power production required for criticality by changing the power production based on the temperature feedback coefficient of the graphite-salt lattice calculated previously, and the excess reactivity and the temperature fields in the core.
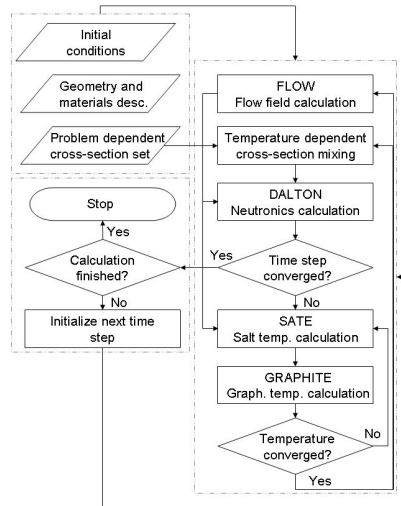
Figure 6.2: The calculation scheme for steady-state calculations. The top left block contains the input data for the calculation. The calculation block runs until the temperature and flux field converges for time step. The time stepping block (bottom left) drives the calculation through the consecutive time steps.

6.2.2 Coupling scheme for dynamic calculations

The time-dependent calculation scheme uses the components of the steady-state scheme. The calculations start with the results and the prepared cross-sections of the static calculations. The schematic overview of the coupling is given in Figure 6.2. This scheme is similar to the steady-state one, the inner loop couples the salt and graphite temperature calculations. The neutronics and flow field calculations of the outer loop use this converged temperature field. This outer loop is repeated until the corresponding flux and temperature fields are converged. The outmost loop drives the scheme through the time domain. It is assumed in the dynamic calculations that the residual heat of the fission products is deposited uniformly in the salt, and that the power production of the FPs is constant during the transient. This assumption was chosen because the simulated transients are short in time and the power production is not expected to increase significantly during the transients.

6.3   Reactor model

The reactor considered in this chapter is a graphite-moderated MSR with the primary heat exchangers located outside the core. The axial and radial reflectors are located inside the reactor vessel. Below the reactor core the flow is distributed to the channels by a plenum and it is re-collected above the core in the collecting plenum. The core consists of hexagonal graphite blocks with a fuel channel in the centerline of each of those. These fuel channels have the same diameter in every graphite block. The dimensions of the graphite blocks were derived from the one-zone one-fluid core used in Chapter 5.3.2 as a reference. The salt flows in radially into the dividing plenum and flows out axially in the centerline of the collecting plenum. The dimensions of the system are listed in Table 6.1.

The modelling of the reactor started with the determination of the mesh for the DALTON calculations. The mesh sizes of the discretized neutronics calculations have been based on the thermal diffusion length of the core, which is over 10 cm at the thermal peak. Then, the radial and axial 1-D cell weighting and homogenization calculations were carried out using the SCALE code package. Here, the mesh sizes correspond to the mesh sizes in the final DALTON mesh and each cell is weighted only with the spectrum in that cell. Each element of the DALTON mesh was filled with the corresponding cross-section either from the radial or from the axial calculation which was evaluated for the actual salt and graphite temperature of the element.

For the flow field calculation of the core and the plena, thes geometry was modelled on a 2-D rz mesh which was built of hundreds of volumes in the radial direction but only three in the axial direction. The calculated flow field was converted to the neutronics mesh and used in the neutronic diffusion calculations. This converted field was used to start the salt temperature calculation as well. During the calculations, the SATE code prepares the salt velocity in every fuel channel based on the initial flow field. This velocity was transferred to the graphite temperature calculations through the heat transfer coefficient between the salt and the graphite, separately for every element in the salt temperature calculation.

Each fuel channel was modelled in the salt temperature calculations as an independent 1-D loop which was connected to the dividing and collecting plena on the two ends, while the plena were modelled on a 2-D rz geometry. The loop outside the reactor vessel was represented as a 1-D loop which connects the outlet of the vessel to the inlet. The axial mesh of the core corresponded to the neutronics mesh. The true 3-D geometry of the moderator was used to calculate the graphite temperature in a finite element calculation which employed 1.27 million elements.

6.4   Static calculations

Static calculations were employed to obtain the nominal operating conditions of the re-actor and feedback coefficients of the core. The thermochemical (melting point, density, heat capacity) and fluid transport properties (viscosity, thermal conductivity) of the molten salts are important parameters for the accurate modelling of an MSR. However, the measurement and prediction of some of these properties (typically the heat capacity and

Table 6.1: Description of the reactor model

Parameter	Unit	Value	Parameter	Unit	Value
			Reactor geometry		
Vessel radius	3	m	Plenum height	0.2	m
Vessel height	6.9	m	Core height	5	m
Core radius	2.4	m	No. gr. blocks	1327	#
Radius of outflow	0.4	m	Size of gr. block	0.0725	m
Axial refl. height	0.75	m	Fuel ch. diameter	0.07	m
			Primary loop		
Lenght of pr. loop	30	m	Mass flow rate	5395	kg/s
			Heat exchanger		
Sec. inlet temp.	823	K	Heat trans. surface	1459	m^2
Total flow area	5.11	m^2	Mass flow rate (sec.)	2876	kg/s
Density (sec.)	1877	kg/m^3	Heat capacity (sec.)	1507	J/kgK
Heat trans. coeff.	4820	W/m^2K	which equals	850	Btu/hr ft^2 F°
			Discretization for the flow field calculations		
No. radial volumes	500	#	No. axial volumes	3	#
Porosity	0.2818	-	Turning loss	0.9	-
Pr. regain coeff.	0.95	-	Pr. decrease coeff.	-0.9	-
			Discretization for the reactor physics calculations		
No. radial volumes	28	#	No. axial volumes	60	#
No. rad. vol. (core)	24	#	No. ax. vol. (core)	40	#

the thermal conductivity) is difficult and no accurate data is available for the salt mixtures used in the MSR. The different measured and predicted data show differences in the available compilations (Konings and Van der Meer, 2003; Williams et al., 2006). Therefore, one objective of the study was to show the impact of the substance properties on the steady state conditions of the reactor and on the reactivity coefficients. In order to achieve this, the steady state calculations were performed with several different measured and predicted substance property correlations.

6.4.1 Material properties
Several correlations of different material properties were applied in the calculations which are listed below. Two measured correlations, Eq. 6.1 (Konings and Van der Meer, 2003) and Eq. 6.2 (Robertson, 1971), and one prediction was used for density. The first correlation was measured for a ternary salt mixture of $LiF-BeF_2-ThF_4$ (0.6998-0.1499-0.1503) while the second one was measured for the salt of the MSBR.

$$\rho(T) = 4441.3 - 0.9526T(K) \ (kg/m^3) \tag{6.1}$$

$$\rho(T) = 3752 - 0.668(T(K) - 273) \ (kg/m^3) \tag{6.2}$$

The following relationship was employed for prediction of molar volume and density for salt mixtures:

$$\rho(T) = \sum_i X_i M_i / \sum_i X_i V_i(T), \tag{6.3}$$

where X, M and V denote the mole fraction, molar mass and molar volume of each component, respectively. The temperature-dependent molar volumes of the components were taken from (Konings and Van der Meer, 2003) and (Williams et al., 2006). Only one correlation was found for the viscosity of a molten salt mixture which contains actinides (Robertson, 1971). This one is used in several reports:

$$\nu(T) = 0.1094e^{4092/T(K)} \ (mPa/s) \tag{6.4}$$

No temperature-dependent correlation of heat capacity is known for FLiBe salt containing actinides. In the design of the MSBR reactor only one value, 1357 J/kgK, is given (Robertson, 1971). For the salt mixture two approximations were used in order to obtain the heat capacity of the salt, the first being the Dulong-Petit estimation while in the second approach the heat capacity is approximated as a sum of heat capacities weighted with the molar fraction of the components. Data for the latter is taken from (Konings and Van der Meer, 2003). The thermal conductivity is both difficult to measure and to predict. The measured data for the MSBR salt mixture is 1.19 W/mK at its normal operating temperatures (Robertson, 1971). Two different methods were used to approximate the thermal conductivity. The first one is the Rao-Turnbull prediction:

$$k(T) = 0.119T_m^{0.5}\rho^{0.667}/(M/n)^{1.167} \ (W/mK), \tag{6.5}$$
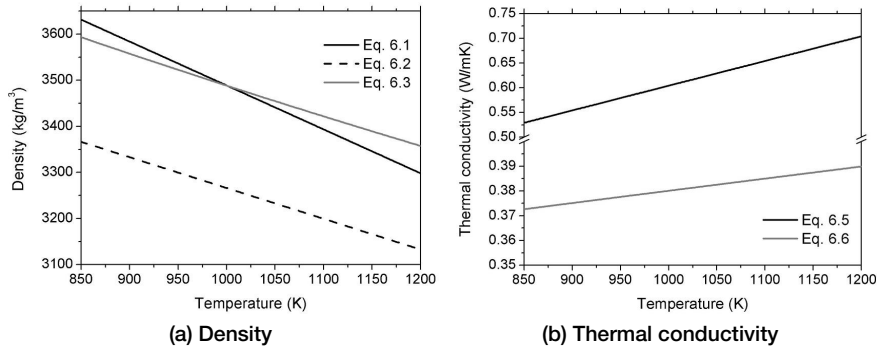
Figure 6.3: Comparison of the different temperature dependent material property definitions.

where T_m is the melting point of the mixture, M is the average formula weight of the salt and n is the number of discrete ions per salt formula. An empirical equation is recommended by (Williams et al., 2006) that is a function of temperature and salt formula weight:

$$k(T) = 0.0005T(K) + 32/M - 0.34 \ (W/mK), \tag{6.6}$$

The different density and thermal conductivity definitions are compared in Figure 6.3.

6.4.2 Normal operating conditions

The static calculation scheme was applied to achieve the nominal operating conditions of the reactor with a given salt composition, which was derived for the applied lattice in Chapter 4.4.3. The temperature-dependent density of the salt was calculated using Eq. 6.3. The measured heat capacity and thermal conductivity together with the only viscosity correlation was used in the calculation. The gamma radiation and the neutrons were assumed to deposit the same amount of heat in a unit volume of the salt and the graphite. Using this assumption, 4.12% of the total power was deposited in the moderator graphite. A search was performed to find the total power at which the reactor is critical. The resulting power production is 792 MW. The reactivity loss due to the fuel flow was also calculated as the difference of two reactivities, with and without flow in the reactor while the temperature fields were not changed, and the reactivity loss was found to be 103 pcm. First, the radial distribution of the velocity in the fuel channels is shown in Figure 6.4. The fuel flows faster closer to the centerline of the reactor and a strong peak can be found which is located under the outflow pipe. This is a result of the geometry of the outflow because the flow has to accelerate near the outflow. This causes a local pressure
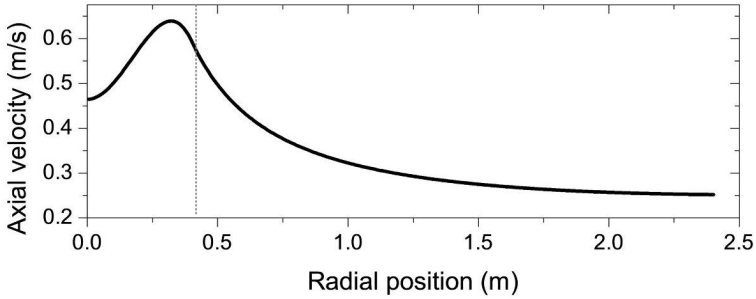
Figure 6.4: The axial velocity in the reactor core as a function of radial position. The dotted line shows the radius of the outflow. The outflow pipe is located in the axial centerline of the reactor vessel. The detailed description of the geometry can be found in Chap. 6.3.

drop in the plenum under the outflow which accelerates the salt in the channels under the outflow. The full explanation of this result is given in Appendix C.

The results of the neutronics calculation is shown in Figure 6.5. The figures show the core and the plena in an $r - z$ cut. Although the fuel is flowing in the reactor, the power density has a distribution which would be expected from a solid fuel reactor. The interface between the core and the plena is visible on both the top and the bottom of the figures as the local power production increases. This is due to the fact that the neutron spectrum is thermalized next to the core in the plenum but the whole volume of the plenum is filled with fuel salt. The distribution of the precursors is also shown for three different precursor groups, namely the first, third and sixth. The half-life of the precursors in the sixth group $(T_{1/2} = 0.216s)$ is the shortest and the distribution of these shows the less deviance from the power profile as these nuclides decay before travelling far with the flow from their point of origin. For the third group $(T_{1/2} = 5.17s)$, the effect of the fuel velocity is well noticeable as the maximum value of the concentration moved streamwise. The effect of the radial velocity distribution is also visible, the concentration is lower in the channels with high fuel velocity because the salt spends less time in these channels than in the other ones. Finally, the distribution of the first group $(T_{1/2} = 53.73s)$ is the most decoupled from the power distribution among the precursor groups. Since this half-life is longer than the recirculation time of the primary loop, there is only 30% difference between the maximal and the minimal concentration. The maximal concentration is not located in the centerline of the reactor but in a ring where the fuel velocity is low but the power density is still relatively high. Furthermore, it is clearly visible as the precursors radially enter the dividing plenum from the primary loop and as they exit through the outlet in the centerline after mixing in the collecting plenum.

The temperature of the salt and the graphite is shown in Figure 6.6. The figures show the core and the plena in an $r - z$ cut although the temperatures were calculated for every channel separately for the salt and on the full 3D geometry of the graphite. The cold salt heats up as it moves upwards in the reactor. The exit temperature of the salt from the
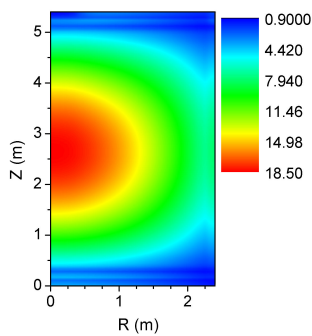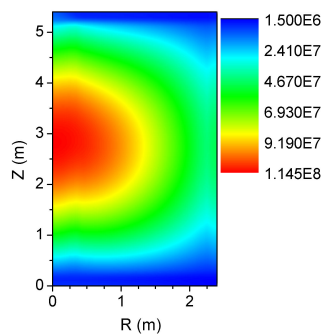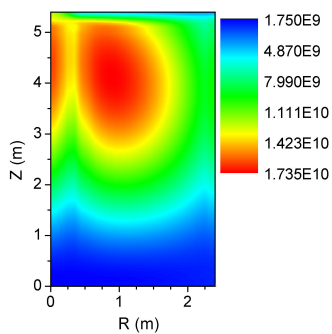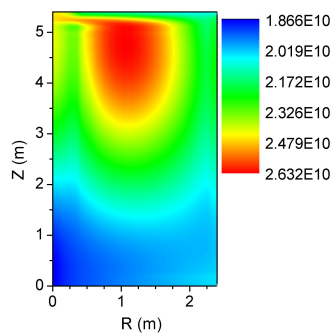
(a) Power density (Mw/m^3)

(b) Concentration of the sixth precursor group ($T_{1/2} = 0.216s$) (#/cm^3)

(c) Concentration of the third precursor group ($T_{1/2} = 5.17s$) (#/cm^3)

(d) Concentration of the first precursor group ($T_{1/2} = 53.73s$) (#/cm^3)

Figure 6.5: The distribution of the power production and the precursors in normal operating conditions. Note the different scales of the plots.
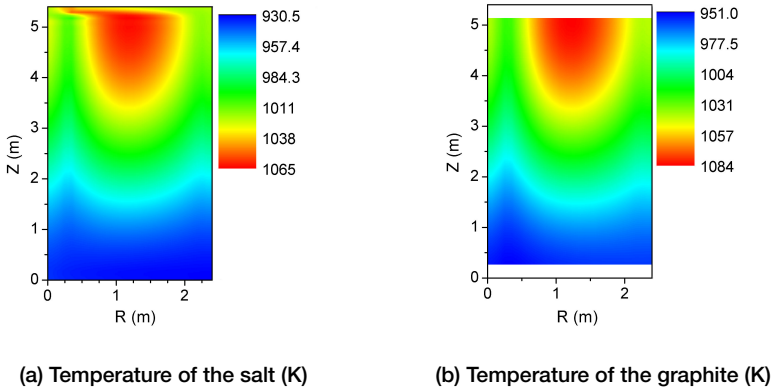
(a) Temperature of the salt (K)   (b) Temperature of the graphite (K)

Figure 6.6: The temperature field in the salt and in the graphite in normal operating conditions

channels depends inversely on the travel time through the channel; therefore the highest temperatures are not found in the centerline of the reactor but radially shifted to a zone where the salt velocity is low but the power density is relatively high. After mixing in the collecting plenum, the salt leaves the core through the outlet. The temperature distribution in the graphite follows the temperature distribution of the salt in the core but the graphite is warmer in every point of the reactor because the salt is cooling it.

6.4.3   Feedback coefficients

The calculations need the material properties of the salts as an input but these properties are often not well known for the salt mixtures as no experimental data is available and the predicting correlations are inaccurate. Therefore, the static calculations were performed with different measured or theoretical correlations to show the impact of the properties on the steady state conditions and feedback coefficients of the reactor. In all the steady state calculations the reactor was forced to produce the total power which resulted in a critical core in the previous section while the different properties were varied in the input. The feedback coefficients of the salt temperature, graphite temperature, power production and uranium mass were calculated.

All the possible combinations of the different properties were used in the coupled static calculations. A part of the calculated results is shown in Table 6.2. The different density correlations are not included in the table because the measured correlations and the theoretical prediction cause small differences in the results. Although the density is expected to have a strong influence on the results, this was not observed because of the small difference between the accurately measured correlations and theoretical prediction. Two feedback coefficients, namely the graphite temperature feedback and the uranium concentration feedback were omitted from the table as the value of those does not vary with the varying material properties of the salt. In each case, the reactivity feedback of

Table 6.2: Calculated reactivity, outlet temperature and feedback coefficients with different correlations for the heat capacity and thermal conductivity of the fuel salt.

H. cap. corr.	Th. cond. corr.	ρ pcm	$\partial\rho/\partial T_s$ pcm/K	$\partial\rho/\partial P$ pcm/MW	T_{in}/T_{out} K
MSBR	MSBR	0.4	-3.86	-0.447	931 / 1041
MSBR	Khoklov	16.7	-3.87	-0.423	931 / 1041
MSBR	R. - T.	29.5	-3.87	-0.407	931 / 1042
w. sum	MSBR	-15.3	-3.79	-0.432	931 / 1054
w. sum	Khoklov	1.7	-3.79	-0.421	931 / 1055
w. sum	R. - T.	20.6	-3.84	-0.404	931 / 1055
D. - P.	MSBR	45.6	-4.04	-0.452	932 / 1005
D. - P.	Khoklov	59.6	-4.07	-0.441	932 / 1005
D. - P.	R. - T.	70.6	-4.07	-0.430	932 / 1005

MSBR - Measured in the MSBR project
w. sum. - Weighted sum prediction for the heat capacity
D. - P. - Dulong-Petit prediction for the heat capacity
Khoklov - Empirical correlation for the thermal conductivity (Eq. 6.6)
R. - T. - Rao-Turnbull prediction for the thermal conductivity

the graphite temperature is 2.16 pcm/K while the reactivity feedback of the uranium mass is 25.6 pcm/kg. The reactivity feedback of the salt temperature is always negative and the sum of the feedback of the salt and the graphite temperature is negative (from -1.7 pcm/K to -1.9 pcm/K) as well. However, these values were calculated with a spatially uniform increase of the temperatures. Therefore, the reactivity feedback of the power is a more realistic measure of the safety of the reactor as in the calculations only the produced power was fixed and not the temperature fields. The value of this feedback is less negative than the sum of the temperature feedbacks because temperature of the graphite increases more than the temperature of the salt.

The results of the calculations employing the two estimations for the heat capacity of the mixture (Dulong-Petit and weighted sum) differ much from that obtained using the measured data, which is due to the differences in the calculated temperature field. The calculated reactivities differ 60 pcm while the difference of the outlet temperatures is 50 K. The thermal conductivity predictions introduce a smaller difference than the heat capacity. As most of the heat is directly deposited in the salt the thermal conductivity has mainly an influence on the heat transfer from the graphite to the salt. This can be observed in the results; although the different thermal conductivity predictions do not change the outlet temperatures of the core, they have an influence on the reactivity and on the reactivity feedback of the power through the graphite temperature.

6.5 Dynamic calculations

Finally, several transients, which are typical for MSRs, are studied. These include pump-driven, cold slug induced and reactivity insertion transients and these were chosen to prove the inherent safety of the reactor design. All the transients presented here are unprotected. Although it is very unlikely for the freeze plug to fail, it was also omitted in each transient simulation. This approach was chosen to demonstrate that the reactor is stable and that the temperatures during the transients are far below 1800 K, the boiling point of the salt. Before the calculations on nominal power, zero-power pump-driven accidents were also investigated.

6.5.1 Pump-start at zero power

The pump start-up is certainly the most interesting zero power experiment for a MSR. Before the transient there is no flow in the critical reactor at low power level. When the fuel circulation is started, the delayed neutron precursors leave the core which results in a decrease of the produced power. A part of these precursors re-enter the core after a full recirculation and this affects heavily the neutron economy of the core and finally results in an oscillation in the power production. In the current simulation, the precursors are allowed to mix in the plena below and above the core and this is expected to introduce a dampening effect on the oscillations. The simulation was started from a critical core and the fuel circulation was turned on at $t = 20s$ and the fuel velocity increases to its nominal value according to an exponential rise. The time constant of the exponential rise was set to 0.05.

Figure 6.7 shows the produced power and the flow rate in the core. After the start of the pump, the power production decreases quickly in the core until it reaches a local minimum after 36.6 s after the pump-start (at $t = 56.6s$). At this point, the precursors which have not decayed outside the core enter the dividing plenum and the power production begins to increase. As the precursors leave the core again, the power production drops and this oscillation repeats until the precursors are homogeneously mixed in the whole primary loop. The reason for the rise of the power is the fact that the concentration of the re-entering precursors is higher than the concentration which would correspond to the actual power production in the reactor.

The concentration of the longest-lived precursor group is shown in Figure 6.8 at four different times: before the pump-start, at the first local minimum of the power production (36.6 s after the pump-start), at the first local maximum (50.8 s after the pump-start) and at three minutes after the start. Before the pump-start, the precursor distribution follows the distribution of the thermal flux. At the first local minimum, the high concentration regions can be observed near the outflow and the inflow, while the most of the precursors are located in the external circuit. The opposite of this can be seen at the time of the power peak, the precursors which have not decayed in the external circuit fill the core. Three minutes after the pump-start the remaining precursors are homogeneously mixed in the reactor and in the external circuit.
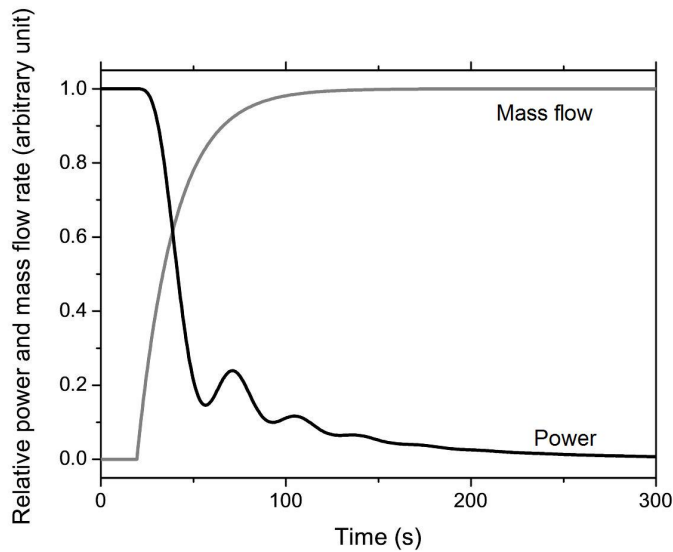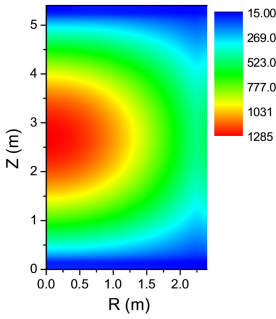
Figure 6.7: The produced power (black) and the mass flow rate (gray) in the core during the pump-start transient. The power was scaled to the initial power production of 10 W while the mass flow rate was scaled to its nominal value.

6.5.2 Pump-coastdown at zero power

This transient is the opposite of the previous one, the pump is turned off while the reactor is critical at low power level. The simulation was started from a critical core at the nominal mass flow rate and the fuel circulation was turned off at $t = 20s$. The fuel velocity decreased zero according to an exponential decline with the same time constant which was used for the pump-start. Note that there is no other way to control reactivity in the model than changing the uranium concentration. Therefore, the uranium concentration was increased compared to the previous transient to achieve criticality when the pump is running. The decrease of the mass flow rate introduces reactivity as the precursors no longer leave the core and this results in an increase of power production. In order to keep the validity of the model, the initial power of the reactor was set to 10 W and the calculation was stopped when the power production reached 100 W.

Figure 6.9 shows the produced power and the mass flow rate during the transient. The power production is constant at the nominal mass flow rate. After the pump is turned off, the fuel velocity starts to decrease and the power production starts to increase shortly after it. As the fuel circulation stops, the increase of the power production approaches an exponential asymptote. This steep increase would eventually turn into a decrease if the simulation would run long enough to capture the salt warming up. The stabilizing effect of the salt temperature feedback is demonstrated in the full power pump-driven transients.
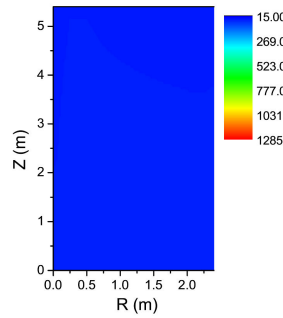
(a) t=20s
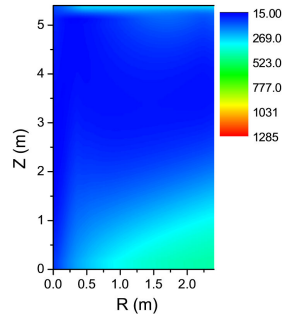
(b) t=56.6s
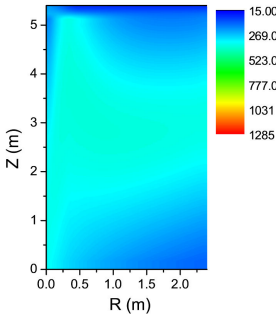
(c) t=70.8s

(d) t=200s

Figure 6.8: The distribution of the longest-lived precursor group in the reactor during the pump-start transient (#/cm^3). Figures a to d capture the distribution at the pump start-up, at the first local minimum of power production, at the first local maximum of power production and three minutes after the start-up when the dsitribution is homogeneous and the power decreases eponentially.
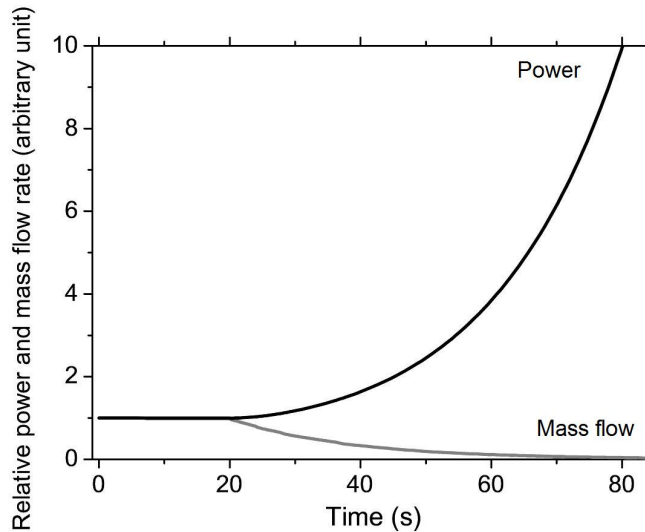
Figure 6.9: The produced power (black) and the mass flow rate (grey) in the core during the pump-coastdown transient. The power was scaled to the initial power production of 10 W while the mass flow rate was scaled to its nominal value.

6.5.3 Slug flow transient

The fuel salt gives a strong negative temperature feedback; therefore, an insertion of cold salt (e.g. from the chemical processing plant) to the primary loop of the reactor can induce a rapid power increase. In the simulation of this transient, a 50 K overcooled slug was placed between the outlet of the heat exchanger and the inlet of the lower plenum while the reactor was operated on full power. Two cases were considered, insertion of 4.5 m^3 and 6 m^3 of cold salt.

The results of the calculations are shown in Figure 6.10. As the cold salt passes through the core, the produced power increases due to the feedback of the salt. This power rise heats up the salt quickly and results in a power decrease. The temperature changes are small, only 10 K at the outlet of the core while the maximum temperature in the core increases with 15 K. After a few small oscillations induced by the returning precursors produced in the power peak and by the returning warmer salt, the reactor returns to its normal operating conditions. The duration of the whole transient is less than a minute.
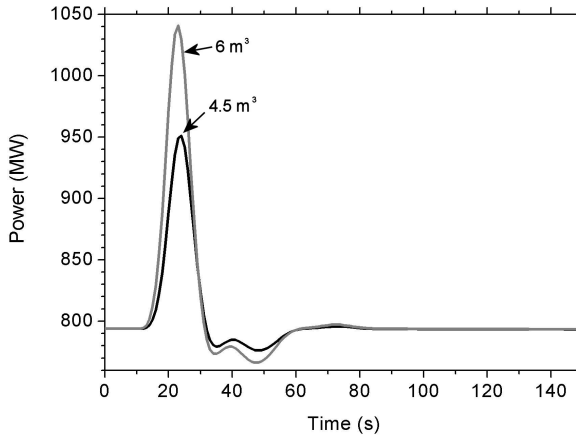
(a) Reactor power
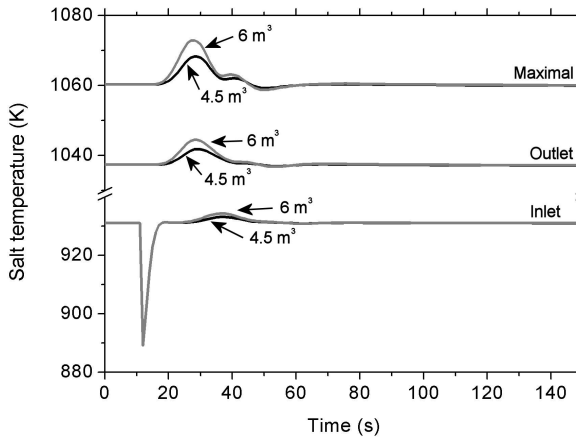
(b) Salt temperature

Figure 6.10: Reactor power and salt temperature as a function of time during the slug flow transient for the insertion of 4.5 m^3 (black) and 6 m^3 (gray) overcooled salt. The power peaks as the salt passes through the core and the reactor quickly returns to steady state.
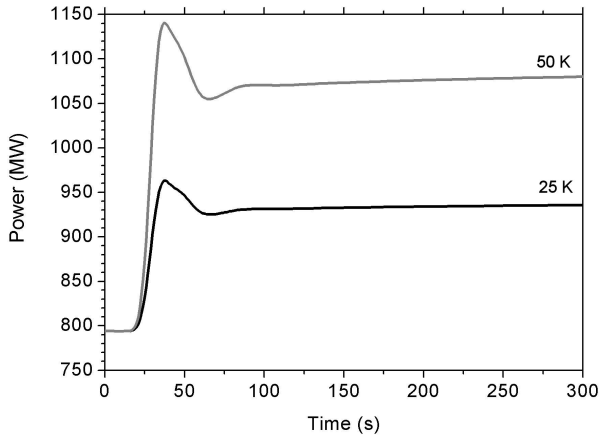
6.5.4   Overcooling transient

Due to the strong negative feedback of the salt, a decrease of the inlet temperature results in an elevated power production and outlet temperature. This transient was simulated by a ramp decrease of the inlet temperature of the secondary side of the heat exchanger. Two transients were calculated with a decrease of 25 K and 50 K while the reactor was operated at its nominal operating conditions. In both cases, this change took 10 s.

The power and the salt temperature as a function of time is displayed in Figure 6.11. When the overcooled salt enters the core, the power begins to increase. The inlet temperature decreases for 15 s and as this decrease stops, the temperatures in the core start to increase. The hot salt leaves the core and passes through the primary loop to return at the core inlet. At this point the power reaches its maximum value and starts to decrease while the temperatures rise in the core. Not much after the power peaks, the outlet temperature reaches its maximum and as this hot salt arrives to the inlet, the reactor power levels out. At this time, the temperature of the graphite begins to rise and all temperatures in the whole system increase slowly. The reactor approaches its new equilibrium state but this process is long compared to the initial phase of the transient. The new power levels and outlet temperatures are 937 MW and 1048 K, and 1085 MW and 1059 K for the cases of 25 K and 50 K reduction of the secondary side inlet temperature, respectively.

6.5.5   Pump-driven transient

A pump shutdown transient is major concern in a MSR because it evokes a reactivity insertion as the precursors do not flow out of the core anymore. Furthermore, the cooling capacity is seriously reduced. Therefore, this transient is interesting from a safety point of view. However, a full pump shutdown cannot be modelled with the codes used in this chapter because the continuity and momentum equations are not solved for natural circulation cases (see Appendix C for details). For this reason, the calculated transients are limited to a partial loss of mass flow in the primary loop. In the three considered cases the mass flow drops to 80 %, 50 % and 20 % following the exponential decline used in the zero-power transient. The results of the transient calculations are shown in Figure 6.12.

Starting with the least severe transient, the power production starts to decrease immediately as the fuel circulation is turned off at $t = 15s$. This is in contrast with the zero-power pump-coast transient as without feedbacks the power begins to rise when the mass flow decreases. This power decrease in the full power case occurs because of the prompt feedback of the salt which is caused by the temperature increase of the salt due to the reduced mass flow. The re-entering precursors cause a short increase of power and after these precursors leave the core, the power production reaches its minimum. The maximum and the outlet temperature of the core increases quickly as the mass flow is reduced. After the negative feedback of the temperature rise compensates the reactivity insertion of the reducing flow, the temperatures stabilize at a higher value. The secondary side of the heat exchanger is not changed during the transient; therefore, the inlet temperature of the core drops. After the quick changes in the power and in the temperature, the graphite starts to warm up slowly because of the heating of the salt. This induces some small but positive feedback to the core. This effect results in a long and

(a) Reactor power
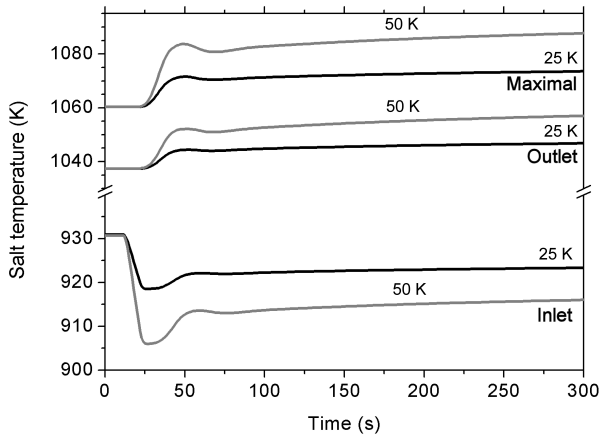
(b) Salt temperature

Figure 6.11: Reactor power and salt temperature as a function of time during the overcooling transient for the decrease of the secondary side temperature of 25 K (black) and 50 K (gray). After an increase of the total power induced by the cold fuel salt, the reactor stabilizes at a new higher power level.
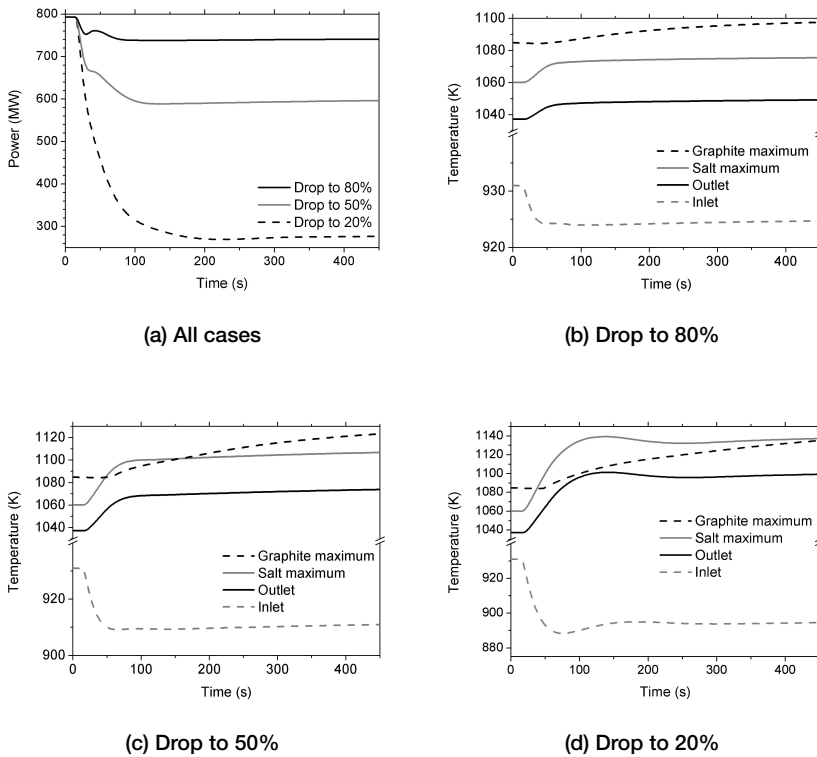
(a) All cases

(b) Drop to 80%

(c) Drop to 50%

(d) Drop to 20%

Figure 6.12: Reactor power and temperatures as a function of time during the pump coast-down transient for the three cases. The prompt feedback of the salt temperature results in an initial decrease of the produced power

weak transient during which the reactor power increases and finally stabilizes at a new steady state with a lower power production compared to its nominal state.

The response is similar in case of the two other transients, when the mass flow drops to 50% and 20%, but the power and the temperatures take more time to stabilize. The time behavior which was discussed in the previous paragraph can be observed during these transients. Firstly, the salt temperature stabilizes close to the new steady state temperatures and right after the power stabilizes as well. This part of the transient is dominated by the temperature feedback of the salt. The graphite takes a long time to heat up and after the salt temperature does not change significantly, the feedback invoked by the graphite temperature change is the strongest feedback in the system. During this second part of the transient, the power increases slowly until the power level and the temperatures stabilize.

6.6   Conclusions

In this chapter, the coupled static calculation scheme was introduced for moderated MSRs. This scheme includes the reactor physics, heat transfer and fluid dynamics calculations which are necessary for the static simulation of this type of reactor. This scheme was applied to a reactor design which was derived from the core optimization calculations in Chapter 4.4.3. The nominal operating conditions of this design were calculated, such as the total power and the reactivity loss due to flow. Although the power density distribution was not affected by the flow of the fuel, the concentration of the precursor nuclei were strongly deviated from the power distribution. The mixing in of the precursors in the plena was also shown as the calculations included these volumes.

Various reactivity feedback coefficients were calculated for the reactor using different substance properties as an input. As the substance property correlations are not well known for fluoride salt mixtures containing actinides, this study was performed to highlight the effect of these on the results of the static calculations. The feedback coefficients on the salt and graphite temperatures, power and uranium concentration were calculated with several temperature dependent material property correlation (theoretical and experimental). According to these calculations, the differences are less than 10% in the coefficients, although the input material properties show a discrepancy up to 50%. The salt temperature feedback coefficient is strongly negative while the feedback on the graphite temperature is positive. In case of the core design chosen in Chapter 4, the sum of these two is sufficiently negative, just as the feedback coefficient of the produced power. For these reasons, the reactor is considered safe. These findings imply that the measurement of substance properties and the validation of the correlations is important but also imply that a sensitivity study on the effect of the material properties should be performed.

Transient calculations were performed to demonstrate the inherent safety of the reactor. As the strongly negative temperature feedback of the salt is prompt, it was expected that the first period of a transient is dominated by it. The heat transfer phenomenon is unique in the moderated core, the salt heats up quickly but the graphite temperature starts to change slowly because the salt is the coolant of the graphite. Due to the large volume of the graphite and the small amount of heat directly deposited to it, the graphite heats up slow. During the second part of a transient (if the transient is long-lasting enough to change the graphite temperature), the change of the graphite temperature generates the dominating feedback; thus, the acting feedback is positive. Fortunately, this effect is weak and it ultimately induces negative feedback through the temperature of the salt but it results in a long approach of the new steady state of the reactor. Both in the presented pump-driven and over-cooling transients, the reactor stabilizes with the above described behavior and the temperature of the salt never approaches its boiling point. Generally, the results of the transient calculations are acceptable from a safety point of view; however, more calculations are needed to fully assess the safety of the reactor. The possible transients include loss of heat sink, channel blockage and loss of flow.
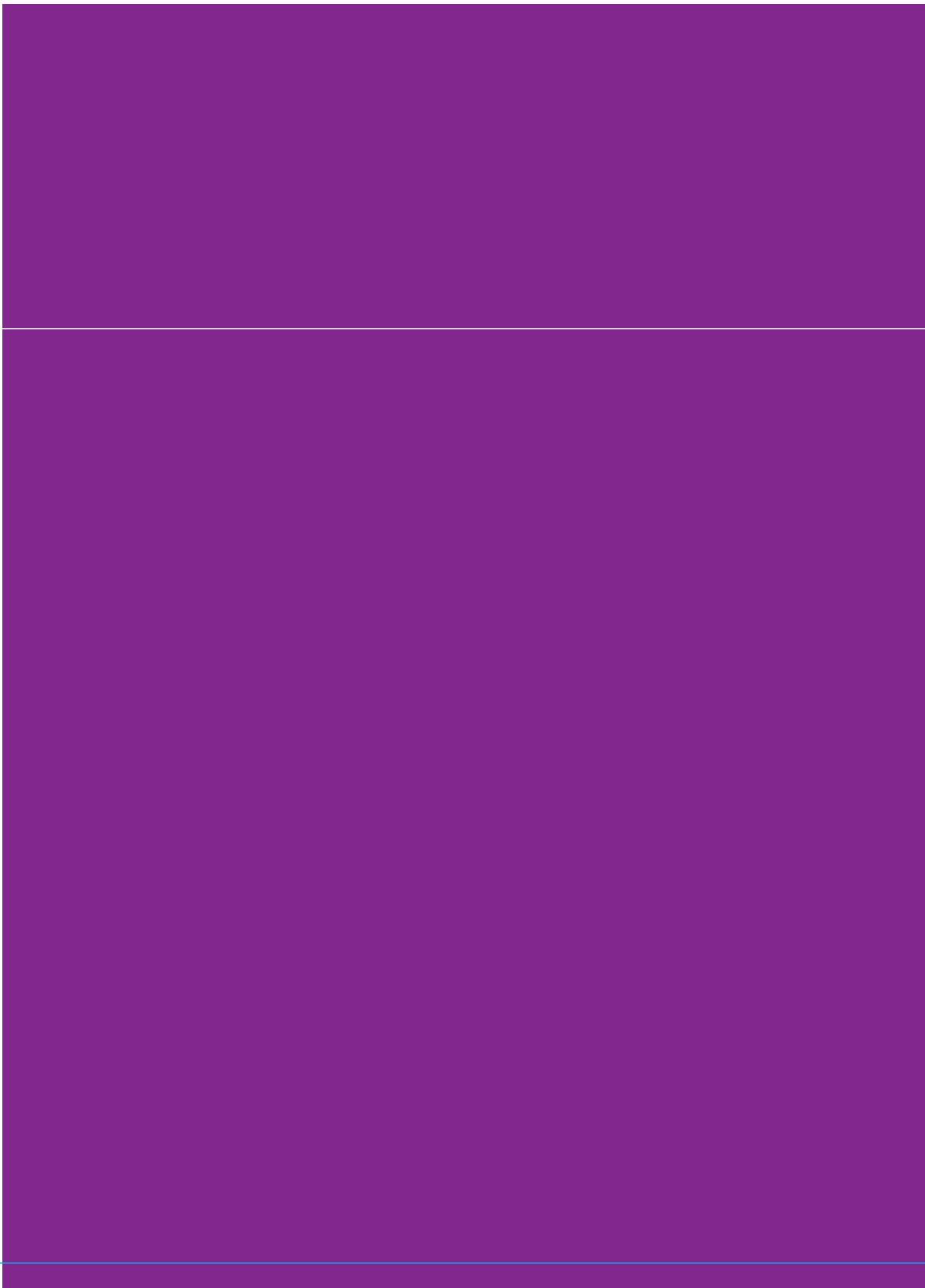
Chapter 7

Conclusions & Discussion

The utilization of the thorium fuel cycle in a Molten Salt Reactor is an attractive combination because it allows to reach breeding in a moderated reactor. Besides the good neutron economy of such a reactor, this is possible due to the salt purification processes which can be applied on- or off-line to the fuel salt. The main objectives of this thesis are to design a moderated MSR and choose its salt processing scheme which provides sustainability and safety by its self-breeder operation and negative feedbacks.

7.1   Conclusions

Core design and optimization
This thesis shows that a practical ratio of the volume of the graphite and the salt, and a realistic fuel channel diameter exist which maximize the breeding performance of the reactor. Unfortunately, the temperature feedback coefficient of these cores is near-zero or positive because of the positive contribution of the moderator. The power density and the applied salt purification scheme have a strong influence on the excess ^{233}U production. The lower the power density is, the better the breeding performance is. As it would be expected, complex salt processing schemes (continuous and Pa removal) are superior to simpler ones in terms of fuel reproduction. However, these complex schemes are not practical at high power densities comparable with the ones in the MSBR because not even these schemes are sufficient for self-breeding. A relatively simple batch-wise processing scheme is enough to reach high conversion ratio operation at a low power density of 5 MW/m^3 while breeding is possible with the continuous and the protactinium removal schemes.

The graphite has positive temperature feedback and a limited lifespan. The results obtained in this thesis indicate that there is a rather narrow range of salt-graphite lattices, described by the amount of graphite in the core, the fuel channel diameter and the thorium concentration in the salt, which provide a sufficiently negative total temperature feedback and still are capable for breeding. According to the optimization study, which was carried out on the basis of the above mentioned salt-graphite lattices, self-breeding can be achieved with an average power density of 5 MW/m^3 and higher, depending on the salt-graphite lattice. However, the graphite lifespan decreases with increasing power density. Therefore, the range of 5 - 10 MW/m^3 average power density is interesting for practical applications because the graphite lifespan is between 10 and 20 years for these cores. Furthermore, these cores contain a relatively low volume of graphite, 65 - 73 m^3; thus, the volume of graphite discharge is limited.

Breeding gain definition
In this thesis, a breeding gain definition is developed for the MSR. This was necessary because the definitions available in the literature assume either irradiation cycles or no change of critical load during operation. The critical load of an MSR increases for several decades of full power operation and as it is shown, the developed definition captures this phenomenon and its effects. The definition is successfully applied to an optimization study of the one-zone MSR and it is used in the comparison of various, one- and two-fluid reactors.

Two-zone and two-fluid core design

The zoning of the graphite moderator in an one-fluid MSR can increase the breeding performance. Some studies have shown that the graphite lifespan can be increased with this method as well. The effects of the zoning are assessed with respect for both the breeding performance and the graphite lifespan by a study presented in this thesis. It was found that zoning has a strong impact on the breeding gain of the reactor, the increase is fourfold in the calculations compared to the one-zone core. However, in these cases the graphite lifespan is reduced because of the increased power peak. It is also possible to design a two-zone, one-zone core which maximizes the graphite lifespan but the increase of the lifespan is modest, up to 20% in the calculated cases. These cores have a lower BG than the one-zone core. Generally, it is concluded that the increase of both the BG and the graphite lifespan is not possible with a two-zone, one-fluid core design.

The processing schemes for two-fluid reactors were compared with each other and with the one-zone and two-zone, one-fluid reactors, using the same core volume and power output. According to the results, the removal rate of uranium from the breeder blanket of the two-fluid reactor does not affect the breeding performance of the reactor. A thorium-containing driver salt is found to be beneficial for breeding in a moderated reactor compared with a fertile-free driver salt. It was also found that in case of the fertile-containing scenario, the increase of the thorium concentration increases the breeding performance of the reactor.

Safety

The steady-state and the dynamic behaviour of the reactor was studied to evaluate its safety. As it was shown in Chapter 6, the total temperature feedback and the power feedback of the one-zone reactor chosen in Chapter 4 is sufficiently negative. Furthermore, these feedback coefficients are not sensitive to the choice of material property correlations so the discrepancy introduced by this uncertainty is small. According to the dynamic calculations, the built-in feedbacks stabilize the reactor during a reactivity-insertion transient. All the performed pump-coast, slug flow and over-cooling transient show that the strong negative feedback of the salt quickly stabilizes the reactor power but the graphite moderator needs more time to adjust its temperature. Thus, the changing graphite temperature results in a long approach to steady state, during which the total feedback acting on the core is positive. There are many ways to introduce positive reactivity in an MSR but certainly the pump shutdown and salt over-cooling transients are the most severe ones. Among other transients, these were shown in this thesis. Generally, the reactor proved to be stable for the introduced perturbations. The temperatures occuring in the core during the transients are far below the boiling point of the salt.

The final conclusion of the thesis is that an inherently safe, graphite moderated self-breeder MSR can be designed and operated. The limiting factors are the positive feedback of the graphite and the efficiencies of salt purification processes. The first one can be controlled by limiting the amount of moderator used in the core but this usually worsens the breeding performance of the reactor. Reduction of the total power can compensate for the loss in breeding performance introduced by the limited amount of moderator or for the penalty of low salt purification efficiency on breeding.

7.2   Recommendations

Many opportunities remain for investigations of the MSR. In this thesis, the thorium fuel cycle was started with available ^{233}U but other fissile materials can be used. As ^{233}U is an currently not available, these studies are of great interest. Two different ways are possible for the start-up. First, the MSR can be started with a mixture of ^{235}U and ^{238}U but this option results in a high MA production compared with the start with ^{233}U. Furthermore, these MAs stay in the salt and lowers the breeding performance unless they are effectively removed during operation. The other option would be to produce ^{233}U in another reactor which is fueled by a low enriched uranium or plutonium mixture. This would have the advantage that the operation of the MSR is not poisoned by the MA production.

The FLiBe mixture is the best choice for the salt of the moderated MSR but it is rather expensive as the lithium has to be enriched in ^{7}Li. The penalty of different salt mixtures on the breeding performance still remains to be quantified. The alternative salt mixtures are even more interesting if the MSR is not designed to reach self-breeding.

As it was shown in this thesis, the graphite moderator in the MSR has a limited lifespan which is shorter than the lifespan of a power plant. However, these results were obtained for the graphite type used in the MSRE and in the MSBR design. The increase of the lifespan can be achieved by introducing new types of graphite which are more resistant against radiation damage so material studies in this field are encouraged. The lifespan of the moderator can be increased if the power distribution is flattened. This is achievable by using more zones both in the radial and in the axial direction. These core optimization studies are important to reduce the waste production of the reactor as well.

The speed of the reactor physics calculations was the limiting factor of the calculations and this is why a 2-D discretization was chosen for the neutronics calculations. For this reason, the coupled transient calculation scheme would benefit from a neutronics code which is suited for high dominance ratio reactors. As the heat transfer calculations were performed in 3-D, the 3-D neutronics calculation would allow for the investigation of spatially localized perturbation, such as channel blockage and unblockage. Furthermore, other transient calculations are necessary to fully assess the safety of the MSR. The most interesting ones are which can result in high temperatures close to or above the boiling point of the reactor. These include the loss of heat sink, channel blockage transients and failure of the freeze plug.

Apart from the continuation of the studies presented in this thesis, numerous other topics have to be addressed before an MSR can be built. Firstly, the thermal hydraulics of the molten salts is not well known. The graphite structure in the moderated MSR is restrictive on the flow, but it is still a challenge to accurately calculate the flow field for any operating condition of a fast MSR. Experimental validation of the calculations is also important. Secondly, a very important area is the development of an effective and afford-able separation process fir soluble FPs, thorium and MAs. Finally, the corrosion induced by the salt of the primary loop is still a problem which needs efforts to be made both in alloy development and experiments.
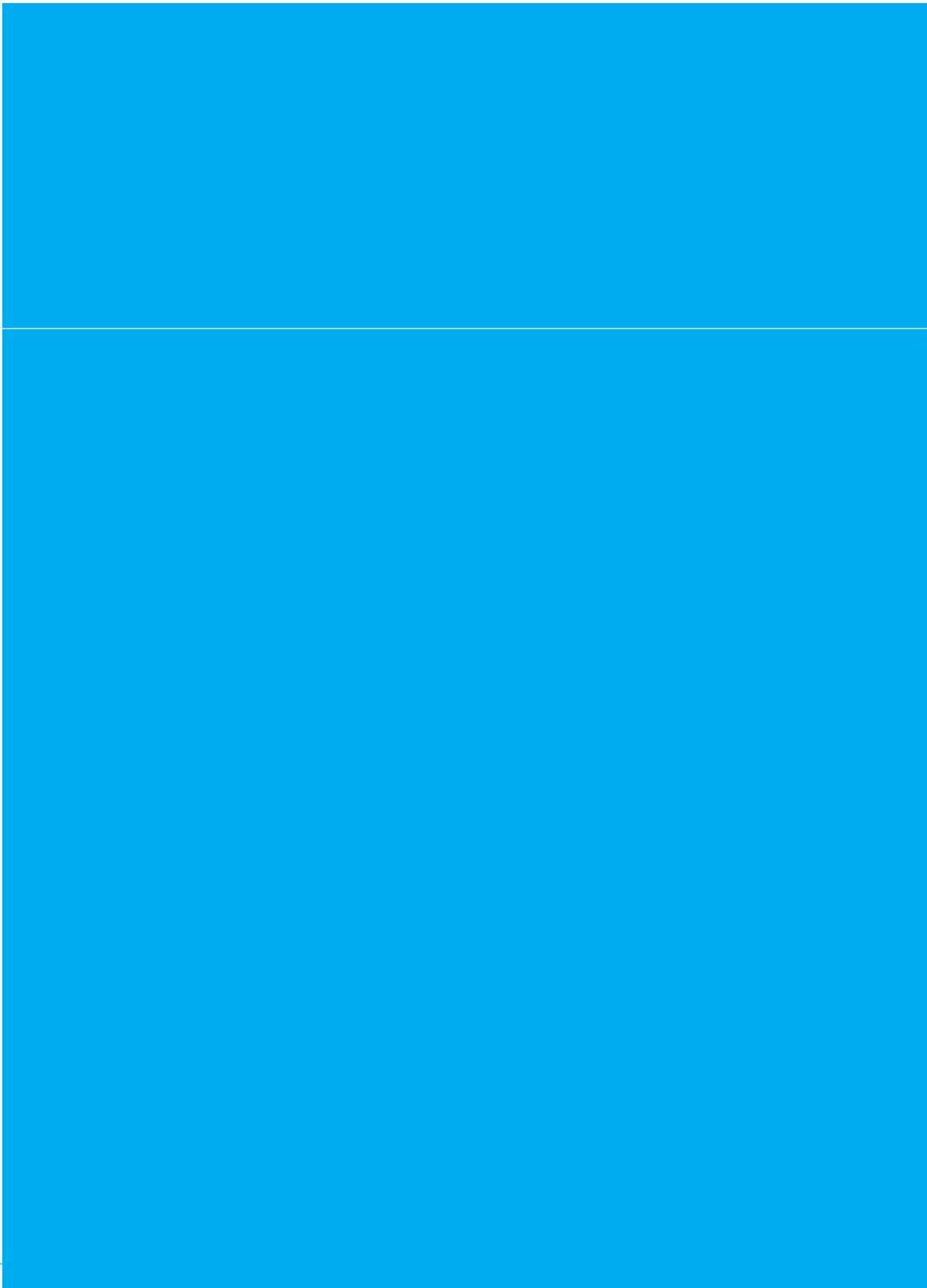
Bibliography

Babcock and Wilcox. *Steam, Its Generation and Use*. The Babcock and Wilcox Company, 1963. 37.

R. A. Bajura and E. H. Jones. Flow distribution manifolds. *Journal of Fluids Engineering*, **98**, 654, 1976.

K. Balakrishnan and A. Kakodkar. Optimization of the initial fuel loading of the indian phwr with thorium bundles for achieving full power. *Annals of Nucl. Energy*, **21**, 1 , 1994.

O. Benes and R. J. M. Konings. Thermodynamic Properties and Phase Diagrams of Fluoride Salts for Nuclear Applications. *Journal of Fluorine Chemistry*, **130**, 22, 2009.

E. S. Bettis and R. C. Robertson. The design and performance features of a single-fluid molten-salt breeeder reactor. *Nuclear Application Technology*, **8**, 190, 1970.

E. S. Bettis et al. The aircraft reactor experiment - design and construction. *Nuclear Science and Engineering*, **2**, 804 , 1957a.

E. S. Bettis et al. The aircraft reactor experiment - operation. *Nuclear Science and Engineering*, **2**, 841 , 1957b.

R. C. Briant and A. M. Weinberg. Molten fluorides as power reactor fuels. *Nuclear Science and Engineering*, **2**, 797 , 1957.

R. B. Briggs. Molten-Salt Reactor Program Semiannual Progress Report for Period Ending August 31, 1965. Technical Report ORNL-3872, Oak Ridge National Laboratory, 1965.

R. B. Briggs. Molten-Salt Reactor Program Semiannual Progress Report for Period Ending August 31, 1966. Technical Report ORNL-4037, Oak Ridge National Laboratory, 1967.

J. E. Brocklehurst and B. T. Kelly. Analysis of the dimensional changes and structural changes in polycrystalline graphite under fast neutron irradiation. *Carbon*, **31**, 155, 1993.

A. Cammi et al. A multy-physics modelling approach to the dynamics of molten salt reactors. *Annals of Nuclear Energy*, **38**, 1356, 2011.

G. I. Cathers, M. R. Bennett and R. L. Jolley. The Fused Salt-Fluoride Volatility Process for Recovering Uranium. Technical Report ORNL-2661, Oak Ridge National Laboratory, 1959.

J. M. Chandler and S. E. Bolt. Preparation of Enriching Salt ^{7}LiF-^{233}UF for Refueling the Molten Salt Reactor. Technical Report ORNL-4371, Oak Ridge National Laboratory, 1969.

J. C. Clayton. The shippingport pressurized water reactor and light water breeder reactor. In *25th Central Regional Meeting, American Chemical Society*, 1993.

W. B. Cottrell et al. Operation of the Aircraft Reactor Experiment. Technical Report ORNL-1845, Oak Ridge National Laboratory, 1955.

S. Delpech et al. Reactor physic and reprocessing scheme for innovative molten salt reactor system. *Journal of Fluorine Chemistry*, **130**, 11, 2009.

M. Deplech et al. Benchmark of dynamic simulation tools for molten salt reactors. In *Proceedings of the GLOBAL 2003 International Conference*, 2003.

S. Dulla and P. Ravetto. Interactions between fluid-dynamics and neutronics phenomena in the physics of molten-salt systems. *Nuclear Science and Engineering*, **155**, 475, 2007.

S. Dulla, P. Ravetto and M. M. Rostagno. Neutron kinetics of fluid-fuel systems by the quasi-static method. *Annals of Nuclear Energy*, **31**, 1709, 2004.

W. K. Ergen et al. The aircraft reactor experiment - physics. *Nuclear Science and Engineering*, **2**, 826 , 1957.

J. L. Everett and E. J. Kohler. Peach bottom unit no. 1: A high performance helium cooled nuclear power plant. *Annals of Nuclear Energy*, **5**, 321, 1978.

K. Furukawa, K. Mitachi and Y. Kato. Small molten-salt reactors with a rational thorium fuel-cycle. *Nuclear Engineering and Design*, **136**, 157 , 1992.

K. Furukawa et al. A road map for the realization of global-scale thorium breeding fuel cycle by single molten-fluoride flow. *Energy Conversion and Management*, **49**, 1832 , 2008.

U. Gat and J. R. Engel. Non-proliferation attributes of molten salt reactors. *Nuclear Engineering and Design*, **201**, 327 , 2000.

Generation IV International Forum. A Technology Roadmap for Generation IV Nucleear Energy Systems. Technical Report GIF-002-00, U.S. DOE Nuclear Energy Research Advisory Committe and the Generation IV International Forum, 2002.

A. A. Harms. Fissile Fuel Dynamics of Breeder/Converter Reactors. *Annals of Nuclear Energy*, **5**, 65, 1978.

P. N. Haubenreich and J. R. Engel. Experience with the molten-salt reactor experiment. *Nuclear Applications and Technology*, **8**, 118, 1970.

J. R. Hightower and L. E. McNeese. Low-Pressure Distillation of Molten Fluoride Mixtures: Nonradioactive Tests for the MSRE Distillation Experiment. Technical Report ORNL-4434, Oak Ridge National Laboratory, 1971.

J. R. Hightower et al. Low-Pressure Distillation of a Portion of the Fuel Carrier Salt from the Molten Salt Reacot Experiment. Technical Report ORNL-4577, Oak Ridge National Laboratory, 1971.

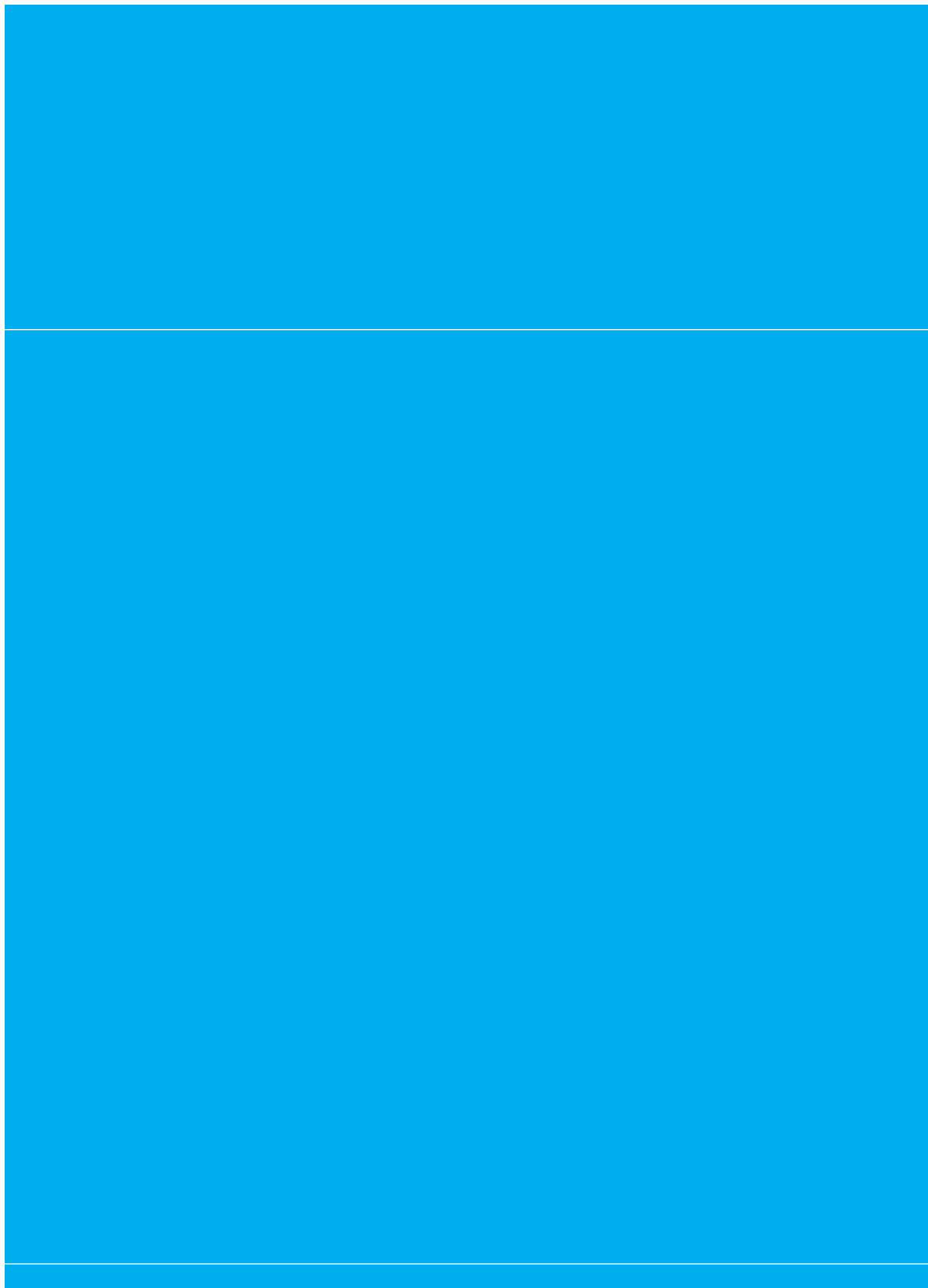IAEA. Thorium fuel cycle - potential benefits and challenges. Technical Report IAEA-TECHDOC-1450, IAEA, 2005.

V. Ignatiev et al. Progress in Development of Li,Be,Na/F Molten Salt Actinide Recycler & Transmuter Concept. In *Proceedings of the ICAPP 2007 International Conference*, 2007.

S. Kakac and H. Liu. *Heat exchangers: selection, rating and thermal design*. CRC Press, 2nd edition, 2002.

P. R. Kasten, E. S. Bettis and R. C. Robertson. Desing Studies of 1000-MW(e) Molten-Salt Breeder Reactors. Technical Report ORNL-3996, Oak Ridge National Laboratory, 1966.

M. Kazimi. Thorium fuel for nuclear energy. *American Scientist*, **91**, 2003.

B. T. Kelly. Graphite - the most fascinating nuclear material. *Carbon*, **20**, 3, 1982.

R. Konings and J. Van der Meer. Chemical Aspects of Molten Salt Reactor Fuel and Coolant. Technical Report MOST-D6, European Commission, FIKW-CT-2001-00096, 2003.

J. Kophazi, D. Lathouwers and J. Kloosterman. Development of a three-dimensional time-dependent calculation scheme for molten salt reactors and validation of the measurement data of the molten salt reactor experiment. *Nuclear Science and Engineering*, **163**, 118, 2009.

J. Kophazi et al. Reactor Physics Study, Design Review and Nominal Operating Conditions, Non Proliferation Issues. Technical Report FIKW-CT-2001-00096, European Commission 5th Framework Programme, 2003.

J. Kophazi et al. Effect of fuel mixing phenomena on the kinetic behavior of molten salt reactors. *Transport Theory and Statistical Physics*, **36**, 227, 2007.

J. Krepel et al. Dyn1d-msr dynamics code for molten salt reactors. *Annals of Nuclear Energy*, **32**, 1799, 2005.

J. Krepel et al. Dyn3d-msr spatial dynamics code for molten salt reactors. *Annals of Nuclear Energy*, **34**, 449, 2007.

J. Krepel et al. Dynamics of molten salt reactors. *Nuclear Technology*, **164**, 34, 2008.

G. Lapenta, F. Mattioda and P. Ravetto. Point kinetic model for fluid fuel systems. *Annals of Nuclear Energy*, **28**, 1759, 2001.

G. Lapenta and P. Ravetto. Basic reactor physics problems in flui-fuel recirculated reactors. *Kerntechnik*, **65**, 250, 2000.

D. LeBlanc. Molten salt reactors: A new beginning for an old idea. *Nuclear Engineering and Design*, **240**, 1644, 2010.

D. Lecarpentier and V. Carpentier. A neutronic program for critical and nonequilibrium study of mobile fuel reactors: The cinsf1d code. *Nuclear Science and Engineering*, **143**, 33, 2003.

D. Lecarpentier et al. Temperature Feedbacks of a Thermal Molten Salt Reactor: Compromise between Stability and Breeding Performance. In *Proceedings of ICAPP 2003 International Conference*, 2003.

H. G. MacPherson. Molten Salt Reactor Program Quarterly Progress Report for Period Ending January 31, 1958. Technical Report ORNL-2474, Oak Ridge National Laboratory, 1958a.

H. G. MacPherson. Molten Salt Reactor Program Status. Technical Report ORNL-2634, Oak Ridge National Laboratory, 1958b.

H. G. MacPherson. The Molten Salt Reactor Adventure. *Nuclear Science and Engineering*, **90**, 374, 1985.

L. Mathieu et al. Thorium Molten Salt Reactor: From High Breeding to Simplified Reprocessing. In *Proceedings of the GLOBAL 2003 International Conference*, 2003.

L. Mathieu et al. The thorium molten salt reactor: Moving on from MSBR. *Progress in Nuclear Energy*, **48**, 664, 2006.

L. Mathieu et al. Possible Configurations for the Thorium Molten Salt Reactor and Advantages of the Fast Nonmoderated Version. *Nuclear Science and Engineering*, **161**, 78, 2009.

H. E. McCoy et al. New developments in materials for molten-salt reactors. *Nuclear Applications and Technology*, **8**, 156, 1970.

E. Merle-Lucotte et al. Influence of the Processing and Salt Composition on the Thorium Molten Salt Reactor. *Nuclear Technology*, **163**, 358, 2008.

E. Merle-Lucotte et al. Optimizing the Burning Efficiency and the Deployment Capacities of the Molten Salt Fast Reactor. In *Proceedings of the International Conference Global 2009*, 2009.

K. Mitachi, T. Yamamoto and R. Yoshioka. Three-Region Core Design for 200 MWe Molten-Salt Reactor with Thorium-Uranium Fuel. *Nuclear Technology*, **158**, 348, 2007.

K. Nagy et al. Parametric Studies on the Fuel Salt Composition in Thermal Molten Salt Breeder Reactors. In *Proceedings of PHYSOR 2008 International Conference*, 2008.

K. Nagy et al. Definition of Breeding Gain for Molten Salt Reactors. In *Proceedings of PHYSOR 2010 International Conference*, 2010.

C. Nicolino et al. Coupled dynamics in the physics of molten salt reactors. *Annals of Nuclear Energy*, **35**, 314, 2008.

A. Nuttin et al. Potential of Thorium Molten Salt Reactors: Detailed Calculations and Concept Evolution with a View to Large Scale Energy Production. *Progress in Nuclear Energy*, **46**, 77, 2005.

K. O. Ott and R. C. Borg. Fast Reactor Burnup and Breeding Calculation Methodology. *Progress in Nuclear Energy*, **5**, 201, 1980.

I. Pazsit and A. Jonsson. Reactor kinetics, dynamic response, and neutron noise in molten salt reactors. *Nuclear Science and Engineering*, **167**, 61, 2011.

A. M. Perry and H. F. Bauman. Reactor physics and fuel-cycle analyses. *Nuclear Applications and Technology*, **8**, 208, 1970.

B. E. Prince et al. Zero-Power Physics Experiments on the Molten-Salt Reactor Experiment. Technical Report ORNL-4233, Oak Ridge National Laboratory, 1968.

C. Renault et al. The MOST project: Key-Points and Challenges for the Feasibility of Molten Salt Reactors. In *Proceedings of the ICAPP 2005 International Conference*, 2005.

A. Rineiski et al. Safety-related neutronics parameters of a molten salt actinide recycler and transmuter. In *Proceedings of the PHYSOR 2006 International Conference*, 2006.

R. C. Robertson. MSRE Design and Operations Report, Part I - Description of Reactor Design. Technical Report ORNL-TM-278, Oak Ridge National Laboratory, 1965a.

R. C. Robertson. MSRE Design and Operations Report, Part I, Description of Reactor Design. Technical Report ORNL-TM-728, Oak Ridge National Laboratory, 1965b.

R. C. Robertson. Conceptual Design Study of a Single-Fluid Molten-Salt Breeder Reactor. Technical Report ORNL-4541, Oak Ridge National Laboratory, 1971.

R. C. Robertson et al. Two-Fluid Molten-Salt Breeder Reactor Design Study. Technical Report ORNL-4528, Oak Ridge National Laboratory, 1970.

M. W. Rosenthal. Molten-Salt Reactor Program Semiannual Progress Report for Period Ending February 28, 1966. Technical Report ORNL-4119, Oak Ridge National Laboratory, 1967.

M. W. Rosenthal. Molten-Salt Reactor Program Semiannual Progress Report for Period Ending August 31, 1968. Technical Report ORNL-4344, Oak Ridge National Laboratory, 1969a.

M. W. Rosenthal. Molten-Salt Reactor Program Semiannual Progress Report for Period Ending February 28, 1969. Technical Report ORNL-4396, Oak Ridge National Laboratory, 1969b.

M. W. Rosenthal. Molten-Salt Reactor Program Semiannual Progress Report for Period Ending August 31, 1969. Technical Report ORNL-4449, Oak Ridge National Laboratory, 1970.

M. Salvatores. Fast reactor calculations. In *Handbook of Nuclear Reactor Calculations*. CRC Press, Bota Raton, Florida, 1986.

H. C. Savage and J. R. Hightower. Engineering Tests of the Metal Transfer Process for Extraction of Rare-Earth Fission Products from a Molten-Salt Breeder Reactor Fuel Salt. Technical Report ORNL-5176, Oak Ridge National Laboratory, 1977.

A. W. Savolainen. Aircraft Nuclear Propulsion Project Quarterly Progress Report for Period Ending December 10, 1954. Technical Report ORNL-1816, Oak Ridge National Laboratory, 1955.

SCALE. *A Modular Code System for Performing Standardized Computer Analyses for Licensing Evaluations*, 2005. ORNL/TM-2005/39, Version 5, Vols I-III, Oak Ridge National Laboratory.

SCALE. *A Modular Code System for Performing Standardized Computer Analyses for Licensing Evaluations*, 2009. ORNL/TM-2005/39, Version 6, Vols I-III, Oak Ridge National Laboratory.

D. Schwarz and R. Baumer. Thtr operating experience. *Nuclear Engineering and Design*, **109**, 199, 1988.

C. D. Scott and W. L. Carter. Preliminary Design Study of a Continuous Fluorination - Vacuum-Distillation System for Regenerating Fuel and Fertile Streams in a Molten Salt Breeder Reactor. Technical Report ORNL-3791, Oak Ridge National Laboratory, 1966.

E. Symons. Lithium isotope separation: A review of possible techniques. *Separation Science and Technology*, **20**, 633 , 1985.

E. Teller. Remarks on the thorium cycle. *Annals of Nuclear Energy*, **5**, 287 , 1978.

J. Uhlir et al. Review and analysis of the fuel processing and waste form studies. Technical Report FIKW-CT-2001-00096, European Commission 5th Framework Programme, 2003.

W. Van Rooijen. *Improving Fuel Cycle Design and Safety Characteristics of a Gas Cooled Fast Reactor*. Ph.D. thesis, Delft University of Technology, 2006.

W. Van Rooijen et al. Definition of breeding gain for the closed fuel cycle and application to a gas-cooled fast reactor. *Nuclear Science and Engineering*, **157**, 185, 2007.

A. van Wijk. *Computational Modeling of the Flow Field in a Molten Salt Reactor Core*. Master's thesis, Delft University of Technology, 2008. PNR-131-2008-009.

J. Vergnes and D. Lecarpentier. The AMSTER concept (Actinides Molten salt TransmutER). *Nuclear Engineering and Design*, **216**, 43, 2002.

S. Wang, A. Rineiski and W. Maschek. Molten salt related extensions of the simmer-iii code and its applications for a burner reactor. *Nuclear Engineering and Design*, **236**, 1580, 2006.

D. F. Williams, L. M. Toth and K. T. Clarno. Assessment of Candidate Molten Salt Coolants for the Advanced High-Temperature Reactor. Technical Report ORNL/TM-2006/12, Oak Ridge National Laboratory, 2006.

D. L. Zhang et al. Analysis on the neutron kinetics for a molten salt reactor. *Progress in Nuclear Energy*, **51**, 624, 2009a.

D. L. Zhang et al. Development of a steady ste analysis code for a molten salt reactor. *Annals of Nuclear Energy*, **36**, 590, 2009b.

E. Ziermann. Review of 21 years of power operation at the avr experimental nuclear power station in juelich. *Nuclear Engineering and Design*, **121**, 135, 1990.

Appendix A

Modification of the LOWFAT code

No material evolution code was available for the author that can perform all the specific tasks required to simulate the operation of an MSR. Most of the software developed for solid fuel reactors incorporate the capability to continuously remove elements from the irradiated material; however, it is necessary to track the evolution of some isotopes which were removed from the fuel salt. A good example for this is the removal of protactinium. The ^{233}Pa is removed from the core to prevent it from capturing a neutron and to allow it to decay to ^{233}U outside of the neutron flux. The formed might be sent back to the core depending on the reactivity control. This mechanism needs to be captured in the model in order to accurately model the fuel cycle of the MSR. For this reason, a new dedicated burn-up code was developed on the basis of the existing in-house developed LOWFAT code. For the full description and validation of the code, the interested reader is referred to (Van Rooijen, 2006).

A.1 Modification of the transmutation equation

The transmutation equatio for any nuclide i is given as:

$$\frac{dN^i}{dt} = -N^i(\sigma_a^i \phi + \lambda^i) + \sum_j y_i^j N^j \sigma_f^j \phi + \sum_k N^k \sigma_{c,i}^k \phi + \sum_l \lambda_i^l N^l + Q^i \qquad \text{(A.1)}$$

where N_i, σ^i, λ^i and y^i are the atomic density, the cross-section, the decay constant and the yield of nuclide i, respectively; and ϕ is the flu in the reactor. Here, Q^i is a source term which describes the continuous feed of nuclide i. However, the continuous removal is not incorporated in the equation. This was added by introducing a pseudo decay constant which is defined based on the throughput of the processing plant and on the efficiency of the removal method. The loss term on the right hand side of Eq. A.1 has to be modified to include the sum of the two effects. The total decay constant of an isotope that is removed is the sum of the two decay constants. The transmutation equation of a given nuclide i which is continuously removed by a purification process is the following, with the notation λ_{pp}^i used for the pseudo decay constant:

$$\frac{dN^i}{dt} = -N^i(\sigma_a^i \phi + \lambda^i + \lambda_{pp}^i) + \sum_j y_i^j N^j \sigma_f^j \phi + \sum_k N^k \sigma_{c,i}^k \phi + \sum_l \lambda_i^l N^l + Q^i \quad \text{(A.2)}$$

The above two equations descibe all the processes occuring in the reactor core but the equation of the nuclide residing in the storage/stockpile are still needed. For these nuclides, another transmition equation is introduced:

$$\frac{dN^{is}}{dt} = \lambda^i(N^i - {}^{is}) + \sum_l \lambda_i^l N^l - Q^i \qquad (A.3)$$

where N^{is} is the atomic density of nuclide i in the storage. The transmutation equation of the salt mixture in the core and in the stockpile consists of a set of coupled ODEs of Eq. A.1, Eq. A.2 and Eq. A.3. This set of ODEs can be re-written in matrix notation as:

$$\frac{\partial \bar{N}}{\partial t} = \bar{\bar{M}} \bar{N} + \bar{Q} \qquad (A.4)$$

A.2   Nuclear data

The LOWFAT code can read the nuclear data library produced by the COUPLE module of the SCALE system. This data is representative for the specific problem because it is based on a cell calculation of the lattice cell geometry. All the nuclides of the library are considered in this version of LOWFAT; thus, all the components of the salt and the FPs are included in the calculations.
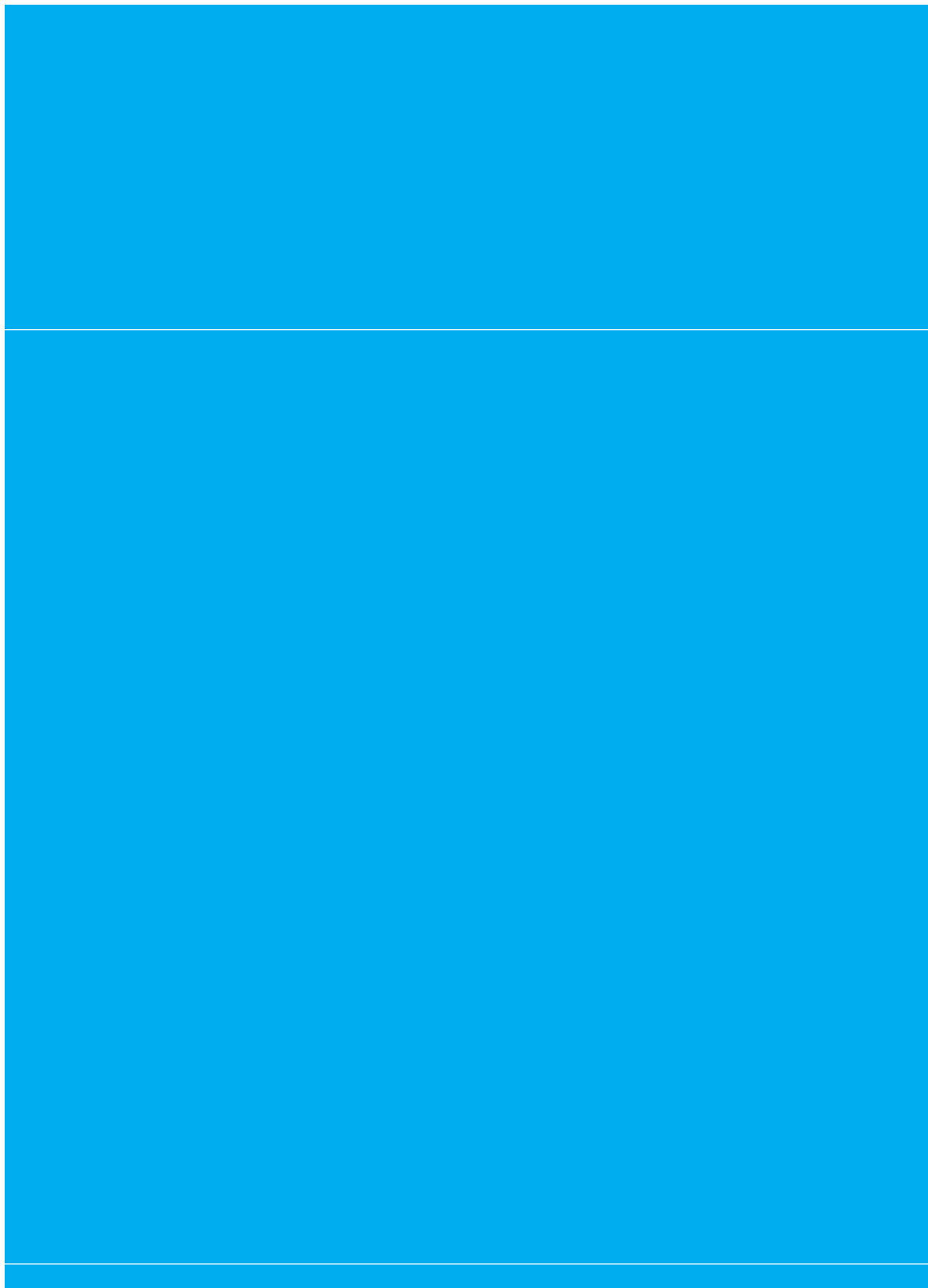
Appendix B

Relation of the proposed BG definitions to the old ones

The breeding ratio of MSR was calculated by several authors (Nuttin et al., 2005; Mathieu et al., 2006; Nagy et al., 2008; Mathieu et al., 2009) in a simple form (see Chap. 3.6 for reaction rate definitions):

$$BR = \frac{R_c^{02} - R_c^{13}}{R_a^{23}} \tag{B.1}$$

This definition is true only after the thorium and protactinium reached their equilibrium concentration so the time dependence is omitted. Breeding gain can be easily formed from this definition by substracting 1 since the consumption rate is in the denominator. The extension to accompany ^{235}U is straightforward:

$$BG = \frac{R_c^{02} - R_c^{13} + R_c^{24}}{R_a^{23} + R_a^{25}} - 1 \tag{B.2}$$

This form can be compared with the BG definitions proposed in this thesis. The main difference is the lack of the decay term of protactinium. Hereby will be proven that the numerator of eq. B.1 equals the total decay rate of ^{233}Pa in the core and in the stockpile together and that eq. B.2 (and eq. B.1) gives the uranium production in the core and the stockpile together at equilibrium. In order to do this, the Bateman equation of the ^{233}Pa is supplemented with a pseudo-decay describing the removal rate of protactinium through its mean residence time.

$$\frac{dN^{13}(t)}{dt} = \sigma_c^{02} N^{02}(t)\phi(t) - \sigma_c^{13} N^{13}(t)\phi(t) - \lambda N^{13}(t) - \frac{1}{\tau^{13}} N^{13}(t) \tag{B.3}$$

In the equation direct production of ^{233}Pa by capture of ^{232}Th is assumed and the residence time is denoted as τ. At equilibrium, the numerator of eq. B.1 equals the total decay of ^{233}Pa in the core:

$$\sigma_c^{02} N^{02}\phi - \sigma_c^{13} N^{13}\phi = \lambda N^{13} - \frac{1}{\tau^{13}} N^{13} \tag{B.4}$$

Similarly a Bateman equation can be written for the ^{233}Pa extracted to the stockpile in which the only production term is the extraction from the core and the loss term is the decay of protactinium. At equilibrium, the two terms equal:

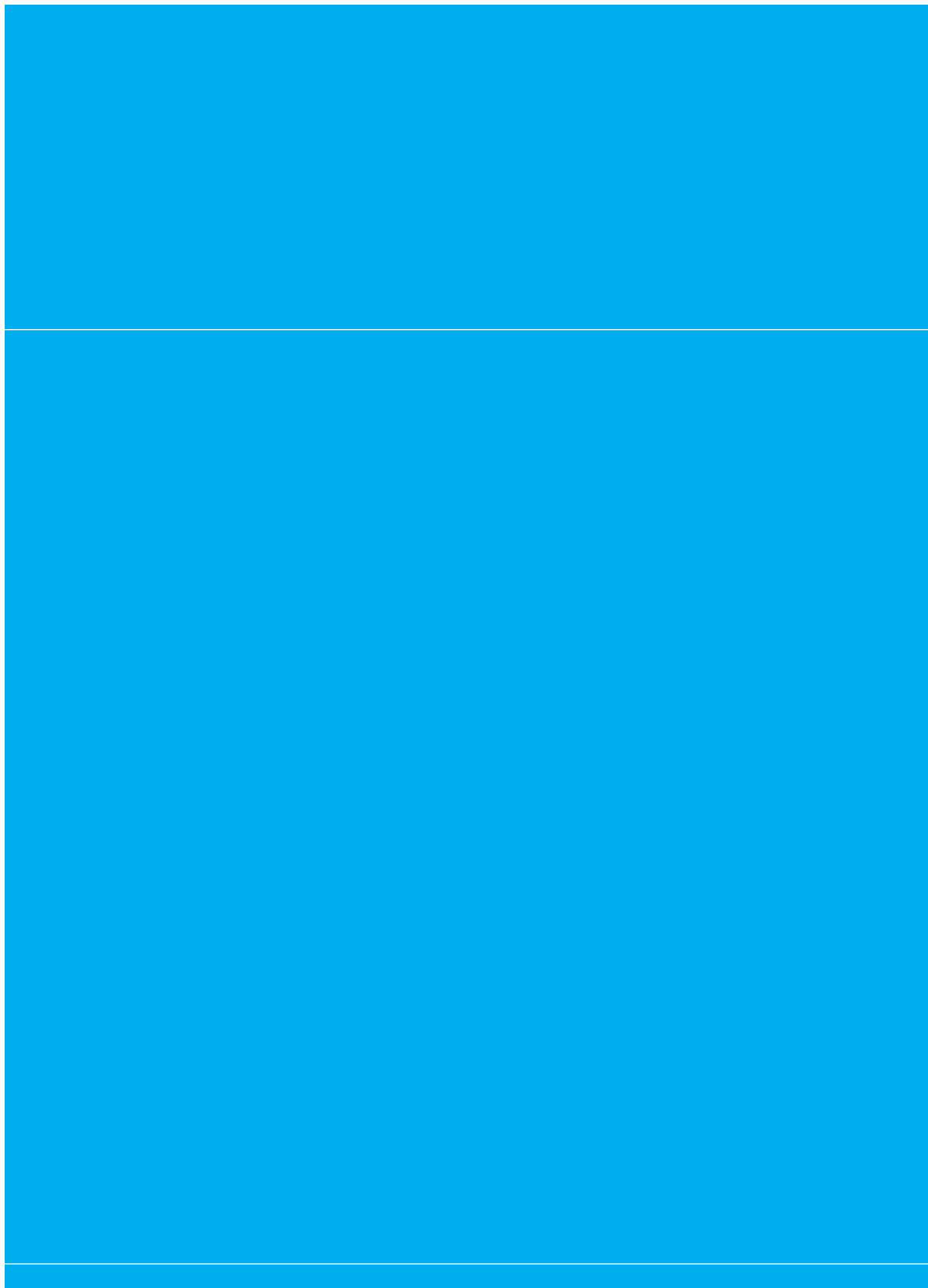$$\lambda N^{13stock} = \frac{1}{\tau^{13}} N^{13}$$

(B.5)

Combining eq. B.4 and B.5 gives that the decay rate of ^{233}Pa in the core and in the stockpile together equals the numerator of eq. B.1:

$$\sigma_c^{02} N^{02} \phi - \sigma_c^{13} N^{13} \phi = \lambda N^{13} + \lambda N^{13stock}$$

(B.6)

The total decay rate can not be found in the BG definitions in eq. 3.11, 3.12 and 3.13 since those are defined separately for the core and the stock. BG describing the core and the stockpile has to be summed to obtain the right hand side of eq. B.6:

$$
\begin{aligned}
BG &= BG_{critical} + BG_{stock} \\
&= \frac{R_d^{13}(t) + R_c^{24}(t) + R_{fe}^{23}(t)}{R_a^{23}(t) + R_a^{25}(t)} - 1 \\
&+ \frac{R_d^{13stock}(t) - R_{fe}^{23}(t)}{R_a^{23}(t) + R_a^{25}(t)} \\
&= \frac{R_d^{13}(t) + R_d^{13stock}(t) + R_c^{24}(t)}{R_a^{23}(t) + R_a^{25}(t)} - 1 \\
&\cong \frac{R_c^{02} - R_c^{13} + R_c^{24}}{R_a^{23} + R_a^{25}} - 1
\end{aligned}
$$

(B.7)

Eq. B.7 is the total increase of fissile material in the core and the stockpile together. It is concluded that the sum of eq. 3.11 and 3.13 equals eq. B.2 as eq. B.6 is applied as an approximation. This expression (eq. B.7) does not distinguish between the increase needed to run the reactor and the increase of the excess material. Thus, eq. B.1 and B.2 describe the total increase of ^{233}U and the total increase of fissile uranium isotopes, respectively. In case of a reactor which employs Pa extraction, these definitions do not describe the evolution of the excess ^{233}U.

Appendix C

The FLOW code

Here the computer code which calculates the flow field in a channel type MSR is described and validated. The calculation is performed on a 2D r-z mesh which is divided into three zones axially, the two plena and the core. The presented code is based on the Bachelor-End-Project of Andreas van Wijk (van Wijk, 2008). The governing equations of the fluid, together with the necessary simplifications and assumptions are discussed. Later, the discretization of the equations and the geometry of the problem is described. Finally, the code is validated against experimental data on the MSRE.

C.1   Description of the geomerty

In a MSR the fuel salt flows from the bottom to the top. In case of a moderated reactor, the active core consists of a graphite moderator interior. The fuel salt passes through the channels of this graphite structure. The fuel salt enters the dividing plenum below the graphite moderator and distributes over the vertical channels. Swirl-straightening vanes eliminate the azimuthal component of the fuel velocity in the plenum. This process reduces the radial pressure gradient and results in a more even flow distribution through the core. The salt is assumed to enter the plenum radially, which is the case in most of the reactor designs. After passing the graphite core, the fuel recombines in the collecting plenum above the core and leaves the reactor vessel through an axial pipe located at the center.

   The model of the reactor core consists of 3 axial zones, such as the two plena and the core. The geometry of the model is shown in Figure C.1. As a result, the radial velocity component is averaged over the height of each zone. A fine discretization in the radial direction makes the full r-z mesh of the MSR. In the zone of the graphite structure, the numerous fuel channels are replaced by a uniformly porous medium. The effects of the fluid entering and leaving the channels is taken into account by using local pressure loss and regain coefficients.

C.2   Governing equations

In this computer code, the Navier-Stokes equations are solved for an incompressible fluid. This assumption was chosen because the density variations are small in the primary loop of the reactor; thus, the effect of a non-uniform density on the flow field is small. Furthermore, the DALTON code - which calculates the precursor concentrations in the primary loop - uses a flow field assuming a constant density. This is necessary because the density is neither provided as an input nor calculated in the DALTON code. In the calculation scheme of the temperature (see Appendix E) of the fuel salt the effect of the non-uniform density is superimposed on the flow field obtained by this code.

   Using the assumption of constant density, the conservation of mass is written as:

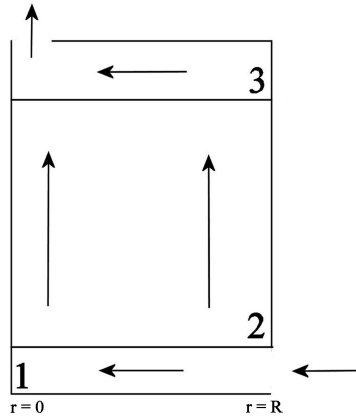$$\nabla \cdot \vec{v} = 0 \tag{C.1}$$

Figure C.1: The modelled geometry of the reactor. The dividing plenum with the radial inflow is labeled as zone 1. The active core of the reactor (zone 2) is is filled with a porous medium. The combinig plenum is denoted as zone 3. The outflow is located on the top of the plenum. The arrows indicate the direction of the flow.

After applying the conservation of mass (eq. C.1), the conservation of momentum reads as:

$$\frac{\partial \vec{v}}{\partial t} + \nabla \cdot \vec{v}\vec{v} = -\frac{1}{\rho}\nabla p + \frac{1}{\rho}\nabla \cdot \bar{\bar{\tau}} \tag{C.2}$$

In these equations v, p, ρ and τ denote the velocity, pressure, density and the stress tensor, respectively. The above equations applied for the r-z mesh become:

$$\frac{1}{r}\frac{\partial ru}{\partial r} + \frac{\partial w}{z} = 0 \tag{C.3}$$

$$\rho\frac{\partial u}{\partial t} + \rho\frac{1}{r}\frac{\partial ruu}{\partial t} + \rho\frac{\partial uw}{\partial z} = -\frac{\partial p}{\partial r} + [\nabla \cdot \bar{\bar{\tau}}]_r \tag{C.4}$$

$$\rho \frac{\partial w}{\partial t} + \rho \frac{1}{r} \frac{\partial rwu}{\partial t} + \rho \frac{\partial ww}{\partial z} = -\frac{\partial p}{\partial z} + [\nabla \cdot \bar{\bar{\tau}}]_z \tag{C.5}$$

in which u and w represent the radial and axial components of the velocity.

At the entrance and exit of the fuel channels the flow has to turn. The fluid loses its radial momentum upon entering the channels and disturbs the flow in the collecting plenum as leaves the channels. Whenever the flow is diverted to a branch and the flow area changes, there is a change in velocity. If there is no loss, the change in the velocity is converted into a regain in static pressure. However, due to dynamic losses, the actual static pressure regain is reduced. The two processes (entering and leaving the branch) are not symmetric, this is represented in the different value of the two coefficients. In the combining flow case a negative loss coefficient can occur which implies that the energy of the through flow is increased by a jet pump action of the high-velocity flow from the channels. Therefore, a static pressure regain and loss coefficients are introduced at the inflow and outflow of the channels, respectively. The cross-term in the radial momentum equation is multiplied with these coefficients:

$$\Delta p \approx K \rho \frac{v^2}{z} \tag{C.6}$$

$$\rho \frac{\partial u}{\partial t} + \rho \frac{1}{r} \frac{\partial ruu}{\partial t} + \rho K \frac{\partial uw}{\partial z} = -\frac{\partial p}{\partial r} + [\nabla \cdot \bar{\bar{\tau}}]_r \tag{C.7}$$

where K denotes the pressure regain or loss coefficient depending on the axial position.

The pressure loss due to the wall shear stress is taken into account in the plena and in the core. Generally, it is written as follows:

$$\nabla \cdot \tau = -4f(Re)\rho v \frac{|v|}{2D_h} \tag{C.8}$$

Here v denotes the radial velocity u or axial velocity w, $f(Re)$ represents the Fanning friction factor and D_h the hydraulic diameter. The friction factor is calculated as:

$$f(Re) = \left\{ \left(16Re^{-1} \right)^{20} + \left(0.079Re^{-0.25} \right)^{20} \right\}^{1/20} \tag{C.9}$$

$$Re = \frac{\rho v D_h}{\mu}$$

The hydraulic diameter of the plenums, assuming swirl vanes but neglecting the thickness of those, is given as:

$$D_h(r) = \frac{4A}{S} = \frac{4 \frac{2r\pi}{n} Z_{pl}}{2\frac{2r\pi}{n} + 2Z_{pl}} = \frac{2Z_{pl}}{1 + \frac{nZ_{pl}}{2r\pi}} \tag{C.10}$$

Z_{pl} and n being the height of the plenum and the number of the swirl vanes, while it is calculated in the porous media in the following way:

$$D_h = \frac{4\alpha}{\beta} \tag{C.11}$$

$$\alpha = \frac{total\ flow\ area\ of\ the\ channels}{flow\ area\ of\ the\ porous\ medium}$$

$$\beta = \frac{total\ wetted\ perimeter\ of\ the\ channels}{flow\ area\ of\ the\ porous\ medium}$$

C.3   Discretization and solution algorithm

The equations are discretized using the finite volume method. The reactor is divided into 3 axial regions and n radial volumes in a cylindrical coordinate system. The scalar variables are stored in the centerpoints of the volumes while the velocities are stored on the faces of the finite volumes. A turning loss coefficient is introduced in order to account for the pressure losses due to turning effects. When pressure is extrapolated to a volume face which is the inflow or outflow surface of the channels, the local pressure is given by the Bernoulli equation of the following form:
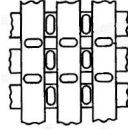
Figure C.2: View from the top of core-support bars with the fuel channels

$$p^{i,j} - p^{i,j}_{z\ +/-} = \rho(1+T)\frac{(w^{i,j}_{z\ +/-})^2}{2} \qquad (\text{C.12})$$

Here T denotes the turning loss and the subscripts refer to the faces of volume i, j. The implicit Euler scheme is used to discretize the equation in time. The non-linear terms of the momentum equations are linearized by replacing some of the variables with the value of those in the previous time step. The flow field is calculated based on a frozen pressure field which is based on the previous time step of the calculation. The use of this pressure field results in a velocity field after solving the momentum balance equations (eq. C.7 and C.5) which does not fulfill the mass conservation. A correction on the velocity field is calculated based on the assumption that the velocity correction is caused by the correction in the pressure is continuity is enforced.

C.4 Validation

The computer code was validated using the results of the hydraulic experiments conducted in the Molten Salt Reactor Programme at ORNL. One-fifth and full-scale model studies were performed to investigate the flow distribution in the reactor (Robertson, 1965b). The volumetric flow was measured in several fuel channels, both in a group of north-south and east-west aligned ones (see Fig. C.2). These flow studies made on the full-scale model showed that the flow through the north-south fuel passages was about 10% less than that through the east-west passages because the upper lattice blocks slightly obstructed the entrance. The volumetric flow rate through a typical core passage was roughly 1 gpm (gallon-per-minute), with about 20% more flowing through the passages toward the center than those near the periphery of the core. A linear equation (volumetric flow as a function of radial position) was fitted on the measured data which is shown in the same figure as the results of the current calculations.

For the actual calculations, the physical properties of the fuel salt of the MSRE were calculated at the mean temperature of the core, 922 K. The geometry and the properties of the salt are listed in Table C.1. The geometrical data and the properties of the fluid, together with the result of the experiments were taken from (Robertson, 1965b). The values for the pressure regain and decrease coefficients and the turning loss were chosen based on experimental values from (Bajura and Jones, 1976).

Table C.1: Input of the code (at nominal MSRE operating conditions)

Parameter	Value	Unit
Height of the plenums	0.1831	m
Radius of the reactor	0.7017	m
Height of the core	1.6256	m
Radius of the outflow pipe	0.0635	m
Number of radial volumes	180	
α	0.225	
β	53.4738	1/m
Hydraulic diameter (single channel)	0.0167	m
Inflow velocity	0.09378	m/s
Density	2082.4	kg/m^3
Viscosity	0.0070274	Pa s
Pressure regain coefficient	0.95	
Pressure decrease coefficient	-0.9	
Turning loss	0.9	

The calculated results and the original linear fit with the error margins is shown on Figure C.3. A strong peak can be found in the results of the calculation which is located under the outflow pipe. This is a result of the geometry of the outflow. The outflow surface area of the combining plenum is much smaller than the cross-section of the reactor so the flow has to accelerate near the outflow. This causes a local pressure drop in the plenum under the outflow which accelerates the salt in the channels under the outflow. The strength of this effect depends on the size of the outflow area; thus, the peak moves and reduces in amplitude if the radius of the outflow is increased. The calculated velocity distribution is in good agreement with the experimental results. The linear fit on the calculated values is $0.01m/s$ off from the fit on the experimental data but most probably a first order function does not describe the velocity distribution properly. Several calculations were performed with different number of radial volumes, pressure coefficients and turning loss. These calculations show that the results are independent of the radial mesh if the radius of the outflow is located on a volume face, and the results are insensitive of the choice of the various pressure loss and regain parameters.
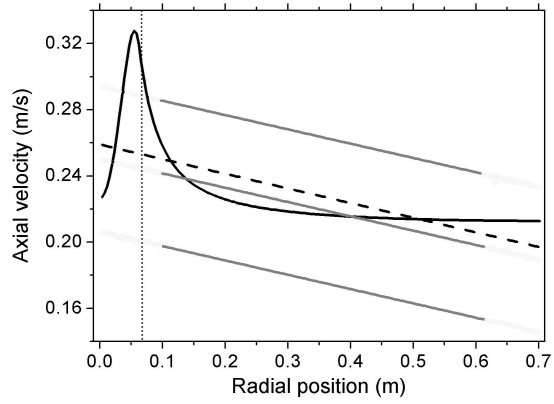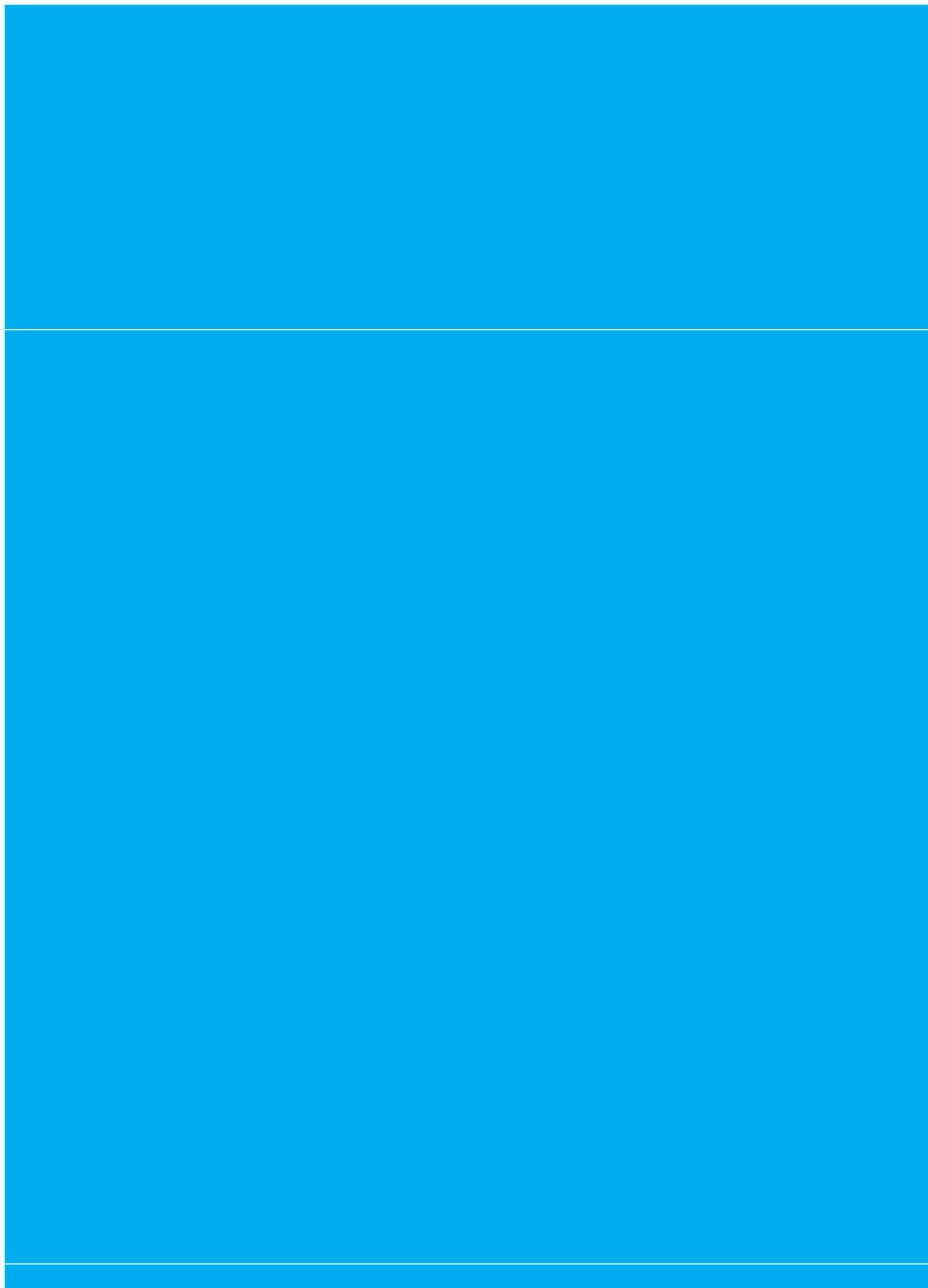
Figure C.3: The axial velocity in the reactor core as a function of radial position (black line). The original linear fit on the experimental data together with the standard deviation is shown in grey (retreived from (Robertson, 1965b)). The dashed black line shows the linear fit on the calculated results. The upright line shows the radius of the outflow.

Appendix D

The DALTON code

The in-house developed oringinal DALTON code can solve the multigroup diffusion equations on structured grid (xyz or $rz\theta$) in 3D. This code was modified in order to take into account the flow of the fuel salt. The original DALTON had been applied to high-temperature reactor neutronics and time-dependent perturbation theory. A past version of the code had been modified to incorporate the drift of the precursor and applied to time-dependent calculations of the MSRE. However, the flow in that code was modelled as a slug flow. The latest version of DALTON was modified for this study and the code can perform its calculations using a 3D flow field.

D.1   Governing equations

The neutron physics in the DALTON is described by the time-dependent multigroup diffusion theory. The precursor equations were extended by a convection term because the precursors move together with the flowing fuel in an MSR. The new equations read as:

$$\frac{1}{v_g}\frac{\partial \Phi_g}{\partial t} = \nabla \cdot D_g \nabla \Phi_g - \Sigma_g^r \Phi_g + \sum_{g \neq g'}^{G} \Sigma_{g' \to g}^s \Phi_{g'}$$

$$+\chi_g^p \sum_{g'=1}^{G} (1-\beta)\nu\Sigma_{g'}^f \Phi_{g'} + \sum_{i}^{l} \lambda_i \chi_g^{d,i} C_i \tag{D.1}$$

$$\frac{\partial C_i}{\partial t} = \sum_{g'=1}^{G} \beta_i \nu\Sigma_{g'}^f \Phi_{g'} - \lambda_i C_i - \nabla \bar{u} C_i \tag{D.2}$$

Here Φ_g, v_g and D_g note the scalar flux, the neutron velocity and the diffusion coefficint in group g, and Σ_g^r, Σ_g^s and Σ_g^f stand for the removal, scatter and fission cross-section in group g, respectively. Furthermore, ν, χ_g^p and $\chi_g^{d,i}$ note the average number of neutrons produced per fission, and the groupwise energy spectra of the prompt neutrons and the delayed neutrons of delayed neutron group i. In equation D.2, C_i, β_i and λ_i represents the precursor concentration, delayed neutron fraction and decay constant of precursor group i, and $\bar{u}$ denotes the velocity of the fuel. The diffusion equation is solved only for the reactor core but the precursor concentration equation is solved for the whole primary loop, if the primary loop of the reactor leaves the reactor vessel. In this case, the primary circuit is modelled as a one-dimensional pipe. This way the precursors are mixed in the external part of the loop. In the volumes of the primary loop the neutron flux is zero.

The spatial discretization of the diffusion equation in the original DALTON code is performed using a second order accurate finite volume method:

$$V^k \frac{1}{v_g} \frac{\partial \Phi_g^k}{\partial t} = -L_g^k - V^k \Sigma_g^r \Phi_g + V^k \sum_{g \neq g'}^{G} \Sigma_{g' \to g}^s \Phi_{g'}$$

$$+ V^k \chi_g^p \sum_{g'=1}^{G} (1 - \beta) \nu \Sigma_{g'}^f \Phi_{g'} + V^k \sum_i^l \lambda_i \chi_g^{d,i} C_i \qquad \text{(D.3)}$$

where V^k and L_g^k denotes the volume of mesh element k and the neutron leakege in group g from mesh element k. The neutron leakage term is approximated using the central differential scheme. In order to be consistent with the spatial discretization of the diffusion equation, the precursor equation is discretized using a second order accurate total variation diminishing (TVD) scheme. This is presented here for a one-dimensional flow. The concentrations on the element faces are estimated by the upwind scheme:

$$C_i^{k-1/2} = C_i^{k-1}$$
$$C_i^{k+1/2} = C_i^k \qquad \text{(D.4)}$$

Here the superscripts $k + 1/2$ and $k - 1/2$ denote the incoming and outgoing mesh element face. This estimation is modified with the TVD scheme:

$$C_i^{k+1/2} = C_i^k + \frac{1}{2} \Psi(r)(C_i^k - C_i^{k-1}) \qquad \text{(D.5)}$$

where the van Leer limiter was applied and r represents the ratio of the local gradients of the precursor concentration on the mesh element faces:

$$\Psi(r) = \frac{r + |r|}{1 + r}$$
$$r = \frac{C_i^{k+1} - C_i^k}{C_i^k - C_i^{k-1}} \qquad \text{(D.6)}$$

The discretized equation of the precursors read as:

$$V^k \frac{\partial C_i^k}{\partial t} = V^k \sum_{g'}^{G} \beta_i \nu \Sigma_{g'}^f \Phi_{g'} - V^k \lambda_i C_i^k$$
$$+ p^1 A^{k-1/2,1} u^{k-1/2,1} C_i^{k-1/2,1} - p^1 A^{k+1/2,1} u^{k+1/2,1} C_i^{k+1/2,1}$$
$$+ p^2 A^{k-1/2,2} u^{k-1/2,2} C_i^{k-1/2,2} - p^2 A^{k+1/2,2} u^{k+1/2,2} C_i^{k+1/2,2}$$
$$+ p^3 A^{k-1/2,3} u^{k-1/2,3} C_i^{k-1/2,3} - p^3 A^{k+1/2,3} u^{k+1/2,3} C_i^{k+1/2,3} \qquad \text{(D.7)}$$

where A, u and p denote the surface area of the element face, the velocity on the face and the ratio of the flow area to the surface area on the face. The superscripts 1, 2 and 3 represent either the directions xyz or $rz\theta$.

In the DALTON model, the cross-sections of the core are homogenized in every unit cell. This way, the calculated precursor concentrations are cell averaged values in every mesh element. To be consistent with this, the velocities need to be scaled on the faces of every mesh element which are not filled with only salt. This typically occurs in the core which consists a graphite - salt lattice. The fuel velocity on the faces of these elements is scaled with the ratio of the flow surface area and surface area of the element.

The velocity field is not calculated by DALTON but it is red as an output of a separate program. There is no expilcit density data in DALTON, only implicitly through the group constants in every unit cell, therefore the flow field has to be calculated for an incompressible fluid.

DALTON uses a second-order accurate time-stepping algorithm based on the Backward-2 scheme. This scheme is fully implicit and unconditionally stable. The time derivative in the diffusion and in the precursor equations are discretized as follows:

$$\frac{\partial X}{\partial t} = \frac{3/2 \cdot X^{n+1} - 2 \cdot X^n + 1/2 \cdot X^{n-1}}{\Delta t} \qquad \text{(D.8)}$$

where X represents either the scalar flux or the precursor concentration.

D.2 Static caluclations

The multiplication factor is calculated with the power method in DALTON. This calculation scheme was modified in order to take the fuel velocity into account. One iteration step in the power method is performed as follows:

- New flux guess is made.
- The prompt fission source is calculated based on the flux guess.
- The precursor concentrations for every precursor group are calculated based on the flux guess and on the velocity field.
- The delayed neutron source is calculated based on the precursor concentrations and the prompt and delayed neutron sources are summed.
- This neutron source is used to calculate the new flux guess in a fixed source problem.

D.3   Validation

In order to validate the changes of the DALTON code, and the choices made in the mesh size and in the number of energy groups, some of the experimental results of the MSRE (see Chap. 2.1.3) had been reproduced. These are the uniform temperature feedback coefficients and the reactivity lost due to the fuel flow for the [235]U-based fuel of the MSRE. This fuel composition was chosen because its composition is better known than the [233]U-based one. The calculations were performed on an rz model of the MSRE. The geometry was simplified; the control rods and the downcomer was neglected in the model. The height of the plenums was 18.31 cm while the height of the core was 162.56 cm. The radius of the core was 70.17 cm. Three different mesh sizes were considered both in the radial and in the axial direction. The mesh sizes in the radial direction were chosen to correspond with the size of the actual unit cell (one graphite bar) of the MSRE. Therefore, the radial mesh size was set to one, two and three times the width of one graphite bar.

The weighted, homogenized cross-section sets of the graphite - salt lattice and the plenums were produced by the SCALE code system (SCALE, 2005). One 1D radial and one 1D axial calculation with the same number of radial or axial volumes as the DALTON model was performed with the XSDRN module, which prepared the collapsed cross-section sets. The graphite - salt lattice of the MSRE was modelled as cylidrical fuel channels in a diagonal lattice. The sets were loaded in the volumes of the DALTON mesh. The fuel salt composition was set to 65% LiF - 29.2% BeF2 - 5% ZrF4 - 0.8% UF4 (molar proportions), which was taken from the MOST report (Kophazi et al., 2003). The uranium composition was 32% [235]U and 68% [238]U. The density of the mixture at different temperatures was calculated as it is explained in Chap 4.4.1. The criticality calculations for the temperature feedback evaluation were performed with a stagnant fuel.

The number of axial elements was set to 14, 20 and 28 while the radial mesh was set to 4, 7 and 14. Three different energy group structure was considered with 7, 14 and 21 groups. The energy boundaries were distributed equidistantly on the logarithmic scale in each case. The results are summarized in Table D.1. The reduction of the number of energy groups results in a decrease of the multipilication factor by 200 pcm. The result is more sensitive to the number of elements in the radial direction than to that in the axial direction. This is associated with the small radius of the reactor core and shows that a fine mesh and proper cross-section generation is necessary in the radial direction. In the finest

159

Table D.1: Results of the benchmark calculations

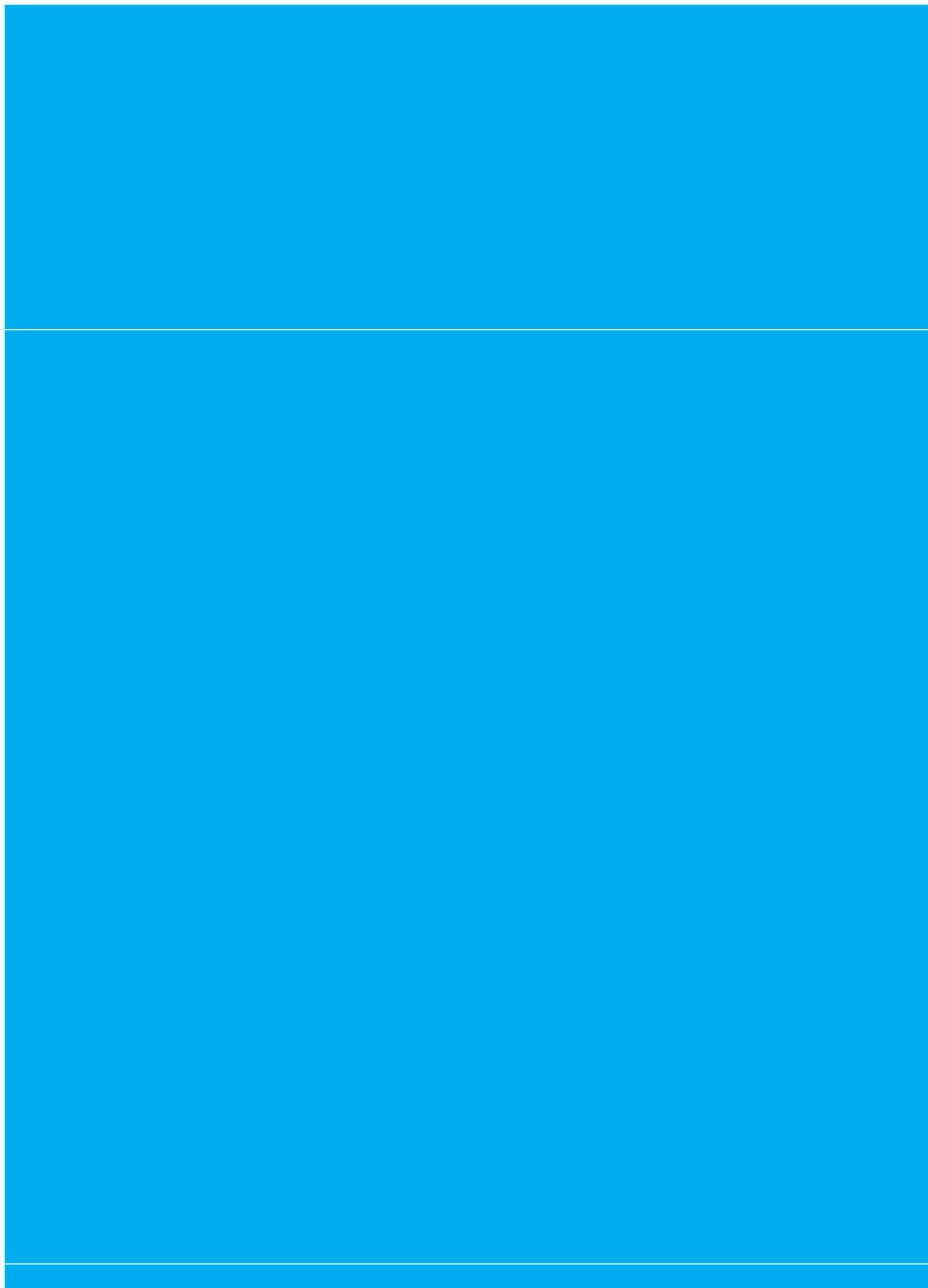| Number of volumes in		Number of energy groups	Temperature of the		Multiplication factor
radial	axial direction		salt (K)	graphite (K)	
14	28	21	923	923	0.996688
14	28	21	1023	1023	0.981846
14	28	21	923	1023	0.990452
14	28	14	923	923	0.994946
14	28	14	1023	1023	0.979811
14	28	14	923	1023	0.988495
14	28	7	923	923	0.994786
14	28	7	1023	1023	0.978426
14	28	7	923	1023	0.987253
7	28	21	923	923	1.001774
7	28	21	1023	1023	0.986967
7	28	21	923	1023	0.995546
4	28	21	923	923	1.012511
4	28	21	1023	1023	0.997724
4	28	21	923	1023	1.006258
14	20	21	923	923	0.997184
14	20	21	1023	1023	0.982368
14	20	21	923	1023	0.990968
14	14	21	923	923	0.997507
14	14	21	1023	1023	0.982675
14	14	21	923	1023	0.991254

radial mesh one element corresponds to one graphite bar in the core. Since the reactor core is homogenized, further decrease of the radial mesh size is pointless as it would cut through the actual unit cell of the core.

Based on the results of the finest mesh and 21 energy group calculations, the temperature feedback coefficients for spatially uniform temperature distributions were calculated and are presented in Table D.2 together with the measured data. The results are considered to be in good agreement with the experimental results.

The flow field in the reactor at normal operation was calculated by the FLOW code and used in DALTON to calculate the reactivity loss due to the fuel flow. See Appendix for the details. The lenght of the primary loop was derived from the description in (Robertson, 1965b). The calculated loss of reactivity is 203 pcm which corresponds well with the original measured value of 212 pcm (Kophazi et al., 2003).

Table D.2: Feedback coefficients of the MSRE

	Salt temperature coefficient (pcm/K)	Graphite temperature coefficient (pcm/K)
Calculation	-8.85	-6.32
Measurement	-8.46	-4.68

Appendix E

The SATE code

The temperature of the fuel salt in the moderated MSR core, plena and primary loop is calculated by the in-house developed code SATE (SAlt TEmperature). All the fuel channels are modeled separately as 1-D loops. These are connected to the dividing and collecting plena which are modelled on a 2-D rz geometry. The primary loop outside the reactor vessel is described as a 1-D loop which connects the collecting plenum to the dividing one. The heat exchanger to the secondary salt is placed in this part of the model. The code reads the flow field in the primary loop, the distribution of power production in the core and in the plena, and the temperature of the graphite on the surface of every fuel channel.

E.1 The numerical model

The temperature balance of the salt in the fuel channels is calculated as follows:

$$\rho(T)c_p(T)\frac{\partial T}{\partial t} + v\rho(T)c_p(T)\frac{\partial T}{\partial z} = \frac{\partial}{\partial z}k(T)\frac{\partial T}{\partial z} + A_{gr}\frac{k(T)}{D}Nu(T_{gr} - T) + q''', \quad \text{(E.1)}$$

where T and v are the temperature and the velocity of the salt. All the material properties of the salt, the density ρ, the heat capacity c_p and the thermal conductivity k are function of the salt temperature in the calculations. The salt is heated by the volumetric source q''' which is the heat induced by fission and by the graphite. In equation E.1 A_{gr} and D represent the surface and the diameter of the fuel channel while Nu and T_{gr} note the Nusselt number and the temperature of the graphite on the surface. In the plena, the balance equation is given as:

$$\rho(T)c_p(T)\frac{\partial T}{\partial t} + v\rho(T)c_p(T)\nabla T = \nabla k(T)\nabla T + q''' \quad \text{(E.2)}$$

Finally, equation E.1 without the source terms is used to describe the primary loop except the position of the heat exchanger, which is modelled with the $\epsilon - NTU$ model (Kakac and Liu, 2002). The temperature of the salt leaving the heat exchanger is calculated with the following equation:

$$T_{out} = (\rho(T_{in})c_p(T_{in})AvT_{in} - \epsilon Q_{max})/(\rho(T_{out})c_p(T_{out})Av) \quad \text{(E.3)}$$

Here T_{in} and T_{out} are the inflow and outflow temperatures of the primary loop and A notes the total flow area of the hot side. The coefficients of the $\epsilon - NTU$ model are calculated as follows:

$$Q_{max} = min\left(Av\rho(T_{in})c_p(T_{in}); A_{sec}v_{sec}\rho_{sec}c_{p,sec}\right)$$ (E.4)

$$NTU = A_{tr}h_{tr}/Q_{max}$$ (E.5)

$$R = \frac{min\left(Av\rho(T)c_p(T); A_{sec}v_{sec}\rho_{sec}c_{p,sec}\right)}{max\left(Av\rho(T)c_p(T); A_{sec}v_{sec}\rho_{sec}c_{p,sec}\right)}$$ (E.6)

$$\epsilon = \frac{1 - exp((R-1) \cdot NTU)}{1 - R \cdot exp((R-1) \cdot NTU)}$$ (E.7)
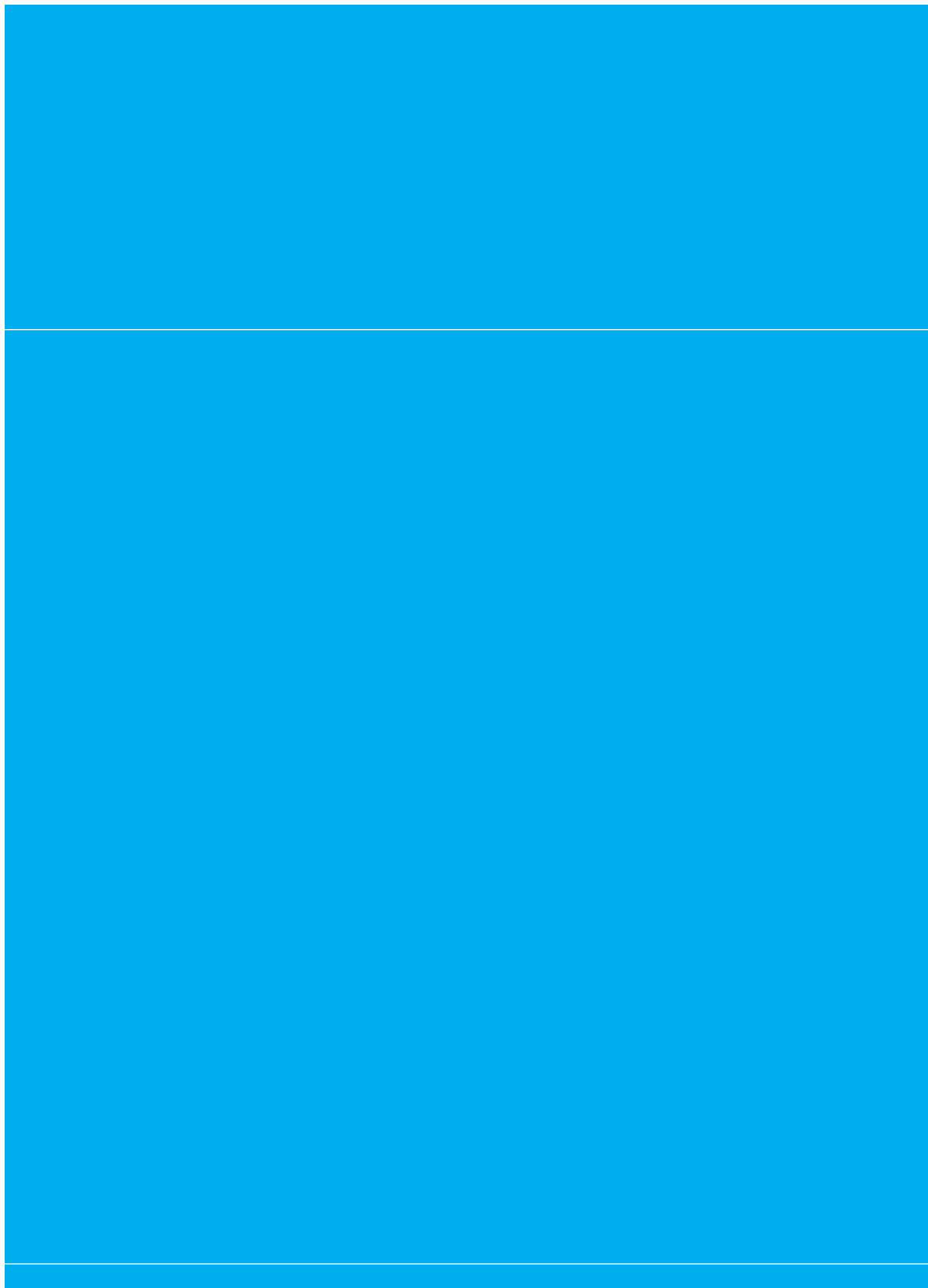
In these equations the subscript sec denotes the properties of the secondary side while A_{tr} and h_{tr} represent the total heat transfer surface and the overall heat transfer coefficient.

The equations E.1 and E.2 are spatially discretized using the finite volume method. The temperatures on the boundaries of the volumes are estimated by the upwind scheme and a total variation diminishing scheme with the van Leer limiter was applied in order to reduce numerical dispersion. The time derivative of the equations is discretized based on the second-order backward differentiation formula (BDF). These discretization schemes are discussed in details in Appendix D.

The mesh of the whole system is not structured, only on the separate parts (channels, plena) of the reactor. At the connection of the dividing plenum and the bottom of the channels, the mass flow leaving the plenum is distributed over the channels based on the overlapping surfaces of the rz mesh of the plenum and the graphite blocks in the cores. The flow leaving the channels is distributed in the similar way in the collecting plenum. The flow leaving the collecting plenum is collected in the 1-D primary loop and distributed evenly in the connecting volumes of the dividing plenum at the end of the loop.

The flow field calculated by the FLOW code (see Appendix C) is calculated using an

average salt temperature in the core. Thus, the effects of temperature variations are not included in it. This flow field is no longer conservative in the SATE calculations since all the material properties, including the density, depend on the temperature of the salt. In order to overcome this, the temperature field is calculated in an iterative way. Before every iteration step, a conservative flow field is prepared by updating the previous flow field with the local density data. The temperature-dependent material properties are updated in every step as well. The iteration stops when the temperature field does not change between two steps.

Appendix F

The GRAPHITE code

The proper calculation of the temperature field of the moderator in a graphite-moderated MSR is crucial because during normal and accidental transients the graphite is the only heat conducting material between the fuel channels. Thus, full 3D modeling of the moderator is necessary in order to capture the localized temperature peaks which might occur for example in a debris-induced incident. Several authors calculated the temperature field on a structured mesh (Kophazi et al., 2009; Krepel et al., 2005). The code presented here is capable of performing calculations on an unstructured mesh which allows correct modeling of complex geometries.

F.1   Description of the code

In an MSR up to 10% of the total power is deposited in the graphite moderator. This results in a unique phenomenon: the internally heating fluid cools the moderator as well while the moderator thermally couples the fuel channels. The equation describing these processes reads as follows:

$$\rho c(T)\frac{\partial T(\bar{x})}{\partial t} = \nabla\lambda_{gr}(T)\nabla T(\bar{x}) + q''' \tag{F.1}$$

Here ρ, c and λ_{gr} denote the density, heat capacity and thermal conductivity of the graphite. The moderator is cooled on the surface of the fuel channels so the following equation holds on the surfaces:

$$\rho c(T)\frac{\partial T(\bar{x}_{surface})}{\partial t} = \nabla\lambda_{gr}(T)\nabla T(\bar{x}_{surface}) + A\lambda_s(T_s)\frac{Nu}{D}(T_s - T(\bar{x}_{surface})), \tag{F.2}$$

where A and D are the surface area and the diameter of the channel.

The Finite Element Method (FEM) is used for the spacial discretization of the problem because allows to solve the differential equation over a complex domain such as the moderator of the reactor. The time derivative is discretized using the second-order backward differentiation formula (BDF). The code can solve the time-dependent and the steady-state equations as well. The thermal conductivity and the heat capacity of the graphite are allowed to depend on the temperature. This dependency makes an iteration necessary for the steady-state calculation. Several correlations are hard-coded in the program because the material properties of the graphite change with the received neutron fluence. The parameters describing the heat transfer on the channel surface (Nusselt number, thermal conductivity of the salt, etc.) are input for the code.
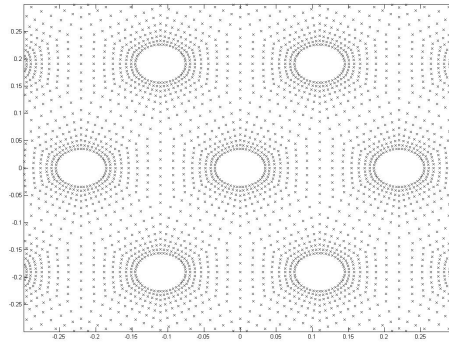
Figure F.1: The points defining the elements in 2D. Only a part of the core is shown. The elements are smaller close to the fuel channel because a large temperature gradient is expected near the surface.

F.2   Input of the code

The code reads one input file which contains all the necessary information. This file is divided into four blocks. The first being the control block defines the problem with the number of nodes, elements and boundary surfaces. The static/dynamic solver routines can be initiated with logical switches together with the restart mode of the dynamic calculations. The length of a time step and the power density in the graphite is read here as well. In the second block the hexahedral elements are defined by the ordered list of their nodes. In the third block the coordinates of the nodes are given line by line. The last block defines the boundary condition by describing a heat transfer coefficient and a bulk liquid temperature for any chosen surface of an element. The initial conditions of the dynamic calculations are taken from the linked files.

F.3   Validation and grid sensitivity

The fuel channels are arranged in a triangular lattice in the reactor core while the graphite structure is built of hexagonal blocks. This geometry of the moderator is described by three-dimensional hexahedral elements. These are defined by 8 points and provide first order accuracy. An illustrative part of the mesh is shown on Figure F.1.

The code was validated against an analytical calculation on a simplified geometry. The hexagonal graphite block was approximated by a cylinder with an inner fuel channel because the solution of the heat conduction problem is known for this geometry. In a cylindrical coordinate system the radial temperature distribution is described as:

Table F.1: Parameters used for validation

Parameter	Value	Unit
Radius of the graphite cylinder	0.07	m
Radius of the fuel channel	0.035	m
Thermal conductivity of the graphite	31.2	W/mK
Volumetric heat source	1.15	MW/m^3
Temperature of the salt	978	K
Thermal conductivity of the salt	1.19	W/mK
Nusselt number	377.1	-

$$T(r) = T_{surface} + \frac{q'''}{2\lambda_{gr}} \left(\frac{R_{surface}^2 - r^2}{2} + R^2 ln \left(\frac{r}{R_{surface}} \right) \right), \qquad \text{(F.3)}$$

where $R_{surface}$ and $T_{surface}$ are the radius of the fuel channel and the temperature of the graphite on the surface of the fuel channel, and R is the radius of the graphite cylinder. The temperature on the surface can be found in the following way:

$$T_{surface} = T_{salt} + \frac{q'''}{2\alpha} \left(\frac{R^2}{R_{surface}} - R_{surface} \right) \qquad \text{(F.4)}$$

Here α is the heat transfer coefficient between the salt and the graphite, $\alpha = \lambda_s Nu/D$. This radial temperature distribution is compared with the results obtained from the code. The calculations were performed with 3 different meshes which differed in the number of elements in the radial direction. This was done to check the sensitivity of the results on the grid size.

The MSBR was chosen as a reference design (Robertson, 1971). The parameters used in the input of the code and in the analytical calculation are listed in Table F.1. The graphite cylinder was described with a mesh which contains 24 elements on the circumference of the cylinder and 2, 5 or 10 elements in the radial direction. Zero heat flux boundary was applied on the outer surface of the graphite cylinder.

The calculated radial temperature distributions are shown on Figure F.2. The results of the code agree with the analytical solution except the case when only 2 elements were used radially. The difference between this and the analytical solution is caused by linear interpolation within the element. This second-order error can be minimized if more elements are used.
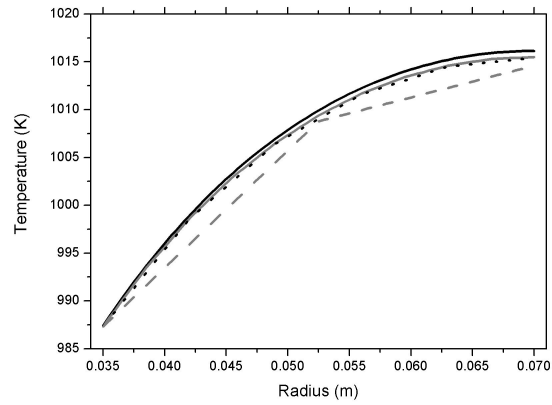
Figure F.2: The radial temperature distribution in the graphite. On the left side of the graph (at r=0.035m) is the inner surface of the graphite cylinder to the graphite. Zero heat flux boundary condition was applied on the outer boundary. The black line shows the analytical solution. The gray, dotted and dashed lines represent the results of the calculations using 10, 5, and 2 elements on the radius of the cylinder, respectively.
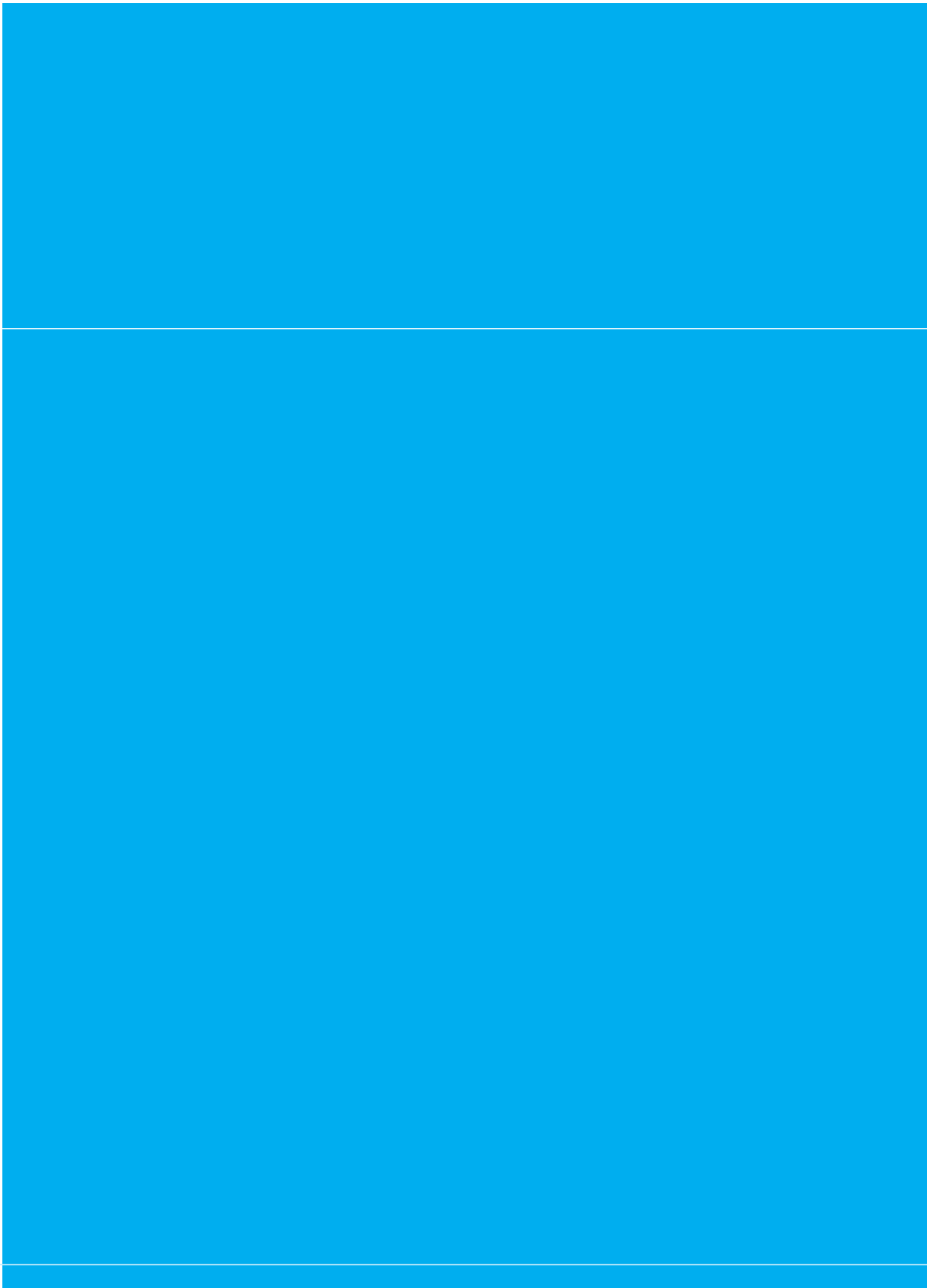
Summary

A Molten Salt Reactor (MSR) operated on the thorium fuel cycle is an attractive breeder reactor. After a two-decade development program at the Oak Ridge National Laboratory, the interest in the MSR rose again with the Generation-IV initiative. The original graphite-moderated ORNL reactor design was the base for these successor research programs. Unfortunately, the original design was found to be unfeasable for its positive reactivity feedback and for its rapid salt purification processes. After some attempts to modify the design to meet the goals of the Generation-IV initiative, the graphite-moderated design was abandoned in favor of fast MSR designs. This thesis aims to prove that it is possible to design and operate an inherently safe, graphite-moderated, self-breeder MSR by modeling the dynamics of its fuel cycle and optimizing the core design according to the results. The safety of the reactor is also evaluated by static and transient calculations.

The breeder MSR designs use different graphite-salt lattice and processing strategies. Therefore, the main objective of the reactor design optimization is to determine which lattice configuration and processing strategy is necessary to reach self-breeding. To be able to model the fuel cycle and the different processing schemes of the MSR, a dedicated code system was developed. It consists of two parts, an in-house time-dependent material evolution calculation and a criticality calculation that provides the spectrum data of the reactor. The resulting code system incorporates the phenomena which are unique for the MSR, such as continuous removal of elements, continuous addition of actinides and storage of actinides outside of the core. This code system is used in several core design studies throughout the thesis. The comparison of different core geometries shows that there is an optimal value of the graphite to salt volume ratio which maximizes the uranium production. Using an undermoderated or overmoderated core by applying less or more graphite results in a decrease of the produced excess uranium because of the increase in the uranium load and of the increase of the power density in the salt, respectively. Salt processing schemes based on the continuous removal of fission products are necessary to reach breeding operation but a relatively simple batch-wise processing scheme allows for high conversion ratio operation at a low power density of 5 MW/m^3.

A breeding gain definition is proposed for the MSR in this thesis. It is shown that the currently used definitions can give wrong prediction about the breeding performance of the reactor because these definitions do not capture all the MSR-specific phenomena. The proposed definitions describe the different actinide-containing volumes of the reactor (such as the primary loop and the stockpiles) with separate equations which can be summed to obtain the total breeding gain of the reactor. The equations also count for the transfer of the nuclides of the thorium fuel cycle between the different volumes. As it is shown, the simplified form of the proposed definition is equivalent with the previously used definition. The definition is successfully applied to an optimization study of the one-zone MSR and it is used in the comparison of various, one- and two-fluid reactors.

The moderator has positive temperature feedback in an MSR operating on the thorium fuel cycle. Calculations presented in this thesis indicate that a narrow range of salt-graphite lattices provide a sufficiently negative total temperature feedback and still are capable for breeding. Therefore, the graphite-salt lattice is optimized with regards to the temperature feedback while the goal is to achieve self-breeding with high power density. During the optimization, the fuel channel diameter, the graphite to salt volume ratio and the thorium

concentration is varied while the temperature feedback coefficient of the core, the breeding gain and the lifespan of the graphite are calculated. It is shown that self-breeding can be achieved in small range of lattices which provide both negative temperature feedback. However, the lifespan of the graphite is 10 to 20 years in the range of 5 - 10 MW/m^3 average power density, which is shorter than the expected lifetime of the reactor.

In the various MSR designs the ratio of the salt and the graphite volume is not uniform. This non-uniform salt distribution is used to either increase the graphite lifespan or improve the breeding gain of the reactor. However, the contribution of this non-uniformity to the final results of lifespan or breeding gain is barely assessed in the literature. The effect of the variation of the salt distribution is investigated on a two-zone core. It is found that both the increase of the breeding gain or the graphite lifespan is possible by zoning the core but at the cost of decreasing the other one. Furthermore, the magnitude of the increase of the breeding gain is higher than that of the graphite lifespan. A two-fluid reactor design offers more options for the fuel cycle of the MSR. These are also discussed and investigated in the thesis.

A coupled calculation scheme, which includes the reactor physics, heat transfer and fluid dynamics calculations, is introduced in this thesis. It is used both for steady-state and for dynamic calculations that aim to evaluate the safety of the graphite-moderated MSR. The calculated feedback coefficients on the salt and graphite temperatures, power and uranium concentration prove that the core design derived in the previous optimization study is safe because the temperature feedback coefficient of the core and of the power is sufficiently negative. Transient calculations are performed to show the inherent safety of the reactor in case of reactivity insertion. As it is shown, the response of the reactor to these transients is initially dominated by the strong negative feedback of the salt. In all the presented transients, the reactor power stabilizes within ten minutes and the temperature of the salt never approaches its boiling point.
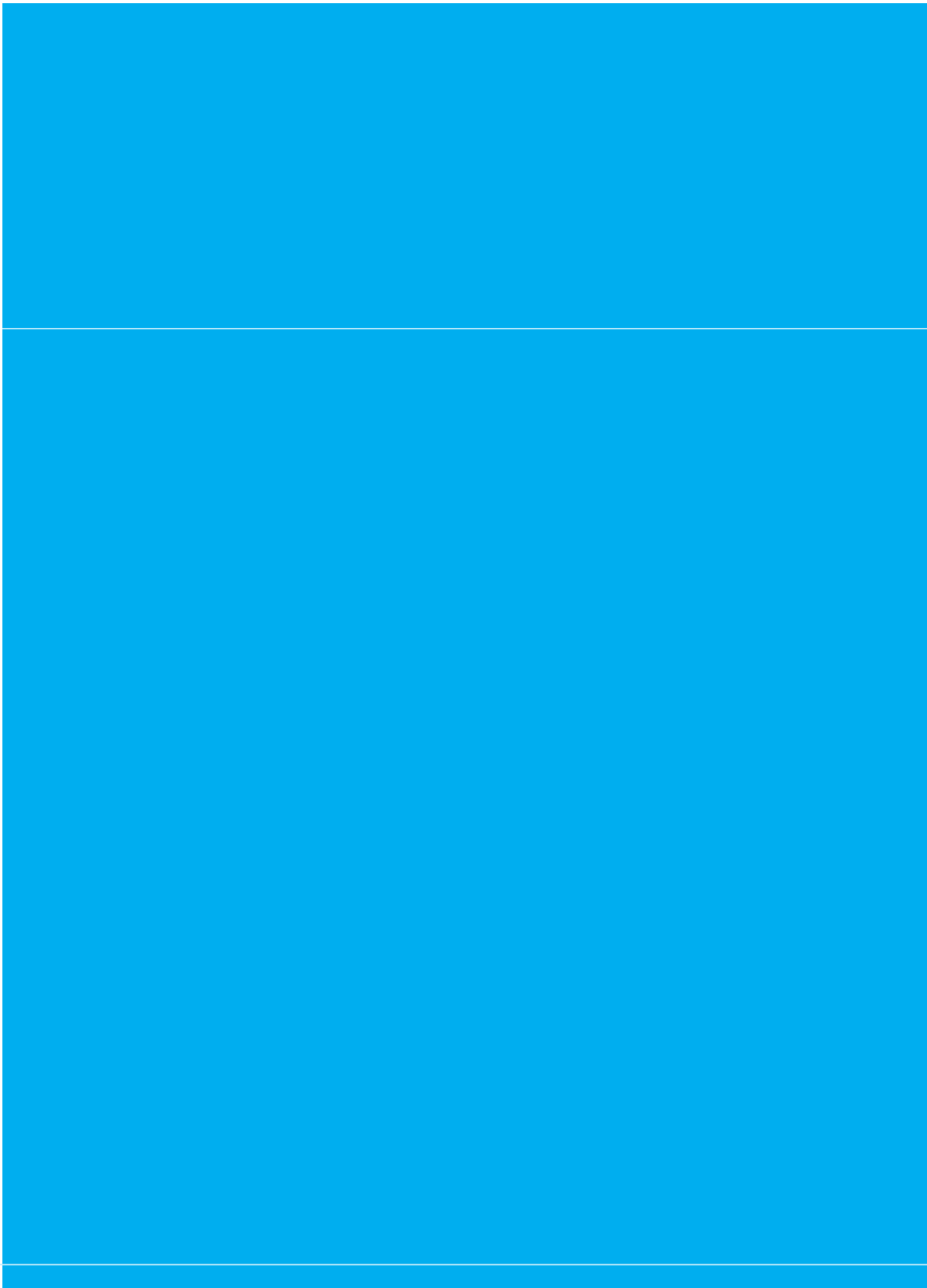
Samenvatting

Een Gesmolten Zout Reactor (met als Engelstalig acroniem 'MSR') werkend op basis van de thorium brandstofcyclus is een aantrekkelijke kweekreactor. Volgend op een twee decennia lang durend ontwikkelingsprogramma bij het Oak Ridge National Laboratory (ORNL), ontstond er kort geleden weer interesse in dit reactortype door het Generation-IV initiatief. De nieuwe gesmolten zout reactorontwerpen die hieruit ontstaan, zijn allen geïnspireerd door het ORNL reactorontwerp wat grafiet gebruikt als moderator. Dit ontwerp bleek jammergenoeg niet haalbaar omwille van de positive reactiviteitsterugkoppeling en de nood aan snelle zuiveringsprocessen voor het zout. Na een aantal pogingen het ORNL ontwerp aan te passen om de doelstellingen van het Generation-IV initiatief te halen, werd de grafiet moderator opgegeven ten gunste van 'snelle' gesmolten zout reactoren. Het doel van dit proefschrift is aan te tonen dat het toch mogelijk is een MSR te ontwerpen en te exploiteren met een grafiet moderator die intrinsek veilig is en werkt als een zelfvoorzienende kweekreactor. Hiertoe werd de brandstofcyclus dynamisch gemodelleerd en uitgaand van deze resultaten werd het ontwerp van de reactorkern geoptimaliseerd. Daarnaast werd ook de reactorveiligheid geëvalueerd door middel van zowel statische als dynamische berekeningen.

De verschillende ontwerpen van gesmolten zout kweekreactoren hebben een andere kernconfiguratie (dus, verschillende zout-grafiet structuur) en verwerkingsstrategie voor het zout. Het voornaamste doel van de optimalisatie van het reactorontwerp is daarom te bepalen welke zout-grafiet configuratie en verwerkingsstrategie nodig zijn om een kweekreactor zelfvoorzienend te maken. Een nieuw computerprogramma werd hiertoe ontwikkeld om de brandstofcyclus en de verschillende zuiveringsprocessen te modelleren. Dit bestaat uit twee delen: een tijdsafhankelijke berekening van de isotoopsamenstelling van de kern en een berekening van de kritikaliteit van de reactor. Dit laatste levert het neutronspectrum op van de reactor. Het computerprogramma houdt verder ook rekening met alle fenomenen eigen aan de gesmolten zout reactor zoals de continue verwijdering en toevoeging van bepaalde stoffen en de opslag van actinides buiten de reactorkern. Dit ontwikkelde computerprogramma werd aangewend voor verschillende ontwerpstudies in dit proefschrift. Een vergelijking van de geometrie van diverse reactorontwerpen toont aan dat er een optimale waarde bestaat voor de verhouding van de grafiet en zout inhoud die resulteert in een maximale uranium productie. Het aanbrengen van minder of meer grafiet resulteert in een lagere productie van surplus uranium, en dit door een toename van respectievelijk de kernbrandstof inhoud en de lokale vermogensdichtheid in het zout. De resultaten geven verder ook aan dat een continue verwijdering van de fissieproducten uit het zout nodig is om als kweekreactor op te treden, maar dat met een eenvoudige discontinue verwerking (lading per lading) het mogelijk is een hoge conversieverhouding te halen en dit bij een lage vermogensdichtheid van 5 MW/m3.

In dit proefschrift wordt aangetoond dat de bestaande definities van de kweekfactor kunnen leiden tot een verkeerde voorspelling van de kweekprestatie van een gesmolten zout reactor en dit omdat deze geen rekening houden met de fenomenen eigen aan dit type reactor. Daarom wordt een nieuwe definitie voorgesteld voor de kweekfactor van een MSR. Deze nieuwe definitie beschrijft de verschillende reactorvolumes (zoals de primaire kringloop of de reservevoorraad) met actinides met een aparte vergelijking. Deze set vergelijkingen kan dan gesommeerd worden om zo de totale kweekprestatie van de

reactor te bepalen. De vergelijkingen houden ook rekening met het transport van actinides afkomstig uit de thorium brandstofcyclus tussen de verschillende reactorvolumes. Men kan aantonen dat de vereenvoudigde vorm van de voorgestelde definitie equivalent is met de bestaande definitie van de kweekfactor. De nieuwe definitie werd aangewend voor de optimalisatie van een gesmolten zout reactor met één zone en voor de vergelijking van verschillende reactorontwerpen met één of twee zoutmengsels.

De grafiet moderator zorgt voor een positieve temperatuursterugkoppeling in een gesmolten zout reactor. Resultaten uit dit proefschrift tonen aan dat onder strikte voorwaarden de kernconfiguratie een voldoende negatieve totale temperatuursterugkoppeling heeft, zelfs wanneer de reactor werkt als een zelfvoorzienende kweekreactor. Aldus wordt de zout-grafiet kernstructuur verder geoptimaliseerd om te werken als een zelfvoorzienende kweekreactor met een voldoende negatieve temperatuursterugkoppeling en strevend naar een zo hoog mogelijke vermogensdichtheid. Tijdens de optimalisatie worden de diameter van het brandstofkanaal, de volumeverhouding van het grafiet tot het zout en de thorium concentratie gewijzigd. Per ontwerp worden de temperatuursterugkoppeling, de kweekfactor en de levensduur van het grafiet berekend. De resultaten tonen aan dat voor zelfvoorzienende gesmolten zout kweekreactoren met een voldoende negatieve temperatuursterugkoppeling de gemiddelde levensduur van het grafiet slechts 10 tot 20 jaar bedraagt bij een gemiddelde vermogensdichtheid van 5-10MW/m3 Dit is aanzienlijk korter dan de verwachte levensduur van de reactor. In verschillende ontwerpen van een MSR wordt in de kern een niet-uniforme zout-grafiet volumeverhouding gebruikt om de levensduur van het grafiet te verlengen of om de kweekfactor te verhogen. Echter, in de literatuur is weinig informatie terug te vinden over de invloed van deze niet-uniformiteit op de kweekfactor, op de levensduur van het grafiet of op de algemene werking van een gesmolten zout reactor. Dit werd onderzocht in dit proefschrift aan de hand van een kern met twee zones. De resultaten tonen aan dat het opdelen van de kern in verschillende zones zowel de kweekfactor als de levensduur van het grafiet kan verhogen, maar niet beide tegelijk. De invloed op de kweekfactor is daarnaast ook sterker dan die op de levensduur van het grafiet. Werken met twee verschillende zoutmengsels zorgt verder ook voor een grotere flexibiliteit in de brandstofcyclus van de gesmolten zout reactor. Dit werd verder onderzocht en beschreven in dit proefschrift.

In dit proefschrift werden vervolgens een aantal statische en dynamische simulaties uitgevoerd om de veiligheid te evalueren van een gesmolten zout reactor met een grafiet moderator. Deze simulaties werden gedaan met een gekoppeld berekeningschema, dat zowel de reactorfysica bevat als warmteoverdracht en vloeistofdynamica. De berekende sterkte van de terugkoppeling van de zout- en grafiettemperatuur, van het reactorvermogen en van de uraniumconcentratie tonen aan dat het kernontwerp bekomen in de eerdere optimalisatiefase veilig is, en dit omwille van de voldoende negatieve terugkoppeling van zowel de kernstructuur en het vermogen. Tijdsafhankelijke berekeningen toonden verder de intrinsieke veiligheid van het ontwerp aan voor een plotse reactiviteitstoename. De resultaten geven aan dat het gedrag van de reactor onmiddellijk gedomineerd wordt door de sterke negatieve terugkoppeling van het zout. In alle tijdsafhankelijke simulaties stabiliseerde het reactorvermogen binnen 10 minuten en bereikte het zout nooit het kookpunt.

(Dutch translation provided by Dr. Christophe T'Joen)
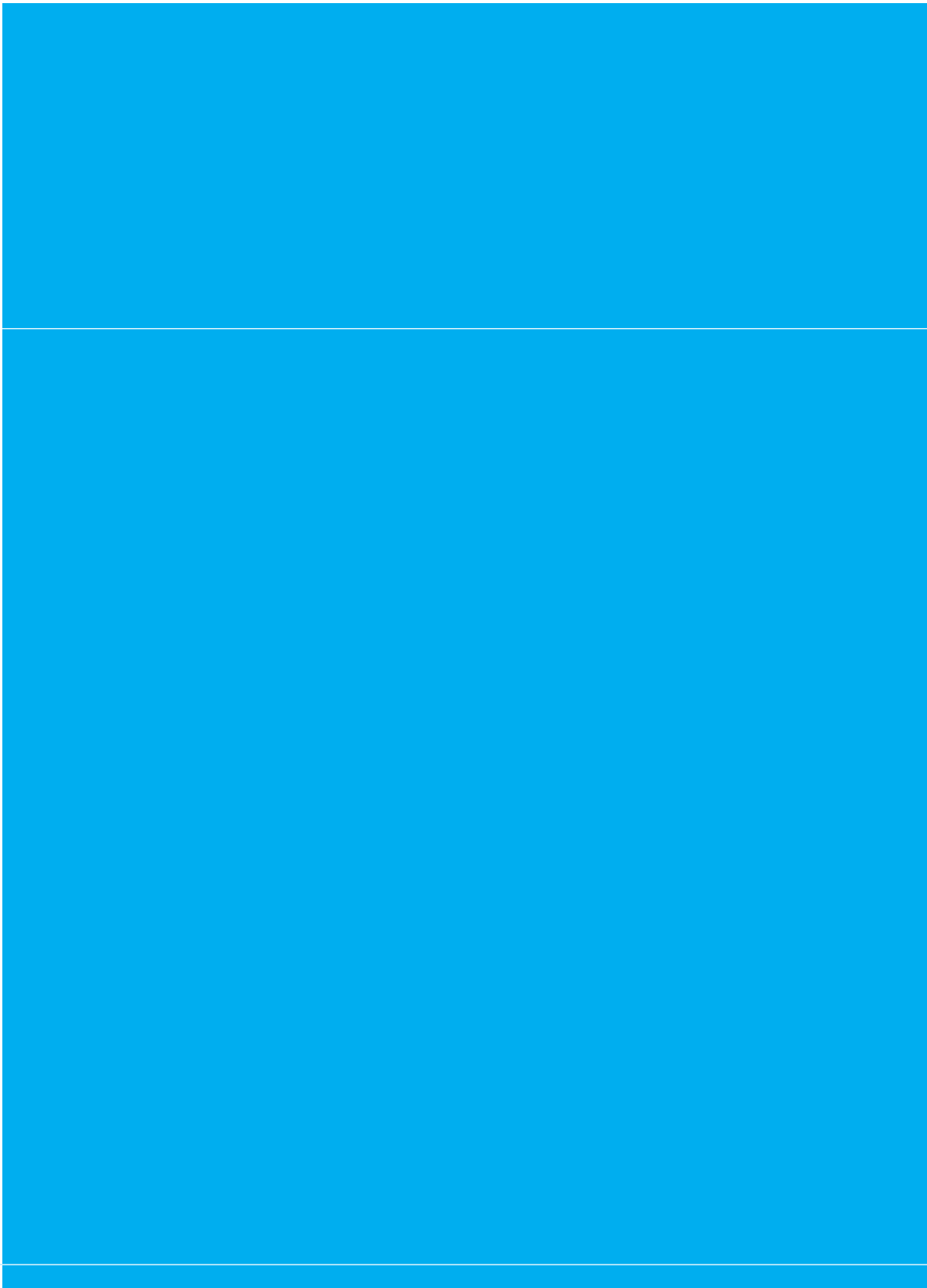
Acknowledgments

Firstly, I would like to thank Tim van der Hagen and Jan Leen Kloosterman for giving me the opportunity to work in the Physics of Nuclear Reactors group of TU Delft. Their guidance and support during the project was invaluable, both in the research and in the management part. Without Tim's drive for perfection this thesis would certainly look different. I feel greatly indebted to my daily supervisor, Jan Leen, for giving me all the freedom in doing my research. I am also grateful for the discussions we had with my Shell supervisors, Wim Wieldraaijer and Herman Kuipers.

It has been a pleasure to work with the staff of PNR. Danny Lathouwers deserves to be mentioned first, given the amount of help and Fortran90 subroutines I got from him. Danny always had an answer for any of my questions regarding modelling approaches and numerical methods. The SCALE experience of Piet was of great value the time I had just started to perform reactor physics calculations. The post-docs of the group were always enthusiastic to share their knowledge with me. Therefore, I thank Christophe for his insight on heat transfer, fluid dynamics and Blizzard games; Dimitrios for citing the PETSc error codes without the manual every time I ran into a new one and for taking every opportunity to share a beer with me; and most importantly József for sharing all his experience and details he has learned on previous MSR projects and on everyday Hungarian politics. The PhDs, visitors and students created a nice environment to work in the group; Stavros, Brian, Jerome, Ming, Johan, Jitka, Luca, Gert Jan, Bart, Zoltán, Frank, and many more, thank you all. And thank you for not forgetting me after I have left the group. One of them, Stuart Christie has influenced my research the most by sharing his collection of vintage fast reactor fuel cycle papers and PS3 games. I am glad that Michiel, Roderik, Frederik and Erik could finish their MSc theses on MSRs having me as their advisor or supervisor. Special thanks goes to Ine who sorted out all the possible problems needed to be sorted out during the four years of a PhD research. Finally, I am grateful for the always-changing regular crowd of 't Koepeltje for making my evenings less boring, and especially grateful for Dr Leon van Heijkamp van Heijkamp [sic] for organising jam sessions and poker nights.

I would like to take this opportunity to thank my parents and my family in Hungary, who supported me and worried about me for these years abroad, and all the years before at home. I was not forgotten by my friends in Gyula and Budapest; no matter how rarely I have contacted them, they have not forgotten me. In the end, running out all the phrases I could use to express my gratitude, I would like to thank Ingrid for everything she did and does, for all the care and love. This thesis would not be finished by now without the important contribution of Kari, my son, who developed a morning routine of waking me up and going back to sleep, only to provide me a quiet environment to work.
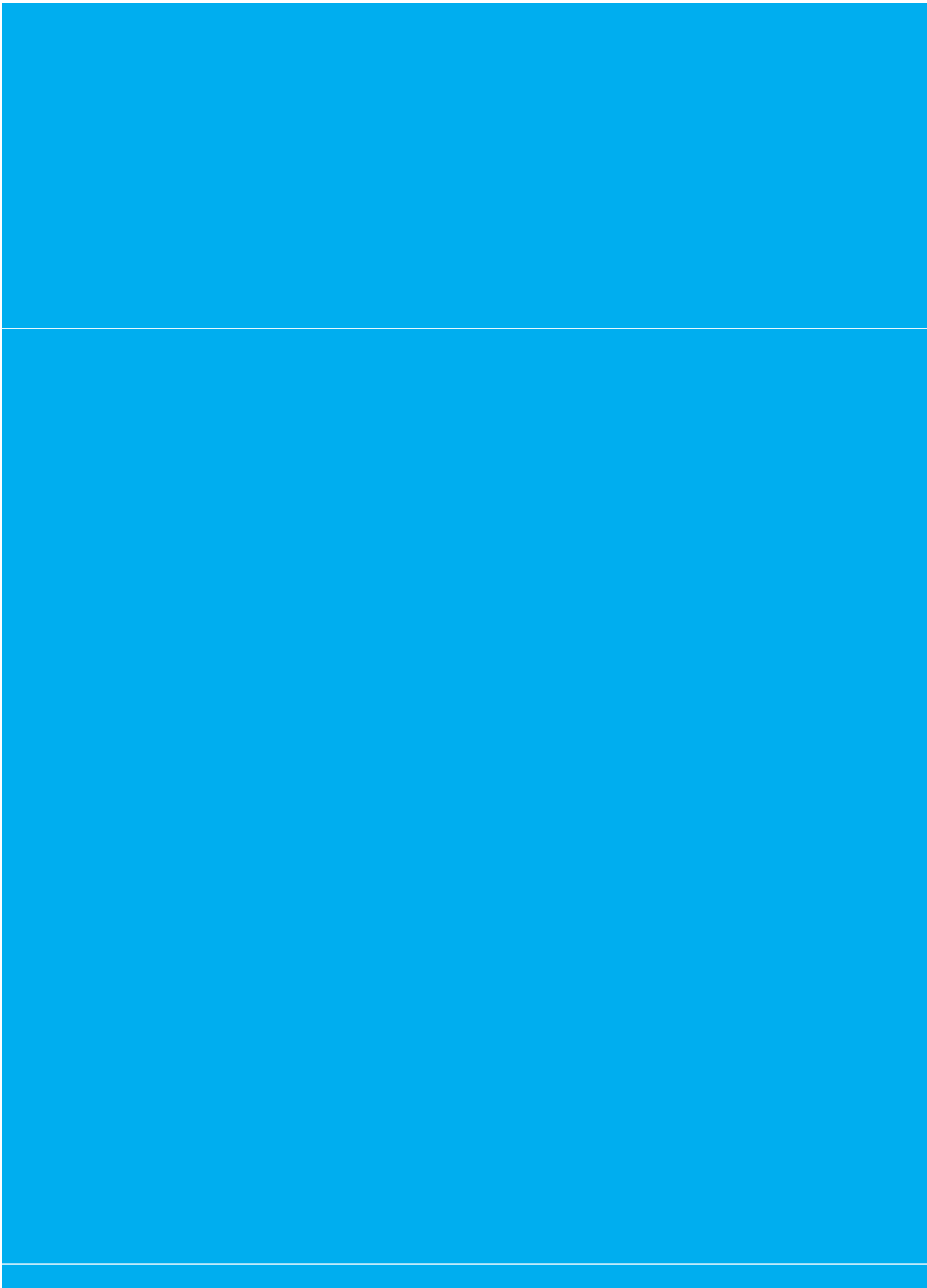
List of Publications

K. Nagy and J. L. Kloosterman and D. Lathouwers and T. H. J. J. van der Hagen. The Effects of Core Zoning on the Graphite Lifespan and Breeding Gain of a Moderated Molten Salt Reactor Design, *Annals of Nuclear Energy*, 43:19-25 (2012).

K. Nagy and J. L. Kloosterman and D. Lathouwers and T. H. J. J. van der Hagen. New Breeding Gain Definitions and their Application to the Optimization of a Molten Salt Reactor, *Annals of Nuclear Energy*, 38:601-609 (2011).

K. Nagy and J. L. Kloosterman and D. Lathouwers and T. H. J. J. van der Hagen. Definition of Breeding Gain for Molten Salt Reactors, *PHYSOR-2010*, Pittsburgh, USA (2010).

K. Nagy and J. L. Kloosterman and D. Lathouwers and T. H. J. J. van der Hagen. Parametric Studies on the Fuel Salt Composition in Thermal Molten Salt Breedeer Reactors, *PHYSOR-2008*, Interlaken, Switzerland (2008).

Curriculum Vitae

Károly Nagy was born on May 19, 1984 in Szolnok, Hungary.

He grew up in Gyula, a small city in Hungary and received his secondary school diploma from the Erkel Ferenc Gimnázium, one of the school of the city, in 2002. Having generations of mathematics and physics teachers in his close family, no one was surprised that he started his studies in the Budapest University of Engineering and Economics. He obtained hisMaster of Science degree in Engineering Physics in 2007.

In July 2007 he started his PhD research in the Physics of Nuclear Reactors group of Delft University of Technology under the supervision of dr. ir. Jan Leen Kloosterman.His research focused on graphite-moderatedMolten Salt Reactors, culminating in this thesis.